ABSTRACT

TALUJA, PAWANDEEP S. Information-Theoretic Limits on Broadband Multi-Antenna Systems in the Presence of Mutual Coupling. (Under the direction of Dr. Brian L. Hughes.)

Multiple-input, multiple-output (MIMO) systems have received considerable attention over the last decade due to their ability to provide high throughputs and mitigate multipath fading effects. While most of these benefits are obtained for ideal arrays with large separation between the antennas, practical devices are often constrained in physical dimensions. With smaller inter-element spacings, signal correlation and mutual coupling between the antennas start to degrade the system performance, thereby limiting the deployment of a large number of antennas. Various studies have proposed transceiver designs based on optimal matching networks to compensate for this loss. However, such networks are considered impractical due to their multiport structure and sensitivity to the RF bandwidth of the system.

In this dissertation, we investigate two aspects of compact transceiver design. First, we consider simpler architectures that exploit coupling between the antennas, and second, we establish information-theoretic limits of broadband communication systems with closely-spaced antennas. We begin with a receiver model of a diversity antenna selection system and propose novel strategies that make use of inactive elements by virtue of mutual coupling. We then examine the limits on the matching efficiency of a single antenna system using broadband matching theory. Next, we present an extension to this theory for coupled MIMO systems to elucidate the impact of coupling on the RF bandwidth of the system, and derive optimal transceiver designs. Lastly, we summarize the main findings of this dissertation and suggest open problems for future work.

Information-Theoretic Limits on Broadband Multi-Antenna Systems in the Presence of Mutual Coupling

by
Pawandeep Singh Taluja

A dissertation submitted to the Graduate Faculty of
North Carolina State University
in partial fulfillment of the
requirements for the Degree of
Doctor of Philosophy

Electrical Engineering

Raleigh, North Carolina

2011

APPROVED BY:

Dr. J. Keith Townsend	Dr. Alexandra Duel-Hallen
Dr. Griff Bilbro	Dr. Brian L. Hughes Chair of Advisory Committee

DEDICATION

To my loving parents and my wife.

BIOGRAPHY

Pawandeep S. Taluja received the B. Tech. degree in Electronics and Communication Engineering from Indian Institute of Technology, Guwahati in May 2004. In July 2004, he joined the Wireless Terminal Division of Samsung Electronics (India) Software Operations where he worked on UMTS Radio Resource Controller design. In August 2006, he began working toward his PhD in Electrical Engineering at North Carolina State University under the advisement of Prof. Brian L. Hughes. He defended his dissertation in February 2011. His research interests include MIMO Systems, Communication Theory, Signal Processing and Communications Systems Design.

ACKNOWLEDGMENTS

First and foremost, I would like to thank my advisor Prof. Brian Hughes for his guidance and support throughout my PhD career. I have greatly benefited from his technical expertise and intuitive approach toward problem solving. His excellent art of communicating ideas, critical analysis and professional attitude have been instrumental in making this experience truly rewarding.

I would also like to thank my committee members Profs. J. Keith Townsend, Alexandra Duel-Hallen, Griff Bilbro and Steve Shannon for their valuable feedback and comments.

I would always cherish the company of my fellow group members Carlo Domizioli and Yuhan Dong for providing a stimulating research environment and years of camaraderie. I would also like to thank one of our undergraduate students, David Fioramonti for his contribution with NEC simulations.

I owe thanks to many of my friends and colleagues who made my stay in Raleigh a memorable one. Finally, this work would not have been possible without the unconditional love and support of my parents, my sister and my wife Sumeet. This dissertation is dedicated to them.

TABLE OF CONTENTS

LIST OF TABLES

LIST OF FIGURES

Chapter 1

Introduction

During the last decade, multiple-input multiple-output (MIMO) systems have received tremendous attention from the research community and industry alike. This interest in MIMO wireless communications was sparked by the pioneering work of Foschini and Gans [39], [38], and Telatar [90], who showed that the use of multiple antennas at the transmitter and receiver combined with sophisticated signal processing can provide high spectral efficiencies in wireless channels with rich scattering environments. This has also led to commercial deployment and adoption of multi-antenna systems in many current and future cellular standards (UMTS, LTE), wireless local area networks (e.g., WLAN-802.11n), and wireless metropolitan area networks (WMAN-802.16e/WiMAX).

A very rich and diverse literature has addressed communication theory, signal processing and implementation aspects of MIMO systems. Although multiple antennas have long been used for radar, military and space applications, the concept of exploiting multiple antennas in order to boost the spectral efficiency of wireless systems through multiplexing techniques was originally proposed in [38], [39]. A detailed information-theoretic analysis of MIMO systems was first presented in [90]. This initial study of MIMO systems

assumed a rich scattering environment such that the *fading* was *spatially uncorrelated*. Later, MIMO channel models that incorporate physical scattering and limited angle-of-arrival (AoA) and angle-of-departure (AoD) spread, were also considered [58], [84]. A study of the impact of spatially correlated fading on MIMO channel capacity can be found in numerous papers [19], [91], [23], [24].

Spatial multiplexing schemes, such as Bell-Labs Layered Space-Time Architecture (BLAST) [110], offer tremendous data rates by transmitting independent streams of data from multiple transmit antennas simultaneously and rely on advanced signal processing capabilities to separate them in space and time at the receiver. Prior to decoding, the MIMO channel is often estimated to aid equalization. A technique to estimate MIMO channels for Vertical-BLAST (V-BLAST) systems by use of training sequences was proposed in [65].

Space-time and space-frequency coding techniques that exploit the spatio-temporal and spatio-spectral diversity of a MIMO wireless channel have been shown to alleviate the problem of signal fading. For example, Alamouti's block coding [2] is a simple yet powerful rate-1 code that transmits modulated symbols over channels with 2 transmit antennas to capture the diversity in space and time/frequency. The use of MIMO systems for *frequency selective* channels has also been a focus of study, particularly in conjunction with spread-spectrum and multi-carrier modulation techniques, such as code-division multiple access (CDMA) and orthogonal frequency-division multiplexing (OFDM) [62], [73], [7]. MIMO-OFDM now forms the air interface of many existing and new standards, namely IEEE 802.11n and 3GPP LTE.

When complete channel state information (CSI) is available at the transmitter (CSIT), optimal transmission strategies are *water-pouring* over space, time and/or frequency such

that the MIMO channel is appropriately decoupled by use of transmit precoding and receive decoding. Generalized linear precoder and decoder design for MIMO systems was proposed in [83]. The capacity of MIMO systems with CSIT can be found in [80], [44], [94]. The capacity of such systems is necessarily greater than or equal to those without CSIT. An analysis of diversity *versus* multiplexing capability of MIMO systems can be found in [122].

The benefits of deploying a large number of antennas at a transceiver come at the cost of an increased system and hardware complexity. Antenna selection (cf. [70], [54], [6], [47], [48]) is a scheme that tries to bridge this gap between complexity and the benefits offered by multi-antenna systems. Antenna selection systems are also popularly known as *hybrid-selection/maximal-ratio-combining* (H-S/MRC). Some of the work on H-S/MRC can be found in [103], [104], [105], [106], [107]. For spatially correlated environments, several designs that improve the performance of selection diversity systems have been proposed, including spatial-FFT [71], phase-shifter based design [121] and RF pre-processing [67]. Some of the implementation issues in antenna selection have been discussed in [69].

1.1 MIMO and Mutual Coupling

The high spectral efficiencies promised by MIMO systems can, in principle, be realized for arrays with large inter-element spacings. However, the demand for high data rates over the air is currently fueled by handheld and portable devices such as cell-phones, laptops and wireless access points. The use of multiple antennas on devices with small dimensions is usually prohibitive because of performance degradation resulting from signal correlation and electro-magnetic (EM) interactions among the antennas (commonly referred to as

mutual coupling).

Several studies have addressed the impact of fading correlation and mutual coupling on the performance of MIMO systems. For conciseness, we highlight here only a few that are relevant to our work. While the impact of correlated fading due to non-richness of the scattering environment has been a topic of interest for quite some time, studies addressing mutual coupling in MIMO systems involving detailed *network analysis* of the RF *front-end* have been a focus of research only recently.

An antenna is a transducer that converts EM signals into electrical signals which are processed by a radio-frequency (RF) chain, which consists of amplifiers, demodulator and analog-to-digital (A/D) converter. The EM wave incident on an antenna induces a voltage across the antenna terminals which is captured by the rest of the RF chain to be processed digitally. For antennas spaced a fraction of a wavelength apart, coupling presents a significant impairment. The current flowing in one element alters the voltage across the other. A key ingredient of modeling compact MIMO transceivers is analyzing the relationship between these terminal currents and voltages, while also incorporating the propagation characteristics and fading correlation into the system model. It is convenient to model an antenna array as a *multiport* network with a Thevenin equivalent *antenna impedance* matrix and an *open-circuit voltage* vector. In the absence of significant coupling, such representations reduce to a bank of uncoupled *two-port* networks and the received signal is a trivial function of the voltage induced across the antenna terminals.

Lee [61] investigated the impact of mutual coupling and spatial correlation on receive diversity systems through a multiport representation of the antenna array. He demonstrated that, by use of appropriate antenna loads, the coupling among the antennas can

be eliminated. In practice however, antenna loads are fixed and special RF circuits called *matching networks* are inserted between the antennas and the rest of the RF network in order to provide maximum power to the digitizer. Such an approach was considered in [99], [100] where the antennas were represented using the *scattering-parameter* matrix or *S-matrix*. This study proposed optimal multiport matching networks, commonly referred to as *conjugate matching*, that decouple the antenna array and deliver maximum power to the rest of the network. By use of EM simulations, it was shown that the diversity gains of an array approach unity as the spacing between the elements is decreased. In this study, the receiver noise was assumed to be spatially-white.

The impact of receiver noise modeling on the system performance for compact transceivers has been considered by several authors. Gans evaluated the impact of antenna thermal noise [42] and (spatially-white) amplifier noise [43], separately. It was shown that matching networks offer no improvement in capacity when antenna noise is dominant, while they have significant impact for amplifier noise dominant scenarios. A more general noise model was presented recently in [29], [30] for state-of-the-art receivers, and an optimal matching network applicable to a variety of MIMO schemes was derived. It was shown that the performance is significantly altered by the location of noise in the RF chain and that mathematically, it was possible to completely eliminate coupling at all spacings and achieve performance close to an ideal system. However, this appears counter-intuitive because, as the antennas are brought close to each other, we expect the system to behave like a single-antenna system.

Although the above mentioned studies paint slightly varying pictures of how close two antennas can be placed while still retaining most of the MIMO benefits, they all share a common underlying theme: with optimal matching, it is possible to pack antennas as

close as a quarter of a wavelength and preserve most of the capacity advantages of MIMO systems. However, conjugate matching networks are often considered impractical because of their multiport structure. They do however, provide an upper bound on the system performance - a useful benchmark to compare other transceiver design methodologies. In this dissertation, we consider relatively simpler architectures, such as *antenna selection*, and investigate alternate transceiver designs that seek to exploit coupling among the antennas.

Another issue with these optimal transceivers - the sensitivity of the diversity gains to the RF bandwidth of the system, was highlighted in [60], [31] recently. All studies thus far have addressed the problem of mutual coupling and optimal matching assuming a *narrowband* communication model. In this dissertation, we also investigate optimal transceiver designs of single- and multi-antenna systems for broadband communications in the presence of mutual coupling.

1.1.1 Antenna Selection

As noted earlier, the benefits of deploying a large number of antennas at a transceiver come at the cost of an increased system and hardware complexity. Typically, each antenna in a receive (or transmit) array is associated with a low-noise amplifier/LNA (power amplifier/PA), a demodulator (modulator) and an A/D (D/A) converter. Together these components constitute the RF chain, which can be expensive. In addition, employing more antennas requires sophisticated digital signal processing (DSP) and for small hand-held devices, it puts a burden on providing an extended battery life. All these factors pose a challenge to the wide scale deployment of multiple-antenna systems.

Antenna selection (AS) is a scheme that tries to bridge this gap between complexity

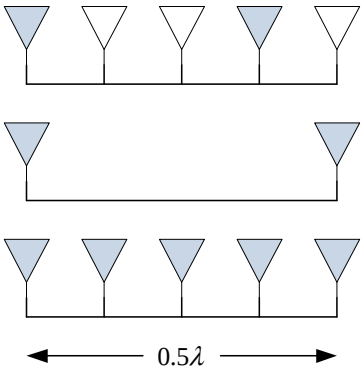

Figure 1.1: Configurations: (a) Antenna selection (AS), (b) Reduced full-complexity (RFC), (c) Full-complexity (FC)

and the benefits offered by multi-antenna systems. An antenna selection system with N antennas and L RF chains, utilizes only L best of the available antennas (by use of a switching network) chosen based on the signal strength at each antenna. The signal from selected antennas is down-converted and fed to the digital signal processor. This reduces the number of RF chains required and hence the system and hardware complexity. Antenna selection systems is often compared with two of its popular counter-parts: (a) *full complexity* (FC) and, (b) *reduced* full complexity (RFC) systems, with the same array size. Fig. 1.1 further illustrates these definitions. Unlike antenna selection, FC and RFC systems employ all of the available antennas, i.e., N and L, respectively. Under independent fading conditions, selection suffers a loss in performance compared to a full complexity system. However, the performance in the presence of mutual coupling is not well established.

A study of receive antenna selection in the presence of mutual coupling has been reported in [111] and [113]. Both the studies offer contradictory results due to differing assumptions about the role of *inactive* elements in determining the system performance. The proposed model in [111] assumes that the inactive elements are transparent to the

rest of the array at all spacings. This assumption may not be valid for compact arrays. The other study [113], [114] models the inactive elements as terminated in the same impedance as the active elements. Although this may not seem like a problem when antennas are separated by large distances, we believe that terminating an inactive element in an impedance with non-zero resistive part will only absorb power and degrade the system performance. Besides, these studies have assumed a simplistic receiver model with spatially-white noise. As mentioned earlier, receiver noise modeling can play a crucial role in determining the system performance.

Traditional antenna selection schemes assume that the inactive elements are left *open-circuited*. While the termination of inactive elements does not matter when the array elements are uncoupled, it is imperative to study the role played by the inactive elements in a compact selection system. One such study that explored this aspect was [120], wherein the impact of an open-circuited antenna placed close to a driven half-wavelength *dipole* antenna was studied numerically. The results show that, for small spacings and practical thickness of these dipoles, the open-circuited inactive elements can not be treated as transparent to the rest of the array.

Inactive elements have long been used to improve performance in some communication applications. For example, Yagi-Uda arrays [112] employ inactive (also called *parasitic*) elements to achieve directivity in the reception of broadcast television. Harrington [52] has shown that it is possible to choose *purely-reactive* loads for the inactive elements of an array in order to steer the radiation pattern over azimuth. Harrington's method involved an exhaustive search for the optimal reactive termination. Vaughan [96] has suggested that, for a circular array of parasitic elements with a single driven element in the center, it is possible to *beamform* the radiation by proper switching of parasites as

open or short.

In this dissertation, we investigate ways in which coupling between the array elements can be exploited to improve the performance of selection systems. The key idea here is to use a different kind of termination that can reflect the power from the inactive elements in order to make more power available to the active antennas.

1.1.2 Coupling and Bandwidth

The other aspect of coupled multi-antenna systems that we study is the impact of mutual coupling on the RF bandwidth of the system, a relatively unexplored territory. As pointed out earlier, some studies have made a passing reference to conjugate matching networks diminishing the RF bandwidth of the system at close spacings [60], [31]. Matching networks built for systems with relatively large bandwidths fall under the purview of *broadband matching theory*. Although a large body of research has addressed the issue of broadband matching for 2-port and *uncoupled* multiport networks (e.g., ideal MIMO systems), relatively little is known about MIMO broadband matching with mutual coupling.

A recent study [50] has derived bounds on the spectral efficiency of an arbitrary antenna array inserted in a sphere, under Rayleigh fading conditions. Each array element is represented by a resonance model and a corresponding antenna *quality factor* while the fundamental limits from the realms of *antenna theory* and broadband matching are used to obtain an estimate of the maximum possible bandwidth of the system. The results are presented in the form of an upper bound on the spectral efficiency in the absence of CSI at the transmitter. However, it does not offer deep insights into the relationship between coupling and its impact on the RF bandwidth of the system. To establish this

dependence, it is imperative to study the design of matching networks for broadband transceivers.

Broadband matching theory was introduced by Bode in 1945 [5], when he addressed the design of a *lumped*, *reciprocal* reactive 2-port network to match an arbitrary *passive*, lumped load to a resistive source. Fano [35] established fundamental *gain-bandwidth* trade-offs on broadband matching of a resistive source to a frequency-dependent load using Darlington's equivalent of a load [27]. Youla [118] introduced an alternative way to solve this problem by use of complex-normalized scattering matrices. Chien [21], [22] further extended this idea to include frequency-dependent sources. Later, Chen [101] extended broadband matching theory to multiport networks. However, unlike our problem, these multiport networks were assumed uncoupled. The text by Chen [16] is an excellent reference for broadband matching theory and implementation techniques. In this work, we investigate the optimal end-to-end design of a broadband MIMO system in the presence of mutual coupling from an information theoretic perspective, while addressing the bandwidth limitations arising from broadband matching theory.

1.2 Overview of Dissertation

This dissertation is organized as follows. In Chapter 2, we develop MIMO channel models and discuss various ways to communicate using multiple antennas at the transmitter and/or receiver. We also introduce a very popular broadband transmission technique known as OFDM which we shall employ to analyze information-theoretic limits on broadband MIMO systems in the presence of mutual coupling. In Chapter 3, we consider an antenna selection system in the presence of mutual coupling and investigate optimal antenna selection strategies for narrowband MIMO systems that seek to exploit coupling

from neighboring antennas. Chapter 4 outlines the fundamentals of broadband matching theory that we use to formulate the problem of matching in broadband systems. We illustrate the information-theoretic approach to optimal broadband matching using a single-antenna, point-to-point communication link. In Chapter 5, we propose an extension of broadband matching theory to coupled multi-antenna systems. In Chapter 6, we formulate the information-theoretic problem of matching and present optimal designs for coupled MIMO-OFDM systems. In Chapter 7, we summarize the main results of this dissertation and suggest topics for future work.

Chapter 2

MIMO for Wireless Communications

In this chapter, we introduce the building blocks of MIMO systems and develop channel and system models for a variety of MIMO communication schemes. This chapter shall serve as a launching pad for the remainder of this dissertation when we develop more generalized system models of compact MIMO transceivers in the presence of mutual coupling.

We begin with a stochastic representation of single-input single-output (SISO) channel models and discuss some of the key physical parameters that characterize a wireless medium followed by the development of a stochastic MIMO channel model. We then present an overview of a variety of MIMO communication schemes based on channel state information at the receiver and/or transmitter. Some of these include eigen-mode transmission, spatial multiplexing, diversity and antenna selection. We then elaborate on broadband channel models useful for analyzing MIMO-OFDM systems and discuss optimal system design and signaling strategies. Lastly, we present some results to demonstrate the impact of fading and its correlation on system performance.

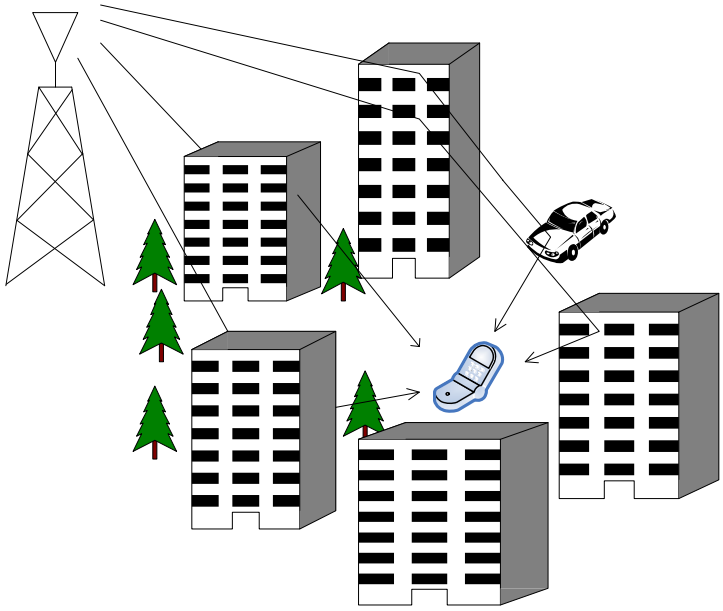

Figure 2.1: Typical wireless signal propagation environment

2.1 SISO Channel Model

Fig. 2.1 shows a typical wireless signal propagation environment. The transmitted signal arrives at the receiver as a superposition of multiple delayed and attenuated copies - known as *multipaths*, corrupted by additive white Gaussian noise (AWGN) at the receiver. If the complex baseband transmitted signal is $s(t)$, the received signal can be represented by

$$r(t) = \sum_i \alpha_i(t) e^{-j2\pi f_c \tau_i(t)} s(t - \tau_i(t)) + n(t) \tag{2.1}$$

where, $\alpha_i(t)$ and $\tau_i(t)$ represent the attenuation and propagation delay associated with the i-th multipath at time t. Here, f_c is the carrier frequency in Hz and $n(t)$ represents AWGN with power spectral density (PSD) $N_0/2$.

A wireless channel is typically characterized by two important time-domain parameters: *delay spread* and *coherence time*. Delay spread (T_m) is a measure of the maximum delay between two (significant) multipath components

$$T_m = \max_{i,j,t} |\tau_i(t) - \tau_j(t)| \ .$$

The reciprocal of delay spread is *coherence bandwidth* (B_c) defined approximately as $B_c \approx 1/T_m$. It is a measure of correlation in the frequency response of the channel. The other channel parameter - coherence time (T_c), captures the time-varying nature of the channel. It is a measure of how correlated in time, various multipath components are. It is usually measured as the reciprocal of *Doppler spread* (D_s) - maximum difference between Doppler shifts $f_c \frac{d\tau_i}{dt}$ of each multipath

$$D_s = f_c \max_{i,j,t} \left| \frac{d}{dt}(\tau_i(t) - \tau_j(t)) \right| \ .$$

Typically, the coherence time of a channel is much larger than its delay spread, i.e., $T_m \ll T_c$. Such channels are sometimes called *underspread* channels.

Since the channel in (2.1) is linear, it can be described by a time-varying response

$$h(\tau, t) = \sum_i \alpha_i(t) e^{-j2\pi f_c \tau_i(t)} \delta(\tau - \tau_i(t))$$

at time t to an impulse transmitted at time $t - \tau$. However, in most part of this study, we shall assume that the transmitter, receiver and the environment are all stationary such that the attenuations and propagation delays are not a function of t. In such a case, we

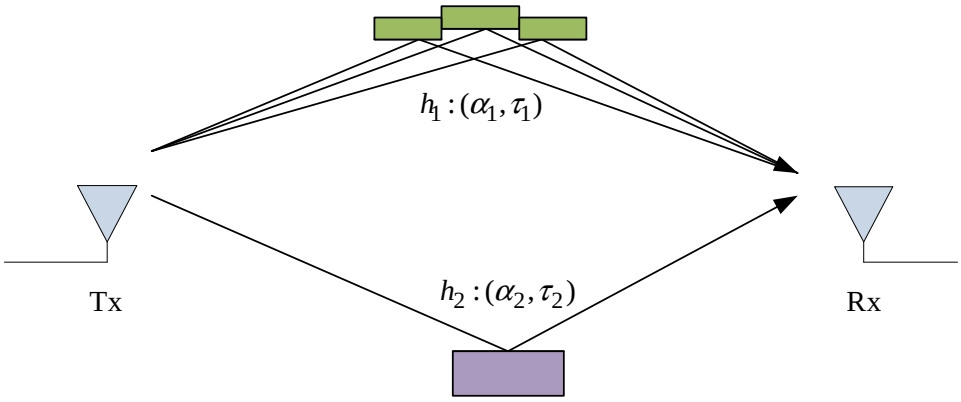

Figure 2.2: Two cluster model for a wireless channel

can model the channel as a linear time-invariant (LTI) system with an impulse response

$$h(\tau) \;=\; \sum_i \alpha_i e^{-j2\pi f_c \tau_i} \delta(\tau - \tau_i) \;,$$

such that

$$r(t) = \int h(\tau) s(t-\tau) d\tau + n(t) \;.$$

For a system with passband bandwidth B (baseband bandwidth $B/2$), the *symbol duration* (T_s) assuming Nyquist's sampling theorem is $T_s = 1/B$, such that the continuous-time channel model can be written in discrete-time as a convolution with N_t-tap *finite impulse response* (FIR) filter [1]

$$r[m] = \sum_{l=0}^{N_t-1} h[l] s[m-l] + n[m] \;. \tag{2.2}$$

A channel with $B \ll B_c$, or equivalently $T_s \gg T_m$ is usually well modeled as a single-tap

[1] The notation $x[m] \triangleq x(mT_s)$.

filter ($N_t = 1$) such that the channel frequency response can be assumed to be fairly constant over the entire bandwidth - hence the name *frequency-flat* channel. For an underspread, frequency flat channel, we can write

$$r[m] = hs[m] + n[m]$$

where

$$h \triangleq \sum_i \alpha_i e^{-j2\pi f_c \tau_i}$$

is called the *fading path gain*. It is modeled as the sum of a number of *unresolvable* multipath components - multipaths with almost equal path delays [93], e.g., cluster 1 in Fig. 2.2.

Without any detailed knowledge of these individual multipaths within a cluster, h is conveniently modeled as a random variable. Assuming a *rich scattering environment* which has a large number of *independent and identically distributed* (i.i.d.) multipaths and no line-of-sight (LOS) component, (using Central Limit theorem) h is modeled as a complex Gaussian random variable with zero mean and variance $\sigma^2 = \sum_i \mathbb{E}[\alpha_i^2]$. The amplitude $|h|$ is thus Rayleigh distributed and phase $\phi = 2\pi f_c \tau$ is well modeled as uniformly distributed over $[0, 2\pi)$. For this reason, such channels are also known as *Rayleigh fading* channels.[2] It is often the case that the channel remains constant over a number of symbols referred to as a *block*. For this reason, such channel models are also called *block fading* channels. The channel is assumed to vary from block to block and completely decorrelate in time with each block or *realization*. When symbols are not

[2]In the presence of a LOS component, the channel is usually modeled as having *Rician fading* distribution.

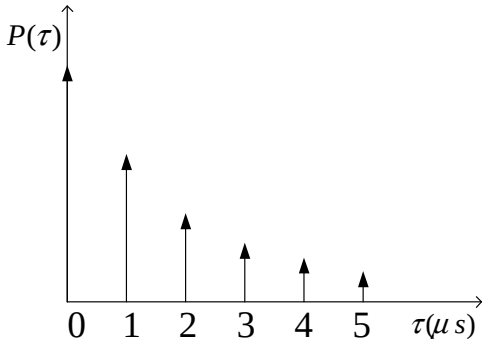

Figure 2.3: Typical wireless power delay profile

coded in time, it is convenient to assume a simplistic model

$$r = hs + n \tag{2.3}$$

by dropping the time-index.

On the other hand, when $B \gg B_c$ multipath clusters are *resolvable* and the channel is called *frequency-selective*. In such a case, the channel is can be modeled as an N_t-tap discrete-time linear filter with coefficients h_l at delays τ_l, $l = 0, \ldots, N_t - 1$. The fading path gains are $h_l \sim \mathcal{CN}(0, \sigma_l^2)$. The strength of each multipath however, usually decays with time, since, the larger the delay, the greater the *path-loss* that the component suffers in propagation. The envelope of multipaths' power vs. the delay is called the *power delay profile* (PDP) and is typically modeled as an exponential decay characteristic. It is a useful tool in analyzing a wireless channel's temporal and spectral characteristics. An example PDP is illustrated in Fig. 2.3.

Based on the relationship between B and B_c discussed above, frequency-flat channels are also referred to as *narrowband* channels and frequency-selective channels as *wideband* or *broadband* channels. Another often-used terms to categorize wireless channels is *fast*

fading and *slow fading*. This is usually associated with whether, for an application, one can transmit coded symbols over multiple fades of the channel (fast fading) or not (slow fading).

2.2 SISO-OFDM

In this section, we provide an overview of orthogonal frequency division multiplexing (OFDM) - a *multi-carrier modulation* technique suitable for broadband communications. For frequency selective channels, *single-carrier* transmission techniques such as code-division-multiple-access (CDMA) and wideband-CDMA currently deployed in IS-95 and UMTS systems, respectively, have been in use for cellular systems for quite some time now. However, OFDM is fast becoming the preferred choice in systems with large delay spreads owing to its ease of channel equalization.

OFDM is currently used in many terrestrial video broadcast systems, DSLs and WLAN systems like 802.11a/Wi-Fi and has been adopted as the air interface for next generation cellular standards like 3GPP LTE and WiMAX. The concept of multi-carrier modulation was originally proposed in 1960s [15], [102]. However, complicated transceiver design and costs, kept it at bay for a long time. With the advent of fast DSP capabilities, OFDM is implemented using Discrete Fourier Transform (DFT) and inverse DFT (IDFT) algorithms. These are readily computed using hardware specially designed for fast Fourier transform (FFT) and inverse FFT (IFFT) algorithms. OFDM offers many distinct advantages over existing single-carrier transmission techniques as we shall see below. In this section, we briefly go over the basics of OFDM and present a SISO-OFDM system model. We shall revisit them as we develop the system model for MIMO-OFDM later in this chapter.

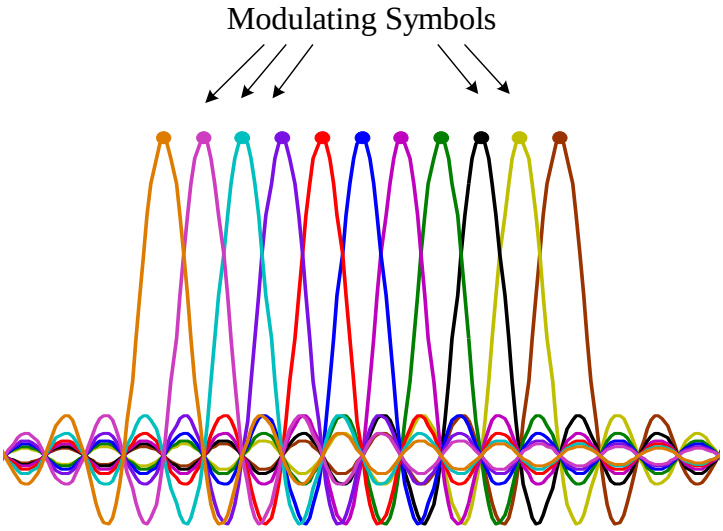

Figure 2.4: *sinc*() pulse shapes for OFDM modulation

OFDM makes it a suitable choice for transmission over channels that exhibit large delay spreads, ($T_s \ll T_m$), or equivalently $B \gg B_c$ such that the channel is essentially broadband. As the name suggests, in OFDM, information symbols are modulated over different frequencies referred to as *orthogonal sub-carriers*. Orthogonality is maintained by use sinc pulse shapes in frequency domain and modulating each sub-carrier at the center, as shown in Fig. 2.4. Given a passband bandwidth B, the number of sub-carriers K is carefully chosen such that the *sub-carrier spacing* (Δf) is small compared to the coherence bandwidth of the channel

$$\Delta f = \frac{B}{K} \ll B_c \ .$$

This ensures that each sub-carrier fades independently of each other and that the fading can be considered frequency-flat within each band.

The complex baseband discrete-time representation of an *OFDM symbol* can be ex-

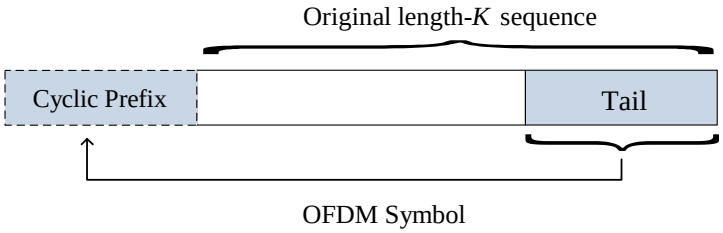

Figure 2.5: Cyclic prefix in OFDM

pressed as

$$s[m] = \frac{1}{\sqrt{K}} \sum_{k=0}^{K-1} \widetilde{s}[k] e^{j2\pi km/K}, \ m = 0, \ldots, K-1$$

where $\widetilde{s}[k]$ is the modulating symbol for the k-th sub-carrier. The time-domain OFDM signal utilizes a special structure which turns a frequency-selective channels into a set of parallel frequency-flat channels. The tail of $s[m]$ comprising N_{cp} symbols, are copied as is and appended to the beginning of the sequence - known as *cyclic prefix* (CP) or *guard interval* (GI) as shown in Fig. 2.5. The resulting sequence $\widehat{s}[m]$ is given by

$$\widehat{s}[m] = \Big[\underbrace{s[K+N_{cp}-2] \ \ldots \ s[K-2] \ s[K-1]}_{\text{cyclic prefix}} \ s[0] \ s[1] \ \ldots \ s[K-1] \Big]$$

The frequency selective channel can be represented by an N_t-tap discrete-time filter $h[m], \ m = 0, \ldots, N_t - 1$, such that the channel output is given by the discrete-time convolution

$$\begin{aligned} r[m] &= h[m] * \widehat{s}[m] + n[m] \\ &= \sum_{l=0}^{N_t-1} h[l] \widehat{s}[m-l] + n[m] \end{aligned}$$

The length of CP ensures zero inter-symbol-interference (ISI) between consecutive OFDM symbols and also renders the otherwise linear convolution with the channel, circulant

$$r[m] = h[m] \circledast s[m] + n[m]$$

From the property of circular convolution, we know that the DFT of the system is a point-by-point multiplication, i.e.,

$$\begin{aligned} \widetilde{r}[k] &= \sum_{m=0}^{K-1} r[m] e^{-j2\pi mk/K} \\ &= \widetilde{h}[k]\widetilde{s}[k] + \widetilde{n}[k] \ , \end{aligned}$$

where the accent tilde denotes a variable's frequency-domain attributes.[3] Henceforth, we shall use a subscript to denote k-th sub-carrier in place of $[k]$

$$\widetilde{r}_k = \widetilde{h}_k \widetilde{s}_k + \widetilde{n}_k \ . \tag{2.4}$$

For this reason, OFDM is known to turn a frequency-selective fading channel into a set of orthogonal frequency-flat fading channels. This provides tremendous savings in equalization at the receiver which is carried out in the frequency-domain[4] with the help of channel estimation techniques using *pilot sub-carriers* - similar to training sequence in a time-domain channel estimation. In the absence of noise and perfect knowledge of channel gains for the k-th sub-carrier, the equation above emphasizes the frequency-domain equalization technique that is one of the biggest advantages of OFDM. The

[3] If x denotes a quantity in time-domain, we shall represent it in frequency-domain by the notation $\widetilde{x}$ in the remainder of this dissertation.

[4] Techniques like CDMA rely on time-domain adaptive equalization which estimates the channel coefficients and requires fast convergence of combiner weights, to estimate the information sequence.

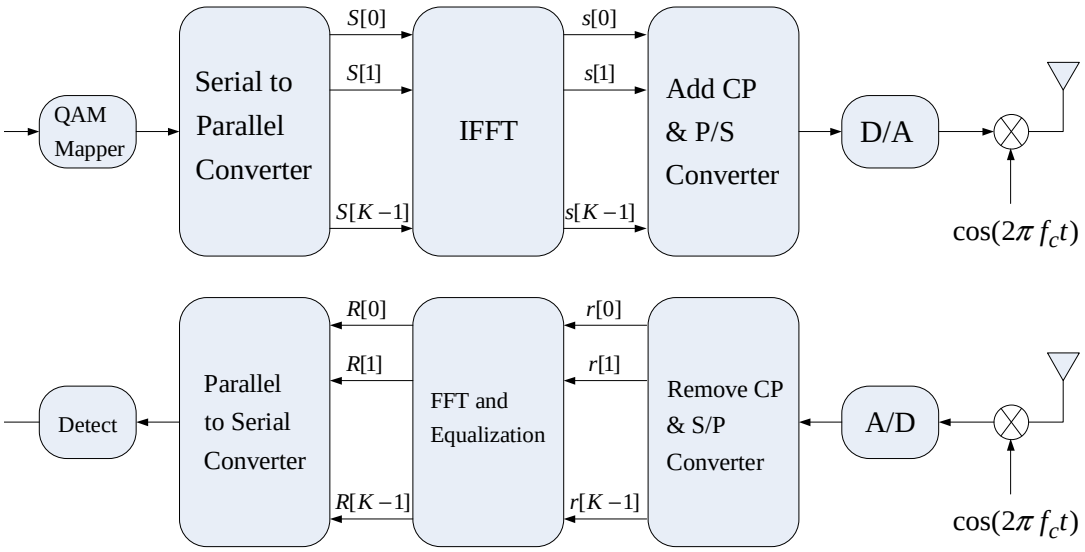

Figure 2.6: OFDM implementation

transmitted symbols are estimated simply as

$$\widetilde{s}_k = \frac{\widetilde{r}_k}{\widetilde{h}_k}$$

The frequency-domain channel for each sub-carrier is related to the channel impulse response by DFT

$$\widetilde{h}[k] = \sum_{m=1}^{K} h[m] e^{-j2\pi km/M} \ , \ k = 0, \ldots, K-1$$

where

$$h[m] = \left\{ \begin{array}{ccc} h[m] & , & 0 < m < N_t - 1 \\ 0 & , & m \geq L \end{array} \right\} .$$

Usually, OFDM is implemented using radix-2 FFT/IFFT techniques, which makes it

convenient to choose the number of sub-carriers to be a power of 2. Fig. 2.6 shows the basic modulation and demodulation techniques used in OFDM.

As can be seen, the overhead due to cyclic prefix in the OFDM symbol results in a loss in capacity but the trade-off over system complexity more than compensates for it. The OFDM symbol, thus spans a duration of $KT_s + T_{cp}$ where $T_{cp} = N_{cp}T_s$ is the duration of cyclic prefix chosen such that $T_{cp} > T_d$ for zero ISI. At the receiver, the first N_{cp} samples are discarded because of ISI from the previous OFDM symbol while the remaining K symbols are directly equalized using the channel estimates for each sub-carrier. For more details about OFDM, the reader is referred to [79].

It is worthwhile to point out another advantage of OFDM (or for that matter, multi-carrier modulation) over single-carrier techniques. It is the ability to adapt the power and bit loading using *adaptive modulation* on each sub-carrier independently. In other words, it provides the ability to achieve a discrete approximation of spectral *water-pouring* strategies. As we shall see later, some of the optimal power allocation schemes we derive shall exhibit a water-pouring characteristic.

2.3 MIMO Channel Model

Next, we consider a channel model for MIMO systems. To begin with, we consider only frequency-flat fading channels, i.e, single tap channels ($N_t = 1$); more generalized frequency-selective MIMO channels will be dealt toward the end of this chapter. Consider a MIMO system with M transmit antennas and N receive antennas as shown in Fig. 2.7. Let $\mathbf{s} = [s_1, s_2, \ldots, s_M]^T \in \mathcal{C}^M$ represent the complex-baseband transmitted symbol vector and $\mathbf{r} = [r_1, r_2, \ldots, r_N]^T \in \mathcal{C}^N$ be the received symbol vector related through

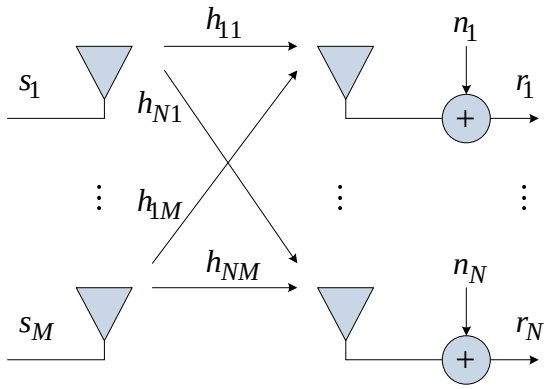

Figure 2.7: MIMO channel model

an $N \times M$ *channel matrix* $\mathbf{H}$ and a receiver noise vector $\mathbf{n} = [n_1, n_2, \ldots, n_N]^T \in \mathcal{C}^N$ by

$$\mathbf{r} = \mathbf{H}\mathbf{s} + \mathbf{n} \ , \tag{2.5}$$

a matrix version of (2.3). The noise vector at the receiver is assumed to be zero-mean, circularly-symmetric, jointly complex-Gaussian (ZMCSCG) in distribution, henceforth denoted as $\mathbf{n} \sim \mathcal{CN}(\mathbf{0}, \mathbf{R_n})$ where, $\mathbf{R_n} = \mathbb{E}[\mathbf{n}\mathbf{n}^H]$ is the noise covariance. For now, we assume that the noise covariance in general is non-diagonal. We shall elaborate on its structure and computation when we address the detailed receiver model used to represent transceivers with mutual coupling. The total transmit power is given by $P_0 = \mathrm{Tr}(\mathbf{R_s})$ where $\mathbf{R_s} = \mathbb{E}[\mathbf{s}\mathbf{s}^H]$ is the *transmit signal covariance.*[5]

[5]Throughout this dissertation, $(\cdot)^*$, $(\cdot)^T$, $(\cdot)^H$, $\mathrm{Tr}(\cdot)$ and $\mathbb{E}[\cdot]$ shall denote conjugation, transposition, conjugate transposition, trace and expectation operator, respectively.

The elements of the MIMO channel matrix specified as

$$\mathbf{H} = \begin{bmatrix} h_{11} & \dots & h_{1M} \\ \vdots & \ddots & \\ h_{N1} & \dots & h_{NM} \end{bmatrix}$$

are also ZMCSCG but are spatially correlated to an extent governed by the physical separation between the elements and scattering environment. In general, the correlation between any two entries of $\mathbf{H}$ is given by a $NM \times NM$ block matrix

$$\mathbf{R_H} = \begin{bmatrix} \mathbb{E}[\mathbf{h}_1\mathbf{h}_1^H] & \dots & \mathbb{E}[\mathbf{h}_1\mathbf{h}_M^H] \\ \vdots & \ddots & \\ \mathbb{E}[\mathbf{h}_M\mathbf{h}_1^H] & \dots & \mathbb{E}[\mathbf{h}_M\mathbf{h}_M^H] \end{bmatrix} \tag{2.6}$$

where $\mathbf{h}_i$ denotes the i-th column of $\mathbf{H}$. We denote this by $\mathbf{H} \sim \mathcal{CN}(\mathbf{0}, \mathbf{R_H})$. Alternatively, $\mathbf{R_H} = \mathbb{E}[\text{vec}(\mathbf{H})\text{vec}(\mathbf{H})^H]$, where vec($\mathbf{H}$) represents the vector obtained by stacking the columns of $\mathbf{H}$.

In MIMO literature, this correlation is often assumed to exhibit the *separable correlation model* behavior [58]. This is particularly true of scenarios when the transmit correlation from two transmit antennas is independent of the receive antenna from which it is observed (and vice-versa for receive correlation). In such a situation, the full correlation matrix can be written as a Kronecker product (denoted by $\otimes$)

$$\mathbf{R_H} = \mathbf{R}_T^T \otimes \mathbf{R}_R$$

where, $\mathbf{R}_T = (1/M)\mathbb{E}[\mathbf{H}^H\mathbf{H}]$ and $\mathbf{R}_R = (1/N)\mathbb{E}[\mathbf{H}\mathbf{H}^H]$ are positive-definite Hermitian *transmit* and *receive spatial-correlation* matrices, respectively. For this reason, this model is also known as *Kronecker correlation model*. The MIMO channel matrix can thus be simplified into a product of known spatial correlation matrices and an $N \times M$ *white* stochastic channel matrix $\mathbf{H}_w$

$$\mathbf{H} = \mathbf{R}_R^{1/2}\mathbf{H}_w\mathbf{R}_T^{1/2} \ ,$$

where $\mathbf{H}_w \sim \mathcal{CN}(\mathbf{0}, \mathbf{I})$ and $\mathbf{I}$ is the $N \times N$ identity matrix. Alternate models for MIMO channels have been proposed in [84].

The extent to which the signals incident on two antennas are correlated is not only a function of the separation between them but also how dense the scattering environment is. For example, a base-station in a cellular network is located at a greater height and has less scatterers/reflectors in the vicinity. A cell-phone on the other hand, is usually surrounded by many objects outdoors or indoors. For this reason, antenna separation required to ensure least signal correlation is lower in cell-phones or portable devices, typically a few wavelengths, while that at the base-station is tens of wavelengths. For simplicity, we shall throughout this study, assume that transmit antennas have a separation large enough so that the signals are perfectly uncorrelated, i.e., $\mathbf{R}_T = \mathbf{I}$ such that

$$\mathbf{H} = \mathbf{R}_R^{1/2}\mathbf{H}_w \ .$$

For a uniform linear array (ULA) with spacing d, the correlation matrix is [25]

$$[\mathbf{R}_R]_{nm} = \int_0^{2\pi}\int_0^{\pi} g_n(\theta,\phi)g_m^*(\theta,\phi)e^{j2\pi d(n-m)\sin\theta\cos\phi/\lambda}p(\theta,\phi)\sin\theta d\theta d\phi \ , \tag{2.7}$$

where $g_n(\theta,\phi)$ is the antenna pattern of dipole n, $p(\theta,\phi)$ is the angular density of mul-

tipaths arriving from (θ, ϕ), λ is the wavelength. When multipaths are uniformly distributed in the plane $p(\theta, \phi) = \frac{1}{2\pi}\delta\left(\theta - \frac{\pi}{2}\right)$ and scattering is neglected so each dipole is omni-directional $g_n(\frac{\pi}{2}, \phi) = 1$, (2.7) reduces to Clarke's [25] formula

$$[\mathbf{R}_R]_{nm} = J_0\left(2\pi\tfrac{d}{\lambda}(m-n)\right) \tag{2.8}$$

where J_0 is the zeroth-order Bessel of first kind.

2.4 Multi-Antenna Communication Schemes

In this section, we briefly discuss some of the popular communication schemes that utilize multiple antennas at the transmitter and/or receiver. We also present some of the relevant metrics to measure the system performance for MIMO systems. Although we address narrowband systems here, an extension to broadband MIMO systems is provided in the next section. Throughout this dissertation, we shall assume that perfect estimates of the channel are available at the receiver at all times, also referred to as channel state information (CSI). [65] highlights the aspects and methods of MIMO channel estimation through training sequences.

Capacity is a measure of maximum data rates that can be transmitted reliably with arbitrarily small probability of error. Based on the knowledge, and slow or fast fading nature of the channel, it is typically expressed in three forms - instantaneous or Shannon capacity, *ergodic* capacity and *outage* capacity. The Shannon capacity is a useful metric to evaluate limits on systems when the channel is constant or known *apriori*. Telatar

derived the Shannon capacity of a MIMO system in AWGN channel [90]

$$C_{awgn} = \max_{\mathrm{Tr}(\mathbf{R_s}) \leq P_0} \log_2 \det \left(\mathbf{I} + \frac{1}{MN_0} \mathbf{H} \mathbf{R_s} \mathbf{H}^H \right) \tag{2.9}$$

where $\det(\cdot)$ denotes the determinant. In cases where the noise is spatially correlated, we have

$$C = \max_{\mathrm{Tr}(\mathbf{R_s}) \leq P_0} \log_2 \det \left(\mathbf{I} + \frac{1}{M} \mathbf{R_n}^{-1} \mathbf{H} \mathbf{R_s} \mathbf{H}^H \right) \tag{2.10}$$

For a fast fading channel, however, it is appropriate to talk about the capacity in a statistical mean or *ergodic* sense, expressed as

$$C_{erg} = \max_{\mathrm{Tr}(\mathbf{R_s}) \leq P_0} \mathbb{E} \left[\log_2 \det \left(\mathbf{I} + \frac{1}{M} \mathbf{R_n}^{-1} \mathbf{H} \mathbf{R_s} \mathbf{H}^H \right) \right] \ . \tag{2.11}$$

In the absence of channel state information (CSI) at the transmitter, the optimal transmission strategy for (2.11) is equal power allocation across the transmit antennas [90]

$$\mathbf{R_s} = \frac{P_0}{M} \mathbf{I}$$

and the capacity achieving transmit vectors have complex normal distribution.

On the other hand, for slow fading channels, a more accurate metric is *outage* capacity. Outage analysis quantifies the level of capacity that is guaranteed with a certain level of reliability. It is the probability that the capacity falls below a certain threshold or goes into an outage

$$\Pr(C \leq C_{out,q\%}) = q\% \ .$$

For example, 1% outage capacity means the information rate $C_{out,1\%}$ is gauranteed for 99% of the channel realizations.

2.4.1 Eigen-Mode Transmission

In certain scenarios, it is possible that complete CSI is available at the transmitter. This information could either be delivered to the transmitter by the receiver through feedback or estimated at the transmitter through reciprocity arguments when the channel on the *forward link* (or downlink) is same as the one on *reverse link* (or uplink). For example, time division duplexing (TDD) systems use the same set of frequency bands for communication in either link which makes it possible to relay the CSI to the transmitter as control information through feedback.

When perfect CSI is available at the transmitter, it is possible to decompose the MIMO channel into $r = \min(M, N)$ orthogonal spatial modes with the help of appropriate *transmit precoding* and *receive decoding*. To observe that, consider the *singular value decomposition* (SVD) of the channel matrix

$$\mathbf{H} = \mathbf{U}\mathbf{\Sigma}\mathbf{V}^H$$

where, $\mathbf{U} \in \mathcal{C}^{N\times N}$ and $\mathbf{V} \in \mathcal{C}^{M\times M}$ are unitary matrices representing the left-hand and right-hand singular vectors of $\mathbf{H}$, respectively and $\mathbf{\Sigma}$ is a rectangular matrix whose diagonal elements are non-negative real numbers and off-diagonal elements are zero. The diagonal elements $\sigma_1 \geq \sigma_2 \geq \ldots \geq \sigma_r$ are the ordered singular values of $\mathbf{H}$, where $r = min(M, N)$. The squared singular values are the *eigen-values* of $\mathbf{H}\mathbf{H}^H$:

$$\sigma_i^2(\mathbf{H}) = \lambda_i(\mathbf{H}\mathbf{H}^H)$$

Incorporating the SVD into the system model (2.5), we get

$$\mathbf{r}' \;=\; \mathbf{\Sigma}\mathbf{s}' + \mathbf{n}'$$

where, $\mathbf{r}' = \mathbf{U}^H\mathbf{r}$, $\mathbf{s}' = \mathbf{V}^H\mathbf{s}$ and $\mathbf{n}' = \mathbf{U}^H\mathbf{n}$ represent equivalent vectors after a *unitary linear transformation* that preserves the energy of signals since $\|\mathbf{s}'\|^2 = \|\mathbf{s}\|^2$ and the distribution of noise $\mathbf{n}' \sim \mathcal{CN}(\mathbf{0}, \mathbf{R_n})$. The last equation represents a set of parallel non-interfering or *orthogonal* channels

$$r'_i = \sigma_i s'_i + n'_i \ .$$

The Shannon capacity can be represented as

$$\begin{aligned} C_{awgn} &= \max_{\mathrm{Tr}(\mathbf{R_s}) \le P_0} \log_2 \det\left(\mathbf{I} + \frac{1}{MN_0}\mathbf{U}\mathbf{\Sigma}\mathbf{V}^H\mathbf{R_s}\mathbf{V}\mathbf{\Sigma}\mathbf{U}^H\right) \\ &= \max_{\sum_i \gamma_i \le P_0} \sum_{i=1}^{r} \log_2\left(1 + \frac{1}{MN_0}\lambda_i(\mathbf{H}\mathbf{H}^H)\gamma_i\right) \end{aligned}$$

where $\gamma_i = \mathbb{E}[|s'_i|^2]$ represents the power allocated to i-th eigen-mode. The optimal power allocation is given by a spatial *water-pouring* solution [26], [62], [23]

$$\gamma_i = \left[F - \frac{MN_0}{\lambda_i(\mathbf{H}\mathbf{H}^H)}\right]^+$$

where, $[x]^+ = \max\{x, 0\}$ and F is the water-level governed by the total power constraint

$$\sum_{i=1}^{r} \gamma_i \le P_0 \ .$$

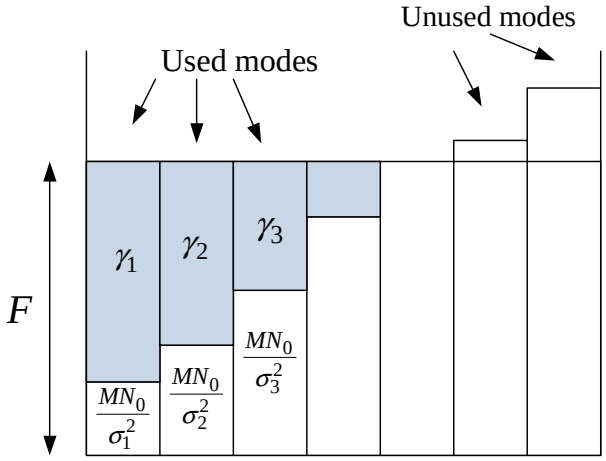

Figure 2.8: Water-pouring schematic

An illustration of this solution is depicted in Fig. 2.8. The optimal signal covariance can be computed using

$$\mathbf{R_s} = \mathbf{V} \begin{bmatrix} \gamma_1 & & \\ & \ddots & \\ & & \gamma_r \end{bmatrix} \mathbf{V}^H \ .$$

2.4.2 Spatial Multiplexing

There are space-time architectures which do not require CSI at the transmitter. Spatial multiplexing (SM) is one such scheme that is based on the principle of parallel transmission of information symbols or *streams* of data through multiple transmit antennas over the same bandwidth. The data rate becomes M-fold and detection at the receiver with $(N > M)$ antennas, relies on sophisticated signal processing techniques that try to cancel the interference from other streams while decoding an individual stream. Some of the popular linear equalizers include zero forcing (ZF) and minimum mean square

error (MMSE), while successive interference cancellation (SIC) is a popular non-linear equalizer. The power allocation strategy (in the absence of CSIT) is uniform across space

$$\mathbf{R_s} = \frac{P_0}{M}\mathbf{I} \ .$$

This idea was originally proposed by Paulraj and Kailath in 1993 and a working model was demonstrated at Bell Laboratories as V-BLAST [110].

2.4.3 Transmit and Receive Diversity

It is not necessary that a MIMO system be equipped with multiple antennas at both the ends of the communication link. A MIMO system with a single transmit antenna and N receive antennas is referred to as a *N-receive diversity* system. An $M \times 1$ MIMO system is called a *transmit diversity* system. Here, we present a receive diversity system and a metric suitable for performance evaluation. The system model of a $1 \times N$ narrowband MIMO system can be written as

$$\mathbf{r} = \mathbf{hs} + \mathbf{n}$$

where the lower-case $\mathbf{h}$ denotes the *channel vector*. With perfect estimates of the channel at the receiver, one of the most widely used linear combining technique is such that the input $\mathbf{r}$ to the combiner is linearly weighted $\mathbf{w}$ as

$$y = \mathbf{w}^H\mathbf{r} = \widehat{h}s + \widehat{n} \ .$$

The optimal weight vector that maximizes the post-processing signal-to-noise ratio (SNR)

$$\gamma = \frac{|\widehat{h}|^2}{\mathbb{E}[|\widehat{n}|^2]} = \mathcal{E}\frac{|\mathbf{w}^H\mathbf{h}|^2}{\mathbf{w}^H\mathbf{\Sigma_n}\mathbf{w}} \ .$$

is given by $\mathbf{w} = \mathbf{R_n}^{-\frac{1}{2}}\mathbf{h}$ where $\mathcal{E} = \mathbb{E}[|s|^2]$. This technique is commonly referred to as *noise-whitening* with *matched filter* or *maximal-ratio-combining* (MRC). Using Kronecker model, we can characterize the channel vector along with the receive spatial correlation

$$\mathbf{h} = \mathbf{R}_R^{1/2}\mathbf{h}_w$$

where $\mathbf{h}_w$ is the $N \times 1$ i.i.d. fading path-gain vector $\mathbf{h}_w \sim \mathcal{CN}(\mathbf{0}, \mathbf{I})$.

2.4.4 Antenna Selection

As outlined in Chapter 1, antenna selection offers a cost- and power-efficient way to realize the benefits of a multi-antenna system. In this section, we provide the system model for a simple receive antenna selection system and evaluate the performance for a variety of configurations toward the end of this chapter.

Consider a receiver with N receive antennas and L RF chains. The array is followed by a noiseless switching network that selects L out of N "active" antennas to connect to the L receiver RF chains. The remaining $\bar{L} = N - L$ "inactive" antennas are left unattended. Let $\mathcal{S} = \{s_1, \ldots, s_L\}$ denote the indices of the L active antennas, and let $\bar{\mathcal{S}} = \{\bar{s}_1, \ldots, \bar{s}_{N-L}\}$ be the corresponding indices of the $\bar{L}_c$ inactive antennas. The received signal can be expressed as

$$\mathbf{r} = \mathbf{I}_{\mathcal{S}}\mathbf{h}s + \mathbf{n}$$

where $\mathbf{I}_{\mathcal{S}}$ is the $|\mathcal{S}| \times N$ selection matrix defined by

$$[\mathbf{I}_{\mathcal{S}}]_{ij} = \left\{ \begin{array}{ll} 1, & \text{if } j = s_i \\ 0, & \text{otherwise} \end{array} \right\} , \tag{2.12}$$

$|\mathcal{S}| = L$ is the cardinality of $\mathcal{S}$ and $\mathbf{h}_{\mathcal{S}} = \mathbf{I}_{\mathcal{S}}\mathbf{h}$. The receiver employs a linear combiner similar to a diversity system. The optimal MRC is given by $\mathbf{w} = \mathbf{R}_{\mathbf{n}}^{-\frac{1}{2}}\mathbf{h}_{\mathcal{S}}$ such that the optimal SNR for the antenna selection system is given by

$$\gamma^o \;\; = \;\; \mathcal{E} \max_{\mathbf{I}_{\mathcal{S}}} \|\mathbf{R}_{\mathbf{n}}^{-\frac{1}{2}}\mathbf{h}_{\mathcal{S}}\|^2 \tag{2.13}$$

The optimal subset $\mathcal{S}$ is the one that maximizes 2.13. We assume a block fading channel such that the optimal subset is computed once every block.

2.5 MIMO-OFDM

In the previous sections, we discussed MIMO channel model for narrowband systems and the broadband transmission technique - OFDM, separately. In this section, we provide insights into MIMO channel models for frequency-selective channels and develop the system model for broadband MIMO communications in conjunction with MIMO-OFDM.

Consider a MIMO-OFDM system[6] with M transmit, N receive antennas and K subcarriers spanning a passband bandwidth B. First, we develop the wideband MIMO channel model by reusing some of the concepts developed in the SISO channel model section. Like wideband SISO channels, each entry of the MIMO channel matrix is essentially a multi-tap channel. Wideband MIMO channels can thus be modeled as a *tensor*

[6]We shall use the term broadband and OFDM interchangeably.

such that the channel impulse response's l-th tap is given by a $N \times M$ matrix

$$\mathbf{H}_l = \begin{bmatrix} h_{11}[l] & \dots & h_{1M}[l] \\ \vdots & \ddots & \\ h_{N1}[l] & \dots & h_{NM}[l] \end{bmatrix}, \; l = 0, \dots, N_t - 1$$

where the entries of $\mathbf{H}_l$ are ZMCSCG - $\mathbf{H}_l \sim \mathcal{CN}(\mathbf{0}, \mathbf{R_H})$. Here, we assume that the time-invariant propagation environment is such that rich scattering near the transmitter and receiver ensures same transmit and receive spatial correlation for each multipath index [7]. The MIMO channel matrix for l-th multipath can thus, similarly be specified using the Kronecker model as

$$\mathbf{H}_l = \mathbf{R}_R^{1/2} \mathbf{H}_{wl} \mathbf{R}_T^{1/2} \; .$$

Here, $\mathbf{H}_{wl}$ represents the stochastic $N \times M$ white channel matrix having i.i.d. complex Gaussian entries $\mathbf{H}_{wl} \sim \mathcal{CN}(\mathbf{0}, \mathbf{I})$.

Like SISO channel models, the underlying complex baseband channel impulse response between r-th receive and t-th transmit antenna can easily be modeled by N_t significant multipaths as

$$h_{rt}(\tau) = \sum_{l=0}^{N_t - 1} \alpha_{rt}[l] e^{-j2\pi f_c \tau_{rt}[l]} \delta(\tau - \tau_{rt}[l])$$

where $\alpha_{rt}[l]$ is the attenuation and $\tau_{rt}[l]$ is the propagation delay associated with l-th multipath. It can be easily shown that the use of OFDM with a cyclic prefix (CP) converts a frequency selective MIMO channel into a set of parallel frequency flat MIMO

channels [76]. The frequency response of each MIMO link pair (r,t) at various sub-carriers is computed using a K-point FFT ($K \geq L$) of the MIMO channel impulse response as

$$\widetilde{h}_{rt}[k] = \sum_{n=1}^{K} h_{rt}[n] e^{-j2\pi kn/M} \ , \ k = 0, \ldots, K-1$$

where

$$h_{rt}[n] = \left\{ \begin{array}{ccc} h_{rt}[n] & , & 0 < n < N_t - 1 \\ 0 & , & n \geq N_t \end{array} \right\} .$$

The MIMO-OFDM channel matrix for the k-th sub-carrier is thus given by

$$\widetilde{\mathbf{H}}_k \ = \ \left[\begin{array}{ccc} \widetilde{h}_{11}[k] & \ldots & \widetilde{h}_{1M}[k] \\ \vdots & \ddots & \\ \widetilde{h}_{N1}[k] & \ldots & \widetilde{h}_{NM}[k] \end{array} \right] \ , \ k = 0, \ldots, K-1 \tag{2.14}$$

An alternative representation of a MIMO-OFDM system with K sub-carriers, is an extension of (2.4) such that the model is expressed in frequency-domain as

$$\widetilde{\mathbf{r}}_k = \widetilde{\mathbf{H}}_k \widetilde{\mathbf{s}}_k + \widetilde{\mathbf{n}}_k \ , \quad k = 1, \ldots, K \tag{2.15}$$

where, $\widetilde{\mathbf{s}}_k$ is the $M \times 1$ transmitted symbol vector on the k-th sub-carrier, $\widetilde{\mathbf{r}}_k$ is the $N \times 1$ received symbol vector and $\widetilde{\mathbf{n}}_k$ is the $N \times 1$ additive white Gaussian noise (AWGN) vector at the receiver with zero mean and covariance $\mathbf{R}_{\widetilde{\mathbf{n}}_k} = \mathbb{E}[\widetilde{\mathbf{n}}_k \widetilde{\mathbf{n}}_k^H]$, denoted by $\widetilde{\mathbf{n}}_k \sim \mathcal{CN}(\mathbf{0}, \mathbf{R}_{\widetilde{\mathbf{n}}_k})$. Observe that the equation above represents a set of K orthogonal flat-fading MIMO systems where the notation $\widetilde{\mathbf{H}}_k$ emphasizes the frequency-domain nature of the model.

Owing to this orthogonal decomposition of the frequency selective channel, the cumulative MIMO-OFDM system can be represented in matrix notation by

$$\boldsymbol{r} = \boldsymbol{\mathcal{H}}\boldsymbol{s} + \boldsymbol{n} \tag{2.16}$$

where, $\boldsymbol{\mathcal{H}}$ is a $KN \times KM$ block diagonal matrix given by

$$\boldsymbol{\mathcal{H}} = \begin{bmatrix} \widetilde{\mathbf{H}}_1 & & \\ & \ddots & \\ & & \widetilde{\mathbf{H}}_K \end{bmatrix} \tag{2.17}$$

and the corresponding vectors by

$$\boldsymbol{r} = \begin{bmatrix} \widetilde{\mathbf{r}}_1 \\ \vdots \\ \widetilde{\mathbf{r}}_K \end{bmatrix}, \ \boldsymbol{s} = \begin{bmatrix} \widetilde{\mathbf{s}}_1 \\ \vdots \\ \widetilde{\mathbf{s}}_K \end{bmatrix}, \ \boldsymbol{n} = \begin{bmatrix} \widetilde{\mathbf{n}}_1 \\ \vdots \\ \widetilde{\mathbf{n}}_K \end{bmatrix}. \tag{2.18}$$

The Shannon capacity in bits/sec per Hz or *spectral efficiency* of the system is a simple extension of the narrowband MIMO Shannon capacity (cf. 2.10)

$$C = \frac{1}{K} \max_{\mathrm{Tr}(\boldsymbol{\mathcal{R}}_{\boldsymbol{s}}) \leq KP_0} \left\{ \log_2 \det \left(\boldsymbol{I} + \frac{1}{N} \boldsymbol{\mathcal{R}}_{\boldsymbol{n}}^{-1} \boldsymbol{\mathcal{H}} \boldsymbol{\mathcal{R}}_{\boldsymbol{s}} \boldsymbol{\mathcal{H}}^H \right) \right\} \tag{2.19}$$

where $\boldsymbol{I}$ is an $NK \times NK$ identity matrix, $\boldsymbol{\mathcal{R}_s}$ represents the transmit signal covariance

$$\begin{aligned} \boldsymbol{\mathcal{R}_s} &= \mathbb{E}[\boldsymbol{s}\boldsymbol{s}^H] \\ &= \begin{bmatrix} \mathbb{E}[\widetilde{\mathbf{s}}_1\widetilde{\mathbf{s}}_1^H] & \dots & \mathbb{E}[\widetilde{\mathbf{s}}_1\widetilde{\mathbf{s}}_K^H] \\ \vdots & \ddots & \\ \mathbb{E}[\widetilde{\mathbf{s}}_K\widetilde{\mathbf{s}}_1^H] & \dots & \mathbb{E}[\widetilde{\mathbf{s}}_K\widetilde{\mathbf{s}}_K^H] \end{bmatrix} \end{aligned} \tag{2.20}$$

and $\boldsymbol{\mathcal{R}_n}$ the noise covariance

$$\begin{aligned} \boldsymbol{\mathcal{R}_n} &= \mathbb{E}[\boldsymbol{n}\boldsymbol{n}^H] \\ &= \begin{bmatrix} \mathbb{E}[\widetilde{\mathbf{n}}_1\widetilde{\mathbf{n}}_1^H] & \dots & \mathbb{E}[\widetilde{\mathbf{n}}_1\widetilde{\mathbf{n}}_K^H] \\ \vdots & \ddots & \\ \mathbb{E}[\widetilde{\mathbf{n}}_K\widetilde{\mathbf{n}}_1^H] & \dots & \mathbb{E}[\widetilde{\mathbf{n}}_K\widetilde{\mathbf{n}}_K^H] \end{bmatrix} . \end{aligned} \tag{2.21}$$

For spatially- and spectrally-uncorrelated noise with variance N_0, $\boldsymbol{\mathcal{R}_n} = N_0\boldsymbol{I}$. By employing the SVD of the MIMO-OFDM channel matrix $\boldsymbol{\mathcal{H}}$, (2.19) can be decomposed into $r(\boldsymbol{\mathcal{H}})$ *space-frequency modes* such that the capacity can be rewritten as

$$C = \frac{1}{K} \max_{\sum_{i=1}^{r(\boldsymbol{\mathcal{H}})} \gamma_i = KP_0} \left\{ \sum_{i=1}^{r(\boldsymbol{\mathcal{H}})} \log_2 \left(1 + \frac{\gamma_i}{MN_0} \lambda_i(\boldsymbol{\mathcal{H}}\boldsymbol{\mathcal{H}}^H) \right) \right\} .$$

Here, $r(\mathbf{A})$ denotes the rank of matrix $\mathbf{A}$. The optimal power allocation is *space-frequency water-pouring* [80]

$$\gamma_i = \left[F - \frac{MN_0}{\lambda_i(\boldsymbol{\mathcal{H}}\boldsymbol{\mathcal{H}}^H)} \right]^+$$

Table 2.1: MIMO-OFDM system parameters

Parameter	Relation	Value
Bandwidth (B)		20 MHz
Relative bandwidth (B_r)	B/f_c	6.67%
Channel taps (N_t)		15
Power delay profile (P_d)	$\exp(-nT_s/T_d)$	
Symbol rate (T_s)	$1/B$	50 ns
Max. delay spread (T_m)		0.8 μs
Coherence bandwidth (B_c)	$1/T_m$	1.25 MHz
Max. Doppler (B_D)		25 KHz
Coherence time (T_c)	$1/B_D$ ($\approx 10T_O$)	40 μs
OFDM symbol duration (T_O)	$KT_s + N_{cp}$ ($\approx 5T_m$)	4 μs
Sub-carriers (K)		64
Cyclic prefix length (T_{cp})	$16T_s$	0.8 μs
Carrier spacing (Δf)	B/K	312.5 KHz

where F is governed by the total power constraint

$$\sum_{i=1}^{r(\boldsymbol{\mathcal{H}})} \gamma_i = KP_0 \ .$$

Example: Let us consider an example MIMO-OFDM system with $M = 2$ transmit antennas and $N = 2$ receive antennas. The OFDM system parameters are taken from IEEE 802.11a WLAN standard and listed in Table 2.1. Fig. 2.9 shows the frequency response for a 2×2 MIMO system for $K = 64$ OFDM sub-carriers spread over a bandwidth $B = 20$ MHz, with each MIMO link represented by $N_t = 15$ taps. The transmit antennas are assumed to be spaced sufficiently far apart, while the spacing at the receiver is $d = 0.25\lambda$. The spatial correlation matrix $\mathbf{R}_R$ at the receiver is calculated using Clarke's model, as highlighted in (2.8). A close observation reveals that the link-pairs $(1,1),(2,1)$ and $(1,2),(2,2)$ are correlated. We shall revisit MIMO-OFDM systems in Chapter 6 to

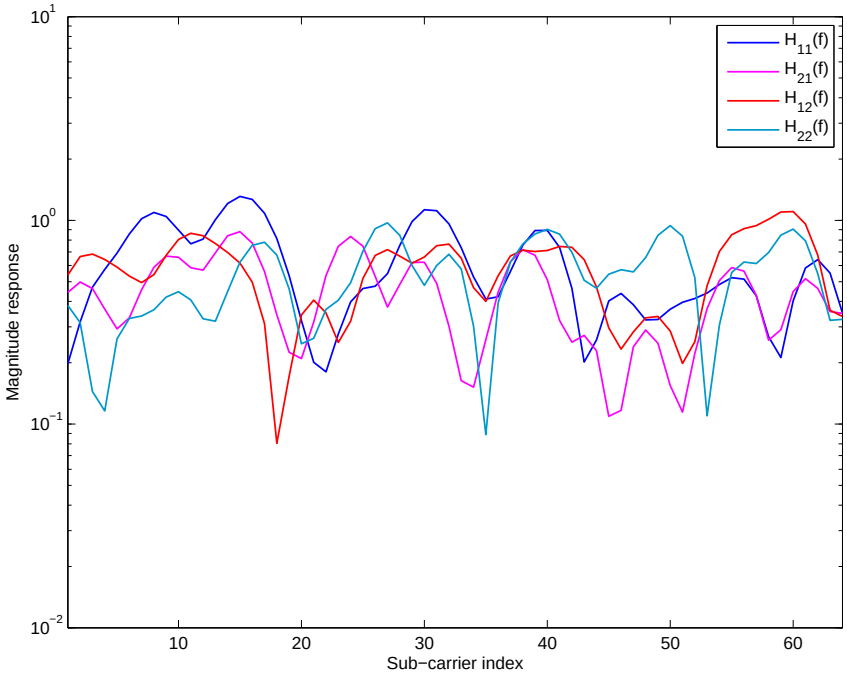

Figure 2.9: Frequency selective MIMO channel, $N = 2$, $d = 0.25\lambda$, $N_t = 15$

address mutual coupling effects on the system model and derive information theoretic limits.

2.6 Performance in Correlated Rayleigh Fading

We conclude this chapter by presenting some results on diversity and antenna selection schemes discussed in previous sections.

2.6.1 Diversity

We consider the outage SNR probability for a N receive diversity system with i.i.d. fading and noise with variance N_0 for different values of N. We consider the performance

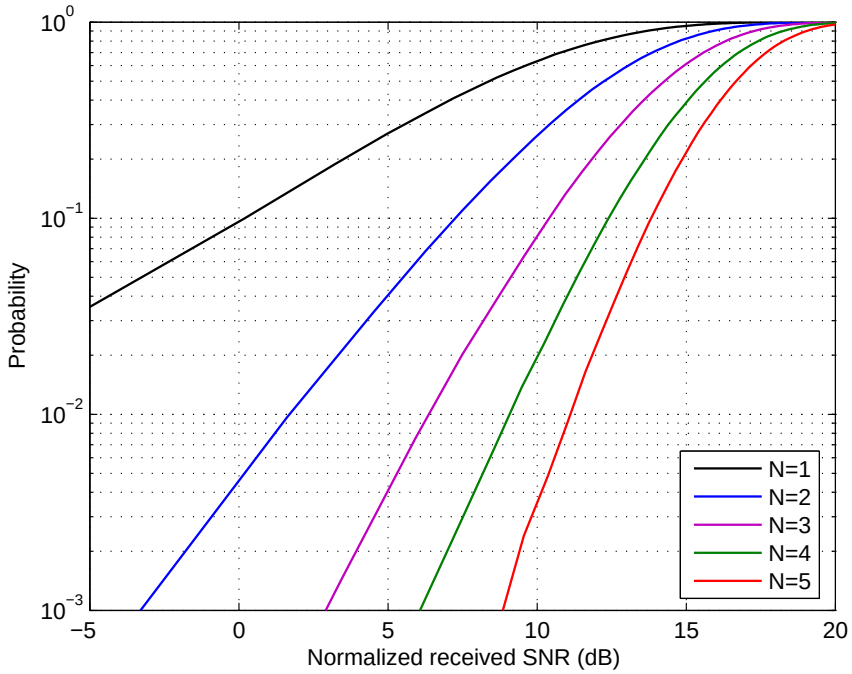

Figure 2.10: Performance of receive diversity in i.i.d. MIMO channels

of diversity systems with i.i.d. fading and noise with variance N_0. The SNR $\mathcal{E}/N_0$ is selected to be 10 dB. Monte-Carlo simulations are carried out for $50,000$ channel realizations. Fig. 2.10 shows the performance - on the x-axis, we have the received SNR and y-axis shows the probability that optimal SNR goes into an outage. For a given outage probability, the difference in received SNR compared to a single antenna system is described as the *diversity gain* of the system. Observe the huge diversity gains offered by diversity receivers as we increase the number of receive antennas. For example, at a 1% outage, $N = 2$ yields a gain of 14 dB while 19 for $N = 3$, 22 for $N = 4$ and 24 dB for $N = 5$. The gains however, become diminishing with each additional element.

In the presence of correlated fading, diversity suffers a loss in performance depending on the extent of correlation denoted by coefficient ρ_{ij} between the (i, j) element pair. To

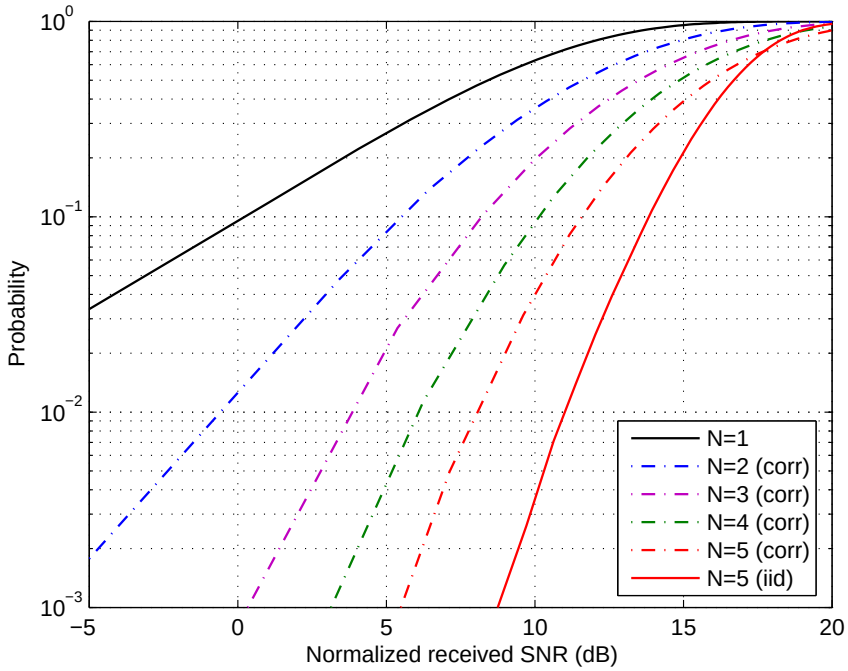

Figure 2.11: Performance of receive diversity in correlated MIMO channels

illustrate the effects of correlation, we assume an exponential correlation model:

$$\rho_{ij} = \left\{ \begin{array}{ll} e^{-\beta|i-j|}\ , & i \neq j \\ 1\ , & i = j \end{array} \right\}$$

where $\beta > 0$. Fig. 2.11 shows the impact of fading correlation for the same set of systems considered above for i.i.d. scenarios. For high degree of correlation, the loss in SNR is noticeable, e.g., 5 dB and 3 dB with $\beta = 0.2$ for $N = 2$ and $N = 3$, respectively.

2.6.2 Antenna Selection

We now analyze the performance of antenna selection with i.i.d. fading and noise with variance N_0 for (N, L) configurations, where N is the number of antennas and L the

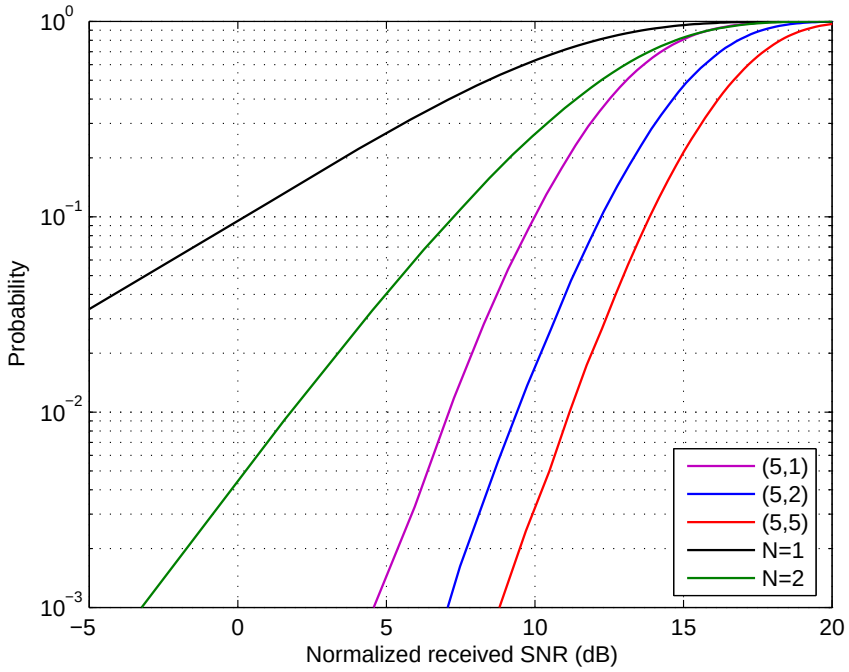

Figure 2.12: Performance of antenna selection in i.i.d. MIMO channels

number of RF chains. The SNR $\mathcal{E}/N_0$ is selected to be 10 dB. Fig. 2.12 shows the remarkable performance improvement offered by antenna selection systems with a single RF chain compared to SISO systems. The gains, however, diminish with increasing number of RF chains. Also notice, how close the $(5, 1)$ system comes to a full complexity system $(5, 5)$. The impact of fading correlation for the same correlation values, as in diversity, is shown in Fig. 2.13. Observe the little impact correlation has on antenna selection compared to diversity systems. This is because of the additional degree of freedom that selection offers over diversity, that is the ability to choose the optimal subset of active antennas. Intuitively, the active subset in correlated fading happens to be such that antennas with least signal correlation (roughly, in other words, large physical separation) are statistically more active than i.i.d. scenarios.

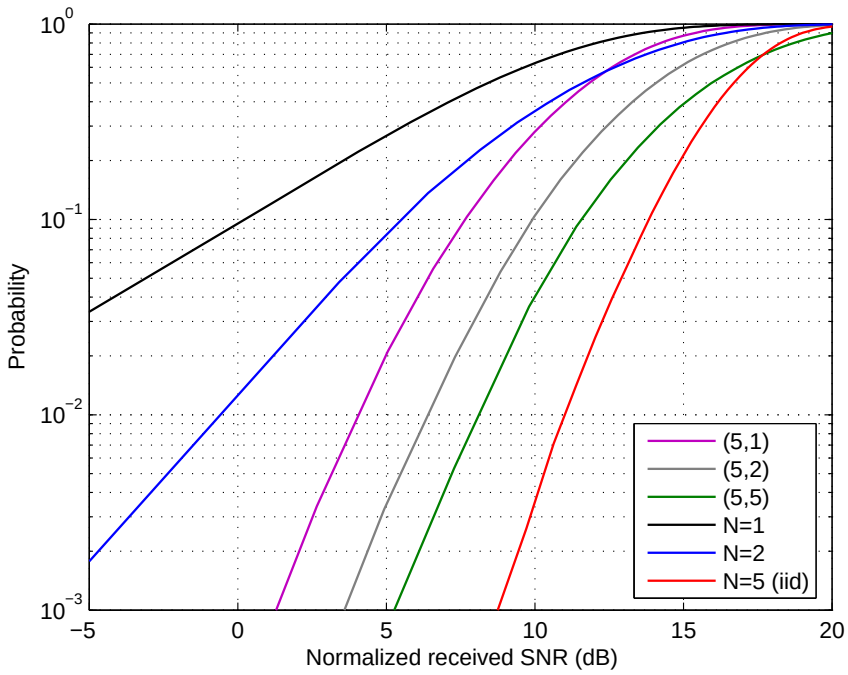

Figure 2.13: Performance of antenna selection in correlated MIMO channels

Chapter 3

Antenna Selection for Compact Arrays

In the previous chapter, we have seen how receive diversity systems offer significant performance improvement over single antenna systems. However, we know that the use of multiple antennas comes at the cost of an increased overhead on hardware complexity and cost. Antenna selection on the other hand, offers a promising trade-off between cost and diversity benefits.

Today's commercial wireless devices have a compact form-factor and realizing MIMO systems on such constrained sizes is a big challenge. An inter-element spacing of half a wavelength is *theoretically* considered sufficient to extract spatial diversity of a wireless environment. In practice however, transceiver impairments such as antenna coupling, limit the deployment of large arrays. Yet, in order to exploit benefits of a multi-antenna system, packing antennas closely seems indispensable. Optimal matching networks proposed in the literature, seem to overcome the problem of coupling, but these multiport

networks are considered impractical and expensive to build, leaving little but no choice than to space the antennas farther apart. In this chapter, we explore alternative avenues to construct low-cost multi-antenna transceivers with improved performance, using antenna selection.

As highlighted in Chapter 1, parasitic antenna structures can leverage significant performance improvement in compact arrays. By way of exploiting coupling, we investigate the design of a compact receive antenna selection system, that puts the inactive elements at use. The underlying motivation is to come up with selection architectures that offer improved diversity performance, compared to a system without selection with an equal number of RF chains and array size. An illustration of this comparison is given in Fig. 1.1. It shows three systems with and without antenna selection, referred to as (a) antenna selection (AS), (b) reduced full-complexity (RFC), and (c) full-complexity (FC).

We begin with a system model for antenna selection in the presence of mutual coupling. In Sec. 3.2, we formulate the problem for a selection diversity system and discuss optimal matching and optimal/sub-optimal parasitic network design. Sec. 3.3 outlines a numerical example and presents the results for various configurations. Sec. 3.4 proposes a simple yet powerful selection strategy that exploits coupling between the active and inactive elements. We conclude this chapter by summarizing the main findings and highlighting some implementation issues in Sec. 3.5.

3.1 System Model for Antenna Selection

Consider an array of N identical antennas spaced a distance d apart from neighboring elements. A receiver circuit model for this selection diversity system is illustrated in Fig. 3.1. It shows N receive antennas together with a switch that selects a subset of these

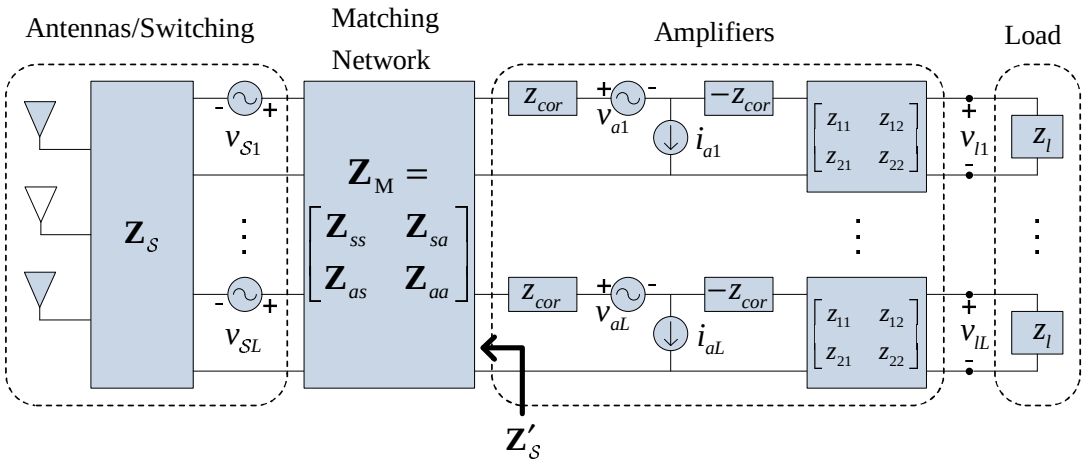

Figure 3.1: A circuit model of a receiver with antenna selection and mutual coupling

antennas to connect to L RF chains. The switch is connected to the front-end amplifiers (LNA) through a matching network, while the rest of the RF chain is represented by an equivalent load z_l. This model is inspired by the receiver model presented in [29] with the inclusion of antenna selection. These components are described in detail below.

3.1.1 Antennas and Switching

The N receive antennas convert the incident electromagnetic (EM) field into open-circuit voltages across the antenna terminals. When the antennas are closely spaced, the terminal voltage of each antenna depends not only on the field at that antenna but also on the currents flowing through neighboring antennas. To account for this coupling, the relationship between the terminal voltages $\mathbf{v}$ and currents $\mathbf{i}$ can be modeled as

$$\mathbf{v} = \mathbf{Z}_A\mathbf{i} + \mathbf{v}_o \ , \tag{3.1}$$

where $\mathbf{Z}_A$ is an $N \times N$ impedance matrix and $\mathbf{v}_o$ is the $N \times 1$ open-circuit voltage induced by the electric field. Here $[\mathbf{Z}_A]_{nn}$ is the *self-impedance* of antenna n, and $[\mathbf{Z}_A]_{nm}$ is the *mutual impedance* between antennas n and m. In the absence of coupling, $\mathbf{Z}_A = z_A\mathbf{I}$ is a diagonal matrix where z_A is the self-impedance of an isolated antenna. In the presence of coupling, [3] offers approximate impedance formulas for a two-element array of infinitesimally-thin dipoles. Since these formulas do not account for antenna scattering, we evaluate the impedances numerically for finite-width dipoles using the Numerical Electromagnetics Code (NEC) [10], a program based on *method of moments* (MoM).

In a flat-fading environment, the open-circuit voltage in (3.1) is given by

$$\mathbf{v}_o = \mathbf{h}_o s + \mathbf{n}_o \ , \tag{3.2}$$

where $\mathbf{h}_o$ is an N-vector of fading path gains, s is the complex transmitted symbol with $\mathbb{E}[|s|^2] = \mathcal{E}$, and $\mathbf{n}_o$ is noise induced in the antennas. If the received signal field consists of a large number of plane waves with independent, uniformly-distributed random phases, then $\mathbf{h}_o$ can be modeled as a zero-mean, circularly-symmetric, complex Gaussian random vector, denoted by $\mathbf{h}_o \sim \mathcal{CN}(\mathbf{0}, \mathbf{R}_{\mathbf{h}_o})$. We shall expand on the fading correlation matrix in our numerical results section.

For perfectly conducting antennas, $\mathbf{n}_o$ in (3.2) is the open-circuit voltage induced by noise sources in the surrounding environment, such as thermal radiation, cosmic background, and interference from other devices. As in [29], we assume the array is surrounded by a black body enclosure at a temperature T_A. Under these conditions, Twiss [95] showed that $\mathbf{n}_o \sim \mathcal{CN}(\mathbf{0}, \mathbf{R}_{\mathbf{n}_o})$ where

$$\mathbf{R}_{\mathbf{n}_o} = 2kT_A B(\mathbf{Z}_A + \mathbf{Z}_A^H) \ , \tag{3.3}$$

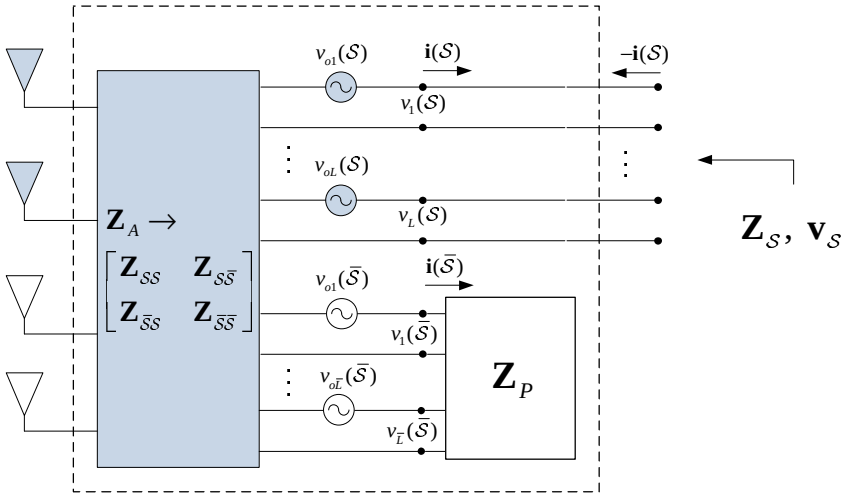

Figure 3.2: Circuit model of the antenna array and switching network

$k = 1.38 \times 10^{-23}$ J/K is Boltzmann's constant, H denotes the conjugate-transpose, and B is the bandwidth in Hz. We shall however, specify the antenna temperature T_A in terms of the standard temperature $T_0 = 290$ K. Observe that $\mathbf{Z}_A$ is essentially diagonal for large d, so the noise is spatially white. For d less than a few wavelengths, however, $\mathbf{Z}_A$ is not diagonal and the noise is correlated.

The array is followed by a noiseless switching network that selects L out of N "active" antennas to connect to the L receiver RF chains. The remaining $\bar{L} = N - L$ "inactive" antennas are not connected directly to the receiver chains but, depending on how they are terminated, they can affect the active antennas through mutual coupling. In traditional antenna selection, the inactive antennas are considered to be open circuit. Here we also consider the possibility that terminating the inactive antennas with some $\bar{L} \times \bar{L}$ parasitic impedance network, say $\mathbf{Z}_P$, may improve performance. Since this impedance may allow currents to flow through the inactive elements, it may alter the open-circuit voltage and impedance of the active antennas in a way that depends on $\mathcal{S}$.

As illustrated in Fig. 3.2, it is convenient to think of the switch as partitioning the antennas into an active group with open-circuit voltage, $\mathbf{v}_o(\mathcal{S}) = \mathbf{I}_{\mathcal{S}}\mathbf{v}_o$, and an inactive group with open-circuit voltage $\mathbf{v}_o(\bar{\mathcal{S}}) = \mathbf{I}_{\bar{\mathcal{S}}}\mathbf{v}_o$, where $\mathbf{I}_{\mathcal{S}}$ is the selection matrix defined in (2.12). If we partition (3.1) as in Fig. 3.2, we obtain

$$\begin{bmatrix} \mathbf{v}(\bar{\mathcal{S}}) \\ \mathbf{v}(\mathcal{S}) \end{bmatrix} = \begin{bmatrix} \mathbf{Z}_{\bar{\mathcal{S}}\bar{\mathcal{S}}} & \mathbf{Z}_{\bar{\mathcal{S}}\mathcal{S}} \\ \mathbf{Z}_{\mathcal{S}\bar{\mathcal{S}}} & \mathbf{Z}_{\mathcal{S}\mathcal{S}} \end{bmatrix} \begin{bmatrix} \mathbf{i}(\bar{\mathcal{S}}) \\ \mathbf{i}(\mathcal{S}) \end{bmatrix} + \begin{bmatrix} \mathbf{v}_o(\bar{\mathcal{S}}) \\ \mathbf{v}_o(\mathcal{S}) \end{bmatrix} \tag{3.4}$$

where $\mathbf{v}(\mathcal{S}) = \mathbf{I}_{\mathcal{S}}\mathbf{v}$, $\mathbf{i}(\mathcal{S}) = \mathbf{I}_{\mathcal{S}}\mathbf{i}$, $\mathbf{Z}_{\mathcal{S}\bar{\mathcal{S}}} = \mathbf{I}_{\mathcal{S}}\mathbf{Z}_A\mathbf{I}_{\bar{\mathcal{S}}}^T$, and the other quantities are defined analogously. Here, T denotes the transpose. Note we also have

$$\mathbf{v}(\bar{\mathcal{S}}) = -\mathbf{Z}_P\mathbf{i}(\bar{\mathcal{S}}) \ . \tag{3.5}$$

Combining (3.4) and (3.5), we obtain

$$\begin{aligned} \mathbf{i}(\bar{\mathcal{S}}) &= (\mathbf{Z}_P + \mathbf{Z}_{\bar{\mathcal{S}}\bar{\mathcal{S}}})^{-1} \left(\mathbf{Z}_{\bar{\mathcal{S}}\mathcal{S}}\mathbf{i}(\mathcal{S}) + \mathbf{v}_o(\bar{\mathcal{S}})\right) \\ \mathbf{v}(\mathcal{S}) &= \mathbf{Z}_{\mathcal{S}}\mathbf{i}(\mathcal{S}) + \mathbf{v}_{\mathcal{S}} \end{aligned} \tag{3.6}$$

where

$$\mathbf{Z}_{\mathcal{S}} = \mathbf{Z}_{\mathcal{S}\mathcal{S}} - \mathbf{Z}_{\mathcal{S}\bar{\mathcal{S}}} \left(\mathbf{Z}_P + \mathbf{Z}_{\bar{\mathcal{S}}\bar{\mathcal{S}}}\right)^{-1} \mathbf{Z}_{\bar{\mathcal{S}}\mathcal{S}} \tag{3.7}$$

$$\mathbf{v}_{\mathcal{S}} = \mathbf{v}_o(\mathcal{S}) - \mathbf{Z}_{\mathcal{S}\bar{\mathcal{S}}} \left(\mathbf{Z}_P + \mathbf{Z}_{\bar{\mathcal{S}}\bar{\mathcal{S}}}\right)^{-1} \mathbf{v}_o(\bar{\mathcal{S}}) \ . \tag{3.8}$$

Comparing (3.6) with (3.1), we see that the switching network and $\mathbf{Z}_P$ essentially change the array impedance and open-circuit voltage from $\mathbf{Z}_A$ and $\mathbf{v}_o$ to $\mathbf{Z}_{\mathcal{S}}$ and $\mathbf{v}_{\mathcal{S}}$, respectively.

Most of the voltages and currents in Fig. 3.1 will, like those in (3.6), (3.7) and (3.8),

depend on the set of active antennas, $\mathcal{S}$. However, to avoid needless clutter, we have chosen to suppress this dependence in (3.7) and (3.8). We also note for future use that (3.8) can be written as

$$\mathbf{v}_{\mathcal{S}} = \mathbf{T}_{\mathcal{S}}\mathbf{v}_o \ , \ \mathbf{T}_{\mathcal{S}} = \mathbf{I}_{\mathcal{S}} - \mathbf{Z}_{\mathcal{S}\bar{\mathcal{S}}}(\mathbf{Z}_P + \mathbf{Z}_{\bar{\mathcal{S}}\bar{\mathcal{S}}})^{-1}\mathbf{I}_{\bar{\mathcal{S}}} \ . \tag{3.9}$$

where $\mathbf{T}_{\mathcal{S}}$ is the equivalent selection matrix.

3.1.2 Amplifiers

According to [81], any linear amplifier can be represented as in Fig. 3.1. Here

$$v_a \sim \mathcal{CN}(0, 4kT_0Br_a) \ , \ i_a \sim \mathcal{CN}(0, 4kT_0Bg_a)$$

are independent random variables that model amplifier internal noise, where r_a and g_a are the *equivalent noise resistance* and *equivalent noise conductance*, respectively. The *correlation impedance*, $z_{cor} = r_{cor} + jx_{cor}$, controls the correlation between the noise observed at the two output terminals. The noise statistics of an amplifier are completely characterized by $\{r_a, g_a, z_{cor}\}$.

When a source impedance $z_s = r_s + jx_s$ at the standard temperature is connected to the amplifier input port, the *noise factor* is defined as

$$F = 1 + \frac{1}{r_s}\left(r_a + g_a\left|z_s + z_{cor}\right|^2\right). \tag{3.10}$$

The noise factor is useful because it relates the input and output signal-to-noise ratios (SNRs) of the amplifier, given in dB by $\mathrm{SNR}_{\mathrm{out}} = \mathrm{SNR}_{\mathrm{in}} - \mathrm{NF}$, where $\mathrm{NF} = 10\log_{10} F$ is

the *noise figure*. Note that F attains its minimum value F_{min} when $z_s = z_{opt}$ where [81]

$$\begin{aligned} F_{min} &= 1 + 2\left(g_a r_{cor} + \sqrt{g_a r_a + (g_a r_{cor})^2}\right) , \\ z_{opt} &= \sqrt{r_a/g_a + r_{cor}^2} - j x_{cor} . \end{aligned} \tag{3.11}$$

3.1.3 Matching Network

The switching network is connected to the amplifiers by a $2L$-port matching network $\mathbf{Z}_M$. Matching networks can be used to alter the antenna array impedance in order to maximize the power transfer or the resulting SNR. We assume an ideal matching network consisting of passive and reactive elements such that it is noiseless, lossless and reciprocal. It can be shown [53] that the network is lossless (no power is dissipated within it) provided the following conditions are satisfied: $\mathbf{Z}_{aa} = -\mathbf{Z}_{aa}^H$, $\mathbf{Z}_{ss} = -\mathbf{Z}_{ss}^H$ and $\mathbf{Z}_{sa} = -\mathbf{Z}_{as}^H$.

The relationship between the voltages and currents at the input and output of the matching network are described by equations similar to (3.4) and (3.5), with $\mathbf{Z}_P$ replaced by $\mathbf{Z}_{\mathcal{S}}$, $\mathbf{v}_o(\bar{\mathcal{S}})$ replaced by $-\mathbf{v}_{\mathcal{S}}$, $\mathbf{v}_o(\mathcal{S})$ replaced by $\mathbf{0}$, $\mathbf{Z}_{as}$ replaced by $\mathbf{Z}_{\mathcal{S}\bar{\mathcal{S}}}$, and so on. It follows from (3.6) that the matching network alters the switch impedance and open-circuit voltage from $\mathbf{Z}_{\mathcal{S}}$ and $\mathbf{v}_{\mathcal{S}}$ to $\mathbf{Z}'_{\mathcal{S}}$ and $\mathbf{v}'_{\mathcal{S}}$, respectively, where

$$\mathbf{Z}'_{\mathcal{S}} = \mathbf{Z}_{aa} - \mathbf{Z}_{as}\left(\mathbf{Z}_{\mathcal{S}} + \mathbf{Z}_{ss}\right)^{-1}\mathbf{Z}_{sa} , \tag{3.12}$$

$$\mathbf{v}'_{\mathcal{S}} = \mathbf{Z}_{as}\left(\mathbf{Z}_{\mathcal{S}} + \mathbf{Z}_{ss}\right)^{-1}\mathbf{v}_{\mathcal{S}} . \tag{3.13}$$

3.1.4 Load

The rest of the RF chain (*aka* downstream components) consists of filters, mixers, amplifiers and other analog circuits. We assume these components to be electrically isolated

from one another, and model them as a diagonal load $\mathbf{Z}_L = z_L\mathbf{I}$.

3.2 Optimal Antenna Selection Designs

The input to the linear combiner given by the voltage $\mathbf{v}_l$ across the load $\mathbf{z}_l$ can be expressed in terms of the $L \times 1$ equivalent fading path-gain vector $\mathbf{h}$ as

$$\mathbf{r} = \mathbf{v}_l = \mathbf{h}s + \mathbf{n} \tag{3.14}$$

where,

$$\mathbf{h} = \mathbf{DCM}(\mathbf{T}_{\mathcal{S}}\mathbf{h}_o) \ , \tag{3.15}$$

$$\mathbf{n} = \mathbf{DC}\left[\mathbf{M}(\mathbf{T}_{\mathcal{S}}\mathbf{n}_o) - \mathbf{v}_a - (\mathbf{Z}'_{\mathcal{S}} + z_{cor}\mathbf{I})\mathbf{i}_a\right] \ . \tag{3.16}$$

Here, $\mathbf{v}_a$ and $\mathbf{i}_a$ are the amplifier noise voltages and currents, respectively and

$$\mathbf{C} = z_{21}(\mathbf{Z}'_{\mathcal{S}} + z_{11}\mathbf{I})^{-1} \tag{3.17a}$$

$$\mathbf{D} = z_l\left[(z_l + z_{22}\mathbf{I}) - z_{12}\mathbf{C}\right]^{-1} \tag{3.17b}$$

$$\mathbf{M} = \mathbf{Z}_{as}\left(\mathbf{Z}_{\mathcal{S}} + \mathbf{Z}_{ss}\right)^{-1} \tag{3.17c}$$

with $\mathbf{Z}'_{\mathcal{S}}$ given by (3.12). The amplifier parameters are denoted by z_{11}, z_{12}, z_{21} and z_{22} and the mutually independent noise sources are distributed as $\mathbf{v}_a \sim \mathcal{CN}(\mathbf{0}, 4kT_0Br_a\mathbf{I})$ and $\mathbf{i}_a \sim \mathcal{CN}(\mathbf{0}, 4kT_0Bg_a\mathbf{I})$. The noise covariance $\mathbf{\Sigma_n}$ for (3.16) is thus, given by

$$\frac{1}{4kT_0B}\mathbf{\Sigma_n} = \mathbf{DC}\left[\frac{1}{2}\mathbf{R}'_{\mathbf{n}_o} + r_a\mathbf{I} + g_a(\mathbf{Z}'_{\mathcal{S}} + z_{cor}\mathbf{I})(\mathbf{Z}'_{\mathcal{S}} + z_{cor}\mathbf{I})^H\right]\mathbf{C}^H\mathbf{D}^H \tag{3.18}$$

where, $\mathbf{R}'_{\mathbf{n}_o} = (\mathbf{M}\mathbf{T}_{\mathcal{S}})\mathbf{R}_{\mathbf{n}_o}(\mathbf{M}\mathbf{T}_{\mathcal{S}})^H$.

The receiver employs a linear combiner to the input $\mathbf{r}$ such that

$$y = \mathbf{w}^H\mathbf{r} = \widehat{h}x + \widehat{n}$$

and the resulting SNR is

$$\gamma = \frac{|\widehat{\mathbf{h}}|^2}{\mathbb{E}[|\widehat{\mathbf{n}}|^2]} = \mathcal{E}\frac{|\mathbf{w}^H\mathbf{h}|^2}{\mathbf{w}^H\mathbf{\Sigma}_{\mathbf{n}}\mathbf{w}} \ .$$

The well-known optimal maximal-ratio-combiner (MRC) is given by $\mathbf{w} \propto \mathbf{R}_{\mathbf{n}}^{-\frac{1}{2}}\mathbf{h}$. Thus, the optimal SNR for the antenna selection system becomes

$$\gamma^o \quad = \quad \mathcal{E}\max_{\mathcal{S}} \|\mathbf{R}_{\mathbf{n}}^{-\frac{1}{2}}\mathbf{h}\|^2 \tag{3.19}$$

where, $\mathbf{h}$ is given by (3.15) and $\mathbf{\Sigma}_{\mathbf{n}}$ by (3.18). It is convenient to normalize (3.19), such that for the i.i.d. scenario, the SNR is given by the familiar expression

$$\gamma_n^{iid} = \frac{\mathcal{E}}{N_0}\max_{\mathcal{S}} \|\mathbf{I}_{\mathcal{S}}\mathbf{h}_w\|^2 \tag{3.20}$$

where, N_0 represents the i.i.d. noise covariance for a single branch (i.e., $\mathbf{R}_{\mathbf{n}} = N_0\mathbf{I}$) and $\mathbf{h}_w$ is the $N \times 1$ i.i.d. fading path-gain vector given by $\mathbf{h}_w \sim \mathcal{CN}(\mathbf{0}, \mathbf{I})$.

To that end, consider a sufficiently large antenna spacing such that the fading path-gain covariance is $\mathbf{R}_{\mathbf{h}} = \mathbf{I}$, and the antenna array is uncoupled ($\mathbf{Z}_A = z_A\mathbf{I}$). From (3.9), $\mathbf{T}_{\mathcal{S}} = \mathbf{I}_{\mathcal{S}}$ and from (3.18), the noise covariance is

$$\mathbf{R}_{\mathbf{n}}^{iid} \quad = \quad 4kT_0B\sigma^2\mathbf{I}$$

where,

$$\sigma^2 = (r_{opt} + \sigma_a^2)|\alpha\beta|^2 \ , \quad \alpha = z_{21}/(z_{opt} + z_{11}) \ , \quad \beta = z_{22}^*/\left(2\,\mathrm{Re}(z_{22}) - \alpha z_{12}\right) \ ,$$

and $\mathrm{Re}(\cdot)$ denotes the real-part. Observe that the equivalent channel vector is given by

$$\mathbf{h}^{iid} = \mathbf{DCMI}_{\mathcal{S}}\mathbf{h}_w = \tau \mathbf{I}_{\mathcal{S}}\mathbf{h}_w$$

where $|\tau|^2 = (r_{opt}/r_A)|\alpha\beta|^2$, such that i.i.d. SNR is given by

$$\gamma_n^{iid} = |\tau|^2 \frac{\mathcal{E}}{4kT_0B\sigma^2} \max_{\mathcal{S}} \|\mathbf{I}_{\mathcal{S}}\mathbf{h}_w\|^2$$

Comparing the equation above with (3.20), we have $N_0 = 4kT_0B\sigma^2/|\tau|^2$. Hence, we normalize the noise covariance by $4kT_0B\sigma^2$ and the output SNR by $|\tau|^2$ such that the normalized output SNR becomes

$$\gamma_n^o = \frac{\mathcal{E}}{N_0} \max_{\mathcal{S}} \|\mathbf{\Sigma}_{\mathbf{n}}^{-\frac{\mathbf{1}}{\mathbf{2}}}\mathbf{h}\|^2 \tag{3.21}$$

where, $\mathbf{h}$ is given by (3.15) and $\mathbf{R_n}$ by (3.18).

3.2.1 Optimal Matching Network

For a given $\mathcal{S}$, any matching network that results in the impedance $\mathbf{Z}'_{\mathcal{S}} = z_{opt}\mathbf{I}$ minimizes the outage probability of selection diversity [30]. Here z_{opt} is the source impedance (3.11) that achieves the minimum noise factor of the amplifier. One lossless, reciprocal network that accomplishes this task is [29]

$$\mathbf{Z}_M = \begin{bmatrix} \mathbf{Z}_{ss} & \mathbf{Z}_{sa} \\ \mathbf{Z}_{as} & \mathbf{Z}_{aa} \end{bmatrix} = j \begin{bmatrix} -\mathrm{Im}[\mathbf{Z}_{\mathcal{S}}] & (r_{opt}\mathrm{Re}[\mathbf{Z}_{\mathcal{S}}])^{\frac{1}{2}} \\ (r_{opt}\mathrm{Re}[\mathbf{Z}_{\mathcal{S}}])^{\frac{1}{2}} & x_{opt}\mathbf{I} \end{bmatrix}. \tag{3.22}$$

While optimal, this network would not be easy to realize in practice. The dependence on $\mathcal{S}$ would generally require some kind of adaptive multiport matching, which would be a complex choice for a diversity scheme whose primary value is simplicity and economy. In some cases (e.g., when inactive antennas are open circuit), it is clear that $\mathbf{Z}'_{\mathcal{S}} = z_{opt}\mathbf{I}$ could also be achieved by a fixed matching network located *between* the antennas and the switch. In any case, we consider (3.22) here primarily because it provides an upper bound on the performance of any fixed matching network.

We also consider a simpler, sub-optimal matching strategy that applies to each antenna - the two-port matching network that achieves the minimum noise figure for that antenna in isolation. This is called *self matching* for minimum noise figure and is accomplished by replacing $\mathbf{Z}_{\mathcal{S}}$ with $z_A\mathbf{I}$ in (3.22), where $z_A = r_A + jx_A$ is the self-impedance of each antenna in isolation:

$$\mathbf{Z}_M = j \begin{bmatrix} -x_A\mathbf{I} & \sqrt{r_{opt}r_A}\mathbf{I} \\ \sqrt{r_{opt}r_A}\mathbf{I} & x_{opt}\mathbf{I} \end{bmatrix}. \tag{3.23}$$

3.2.2 Optimal Parasitic Network

Observe that the optimal matching network discussed above depends on (3.7) which in turn is also dependent on the parasitic network. Hence, it is natural to ask if there is an optimal choice for the parasitic networks (with purely-reactive entries) as well. The

aim here is to choose a $\mathbf{Z}_P$ that depends only on the active subset $\mathcal{S}$ and not on the instantaneous channel conditions, just like the optimal matching network $\mathbf{Z}_M$.

The derivation of optimal non-diagonal $\mathbf{Z}_P$ for a uniform linear array is in general complicated and tedious. However, the solution is analytically tractable for a special but practical class of planar arrays - *uniform circular arrays* - with equal number of active and inactive elements. Again, the optimal parasitic network design presented here serves as an upper bound on the system performance of coupled antenna selection systems. To that end, consider a circular array of N antennas such

$$L = \bar{L} = N - L \ .$$

The impedance matrix $\mathbf{Z}_A$ for a circular array is circulant and the same applies to the permuted impedance matrix in (3.4)

$$\widetilde{\mathbf{Z}}_A = \begin{bmatrix} \mathbf{Z}_{\mathcal{S}\mathcal{S}} & \mathbf{Z}_{\mathcal{S}\bar{\mathcal{S}}} \\ \mathbf{Z}_{\bar{\mathcal{S}}\mathcal{S}} & \mathbf{Z}_{\bar{\mathcal{S}}\bar{\mathcal{S}}} \end{bmatrix} \tag{3.24}$$

Each of the $L \times L$ sub-blocks in (3.24) can be diagonalized by a unitary transformation $\mathbf{Q}$ such that

$$\begin{bmatrix} \mathbf{Z}_{\mathcal{S}\mathcal{S}} & \mathbf{Z}_{\mathcal{S}\bar{\mathcal{S}}} \\ \mathbf{Z}_{\bar{\mathcal{S}}\mathcal{S}} & \mathbf{Z}_{\bar{\mathcal{S}}\bar{\mathcal{S}}} \end{bmatrix} = \begin{bmatrix} \mathbf{Q} & \mathbf{0} \\ \mathbf{0} & \mathbf{Q} \end{bmatrix} \begin{bmatrix} \mathbf{\Lambda}_{\mathcal{S}\mathcal{S}} & \mathbf{\Lambda}_{\mathcal{S}\bar{\mathcal{S}}} \\ \mathbf{\Lambda}_{\bar{\mathcal{S}}\mathcal{S}} & \mathbf{\Lambda}_{\bar{\mathcal{S}}\bar{\mathcal{S}}} \end{bmatrix} \begin{bmatrix} \mathbf{Q}^H & \mathbf{0} \\ \mathbf{0} & \mathbf{Q}^H \end{bmatrix}$$

The set of orthonormal eigen-vectors for each block corresponding to the eigen-values $\mathbf{\Lambda}$

are given by

$$\mathbf{Q} = \frac{1}{\sqrt{L}} \begin{bmatrix} 1 & 1 & 1 & \dots & 1 \\ 1 & \alpha & \alpha^2 & \dots & \alpha^{L-1} \\ 1 & \alpha^2 & \alpha^4 & \dots & \alpha^{2(L-1)} \\ \vdots & \vdots & \vdots & & \vdots \\ 1 & \alpha^{L-1} & \alpha^{2(L-1)} & \dots & \alpha^{(L-1)(L-1)} \end{bmatrix}$$

where $\omega = e^{-j2\pi/L}$ and the eigen-values ($\mathbf{\Lambda}$) are given by the DFT of the first row scaled by $\sqrt{L}$. Physically, the matrix $\mathbf{Q}$ represents an L-point DFT/IDFT operation in space.

Since the sub-blocks of $\mathbf{Z}_A$ are $L \times L$ circulant matrices, it is reasonable to assume (as is also evident from (3.7)), that the optimal parasitic network also admits the same spatial unitary transformation $\mathbf{Q}$ diagonalizing it

$$\mathbf{Z}_P = \mathbf{Q}\mathbf{\Lambda}_P\mathbf{Q}^H \ .$$

Therefore, we can write (3.7) as

$$\mathbf{Z}_{\mathcal{S}} \ = \ \mathbf{Q} \underbrace{\left(\mathbf{\Lambda}_{\mathcal{S}\mathcal{S}} - \mathbf{\Lambda}_{\mathcal{S}\bar{\mathcal{S}}} \left(\mathbf{\Lambda}_P + \mathbf{\Lambda}_{\bar{\mathcal{S}}\bar{\mathcal{S}}}\right)^{-1} \mathbf{\Lambda}_{\bar{\mathcal{S}}\mathcal{S}}\right)}_{\mathbf{\Lambda}_{\mathcal{S}}} \mathbf{Q}^H$$

such that the optimal matching network from (3.22) is given by

$$\mathbf{Z}_M = \begin{bmatrix} \mathbf{Z}_{ss} & \mathbf{Z}_{sa} \\ \mathbf{Z}_{as} & \mathbf{Z}_{aa} \end{bmatrix} = \begin{bmatrix} \mathbf{Q} & \mathbf{0} \\ \mathbf{0} & \mathbf{Q} \end{bmatrix} \begin{bmatrix} \mathbf{\Lambda}_{ss} & \mathbf{\Lambda}_{sa} \\ \mathbf{\Lambda}_{as} & \mathbf{\Lambda}_{aa} \end{bmatrix} \begin{bmatrix} \mathbf{Q}^H & \mathbf{0} \\ \mathbf{0} & \mathbf{Q}^H \end{bmatrix}$$

where

$$\begin{bmatrix} \mathbf{\Lambda}_{ss} & \mathbf{\Lambda}_{sa} \\ \mathbf{\Lambda}_{as} & \mathbf{\Lambda}_{aa} \end{bmatrix} = j \begin{bmatrix} -\mathrm{Im}[\mathbf{\Lambda}_{\mathcal{S}}] & (r_{opt}\mathrm{Re}[\mathbf{\Lambda}_{\mathcal{S}}])^{\frac{1}{2}} \\ (r_{opt}\mathrm{Re}[\mathbf{\Lambda}_{\mathcal{S}}])^{\frac{1}{2}} & x_{opt}\mathbf{I} \end{bmatrix} .$$

The input impedance seen looking into the matching network from the rest of the RF chain is given by (3.12)

$$\mathbf{Z}'_{\mathcal{S}} = \mathbf{Q} \underbrace{\left(\mathbf{\Lambda}_{aa} - \mathbf{\Lambda}_{as} \left(\mathbf{\Lambda}_{\mathcal{S}} + \mathbf{\Lambda}_{ss}\right)^{-1} \mathbf{\Lambda}_{sa}\right)}_{\mathbf{\Lambda}'_{\mathcal{S}}} \mathbf{Q}^{H} .$$

However, we can simplify the network design above by embedding special RF networks popularly known as *Butler matrices*, as shown in Fig. 3.3. These decoupling networks which act as spatial FFT/IFFT matrices [67], are followed by a bank of uncoupled matching networks, i.e., $\mathbf{Z}_M = \mathbf{\Lambda}_M$. The cascade of decoupling network and matching network can be expressed as

$$\mathbf{Z}_C = \begin{bmatrix} \mathbf{Q} & \mathbf{0} \\ \mathbf{0} & \mathbf{I} \end{bmatrix} \begin{bmatrix} \mathbf{\Lambda}_{ss} & \mathbf{\Lambda}_{sa} \\ \mathbf{\Lambda}_{as} & \mathbf{\Lambda}_{aa} \end{bmatrix} \begin{bmatrix} \mathbf{Q}^{H} & \mathbf{0} \\ \mathbf{0} & \mathbf{I} \end{bmatrix}$$

such that the input impedance $\mathbf{Z}'_{\mathcal{S}}$ becomes uncoupled:

$$\mathbf{Z}'_{\mathcal{S}} = \mathbf{\Lambda}_{aa} - \mathbf{\Lambda}_{as} \left(\mathbf{\Lambda}_{\mathcal{S}} + \mathbf{\Lambda}_{ss}\right)^{-1} \mathbf{\Lambda}_{sa} = \mathbf{\Lambda}'_{\mathcal{S}} .$$

We consider amplifiers to be the dominant source of noise in the RF chain, such that

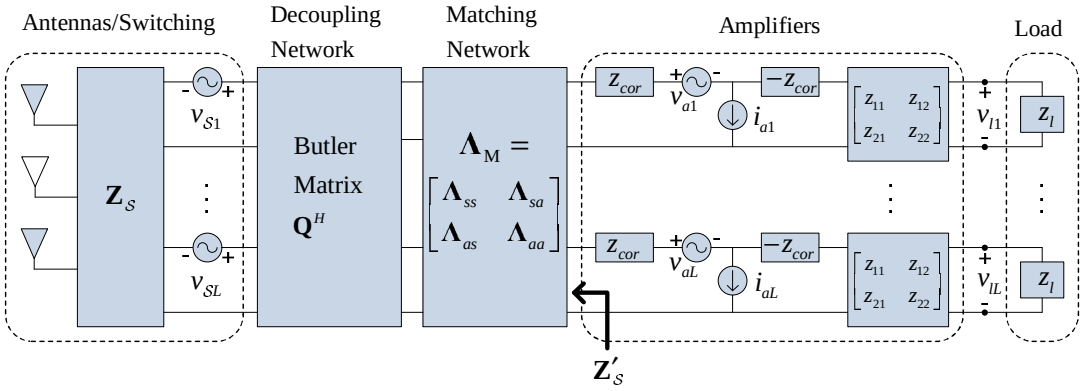

Figure 3.3: A circuit model of a circular array receiver with antenna selection and mutual coupling

the post-MRC output SNR, with optimal parasitic network, is given by (3.19) is

$$\begin{aligned}\gamma^o(\mathbf{\Lambda}_P) &= \mathcal{E} \max_{\mathcal{S}} \left\{ \max_{\mathbf{\Lambda}_P(\mathcal{S})} \|\mathbf{R}_\mathbf{n}^{-1/2}\mathbf{h}\|^2 \right\} \\ &= \frac{\mathcal{E}}{\sigma_a^2} \max_{\mathcal{S}} \left\{ \max_{\mathbf{\Lambda}_P(\mathcal{S})} \Gamma(\mathbf{\Lambda}_P(\mathcal{S})) \right\}\end{aligned}$$

where

$$\sigma_a^2 = r_a + g_a|z_{opt} + z_{cor}|^2 \tag{3.25}$$

represents the amplifier noise variance. The instantaneous output SNR for each subset is

$$\Gamma(\mathbf{\Lambda}_P(\mathcal{S})) = \|\mathbf{\Lambda}_M^H \mathbf{h}'\|^2$$

where, $\mathbf{h}' = \mathbf{Q}^H \mathbf{T}_{\mathcal{S}} \mathbf{h}_o$ and

$$\mathbf{\Lambda}_M \;=\; \sqrt{r_{opt}} \left(\mathrm{Re} \left[\mathbf{\Lambda}_{\mathcal{SS}} - \mathbf{\Lambda}_{\mathcal{S}\bar{\mathcal{S}}} \left(\mathbf{\Lambda}_P + \mathbf{\Lambda}_{\bar{\mathcal{S}}\bar{\mathcal{S}}} \right)^{-1} \mathbf{\Lambda}_{\bar{\mathcal{S}}\mathcal{S}} \right] \right)^{-\frac{1}{2}} \;.$$

Details can be found in Appendix A.1.

The fading-independent, subset-dependent optimal $\mathbf{\Lambda}_P$ is thus given by

$$\begin{aligned} \mathbf{\Lambda}_P &= \arg_{\mathbf{\Lambda}_P} \max \left\{ \mathbb{E}(\Gamma(\mathbf{\Lambda}_P)) \right\} \\ &= \arg_{\mathbf{\Lambda}_P} \max \left\{ \mathbb{E} \left(\sum_{k=1}^{L} \left| [\lambda_M]_k h'_k \right|^2 \right) \right\} \\ &= \arg_{\mathbf{\Lambda}_P} \max \left\{ \sum_{k=1}^{L} \left| [\lambda_M]_k \right|^2 \mathbb{E} \left(\left| h'_k \right|^2 \right) \right\} \;. \end{aligned} \tag{3.26}$$

For a circular array with $N = 4$, $L = 2$

$$\mathbf{Q} = \frac{1}{\sqrt{2}} \begin{bmatrix} 1 & 1 \\ 1 & -1 \end{bmatrix} \;. \tag{3.27}$$

The optimal eigen-values of $\mathbf{Z}_P$ calculated for this example, are shown in Table 3.1. It comes from a simple polynomial maximization given in (3.26). Detailed information can be found in Appendix A.2.

Table 3.1: Optimal parasitic network: Circular array $N = 4$, $L = 2$, $d_{min} = 0.15\lambda$

Active Subset	Parameter	Value
$(1,3)$ or $(2,4)$	$[\mathbf{\Lambda}_P]_1$	$-j60.36$
	$[\mathbf{\Lambda}_P]_2$	Any
Others	$[\mathbf{\Lambda}_P]_1$	$-j137.79$
	$[\mathbf{\Lambda}_P]_2$	$-j55.76$

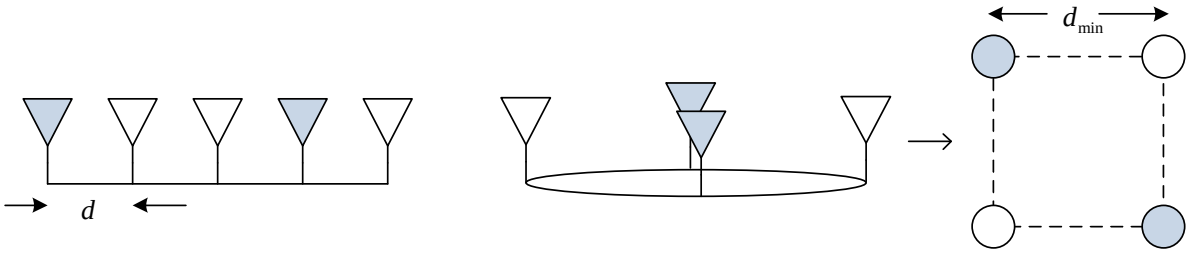

Figure 3.4: Configurations: (a) Uniform linear array (ULA), (b) Uniform circular array (UCA)

The optimal parasitic network designs presented here for circular arrays with equal number of active and inactive elements, can be extended to a broader set of arrays and configurations, although the optimal solution may need to be computed numerically. In Sec. 3.4, we provide some sub-optimal designs applicable to *all* kinds of arrays and configurations. These designs will be shown to achieve near-optimal performance, for linear, as well as circular arrays.

3.3 Simulation and Results

In this section, we present numerical results for two types of antenna arrays considered above. These arrays consist of half-wavelength or $\lambda/2$ dipole antennas spread over a length of 0.5λ (for ULA) and *nearest neighbor distance* $d_{min} = 0.15\lambda$ (for UCA), as shown in Fig. 3.4. The aim is to determine, if employing antenna selection with closely packed antennas can provide benefits over conventional diversity systems in the presence of moderate to strong coupling. We compare three combinations (a), (b) and (c), shown in Fig. 1.1, with and without antenna selection. Monte-Carlo simulations are carried out over $100,000$ channel realizations. The channel is assumed to be quasi-static block fading such that the block length is long enough to determine the optimal subset and

parasitic network. The optimal combination, once determined, is employed for the rest of the block.

The closed form expression for the fading path-gain covariance given in [25] assumes a uniform distribution of infinite EM waves arriving at the antenna, in the azimuth plane. While this may provide accurate values for thin dipole antennas where the active and inactive antennas do not act as scatterers, we resort to the use of NEC to account for the finite thickness (radius 100 mm) of half-wavelength dipoles, and scattering arising due to the presence of neighboring elements. For similar reasons, we choose NEC for computing the antenna array impedance $\mathbf{Z}_A$, over the closed-form expressions for self and mutual impedance of an array of dipoles given in [3].

For an N-antenna uniform linear array with inter-element spacing d, the incident electric field is modeled in NEC as a superposition of $K' = 32$ vertically polarized plane waves with i.i.d. phases uniformly distributed on $[0, 2\pi)$. The angles-of-arrival (AOA) of the plane waves, $\phi_0, \ldots, \phi_{K'-1}$, are uniformly spaced in azimuth from 0 to 2π. Under these conditions, the open-circuit fading path gains are approximately Gaussian with correlation matrix

$$[\mathbf{R_h}]_{nm} = \sum_{k=0}^{K'-1} g_n(\phi_k) g_m^*(\phi_k) e^{j2\pi(n-m)\frac{d}{\lambda}\cos(\phi_k)} \ ,$$

where $g_n(\phi)$ is the open-circuit voltage induced in the nth antenna by a zero-phase plane wave with AOA ϕ, normalized so that $\sum_k |g_n(\phi_k)|^2 = 1$ for an isolated dipole. For a uniform circular array, the correlation entries are given by

$$[\mathbf{R_h}]_{nm} = \sum_{k=0}^{K'-1} g_n(\phi_k) g_m^*(\phi_k) e^{j2\pi d_{nm}\cos(\phi_k)/\lambda} \ ,$$

where d_{mn} is the distance between m-th and n-th antenna.

The amplifier selected for this study is a low-cost SiGe LNA [1] designed for use in the cellular band. In high-gain mode with $R_{bias} = 510\ \Omega$ and $f = 900$ MHz, its impedance matrix and the noise parameters are:

$$\begin{bmatrix} z_{11} & z_{12} \\ z_{21} & z_{22} \end{bmatrix} = \begin{bmatrix} 35.7\angle -82.0 & 2.74\angle 91.8 \\ 325\angle 119 & 46.1\angle -23.3 \end{bmatrix} \Omega$$

$r_a = 9.45\ \Omega$, $g_a = 3.24$ mS, $z_{cor} = 35.3\angle -114$. We assume that the downstream noise is negligible compared to other noise sources [29].

The performance is evaluated in terms of the outage SNR - the probability that the SNR falls below a threshold γ_0:

$$P_{out} = \Pr\left(\gamma_n^o < \gamma_0\right) .$$

We divide the results into two categories: uniform linear arrays and uniform circular arrays.

3.3.1 Uniform Linear Array

Fig. 3.5 shows the results for a linear array with $N = 5,\ L = 2,\ d = 0.125\lambda$ with optimal and sub-optimal matching networks and open-circuited inactive elements. It shows that antenna selection in compact arrays provides a 3-4 dB improvement over conventional RFC systems, at a 1% outage. The results for the configuration (c) in Fig. 1.1, i.e., full complexity systems, lie in between the self and optimal-matching and are omitted for clarity. It clearly demonstrates that antenna selection with 2 RF chains performs

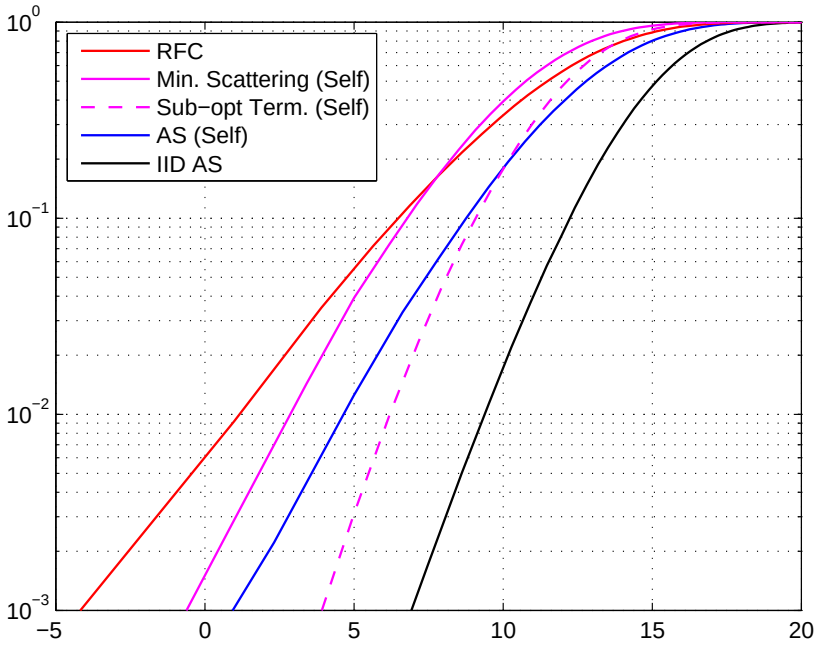

Figure 3.5: Traditional antenna selection (ULA): $(5, 2)$

as good as 5 RF chains. Unarguably, antenna selection in state-of-the-art transceivers is preferred over employing 2 antennas placed 0.5λ apart or using all of the available antennas in compact arrays. The optimal number of RF chains required though, depends on the array length, N and L.

It is worthwhile to note that, if we were to incorporate the model used in earlier studies [111] and [113], into our system, we would need to modify the equivalent channel vector as

$$\mathbf{h}_1 = \mathbf{DCM}(\mathbf{I}_{\mathcal{S}}\mathbf{R}_{\mathbf{h}_o}^{\frac{1}{2}}\mathbf{I}_{\mathcal{S}}^T)(\mathbf{I}_{\mathcal{S}}\mathbf{h}_w) \ ,$$

$$\mathbf{h}_2 = \mathbf{I}_{\mathcal{S}}(\mathbf{DCMh}_o) \ ,$$

respectively.[1] The first model signifies that the inactive elements are transparent to the rest of the array, commonly referred to as *minimum scattering*, while the second model does not distinguish between active and inactive element termination. A termination with non-zero resistive part is clearly a sub-optimal choice for inactive elements. On the other hand, (3.15) suggests that it suffices to capture the accurate open circuit voltage across the active antennas, by taking into account the effect of inactive elements.

The curves reproduced with these models are shown in Fig. 3.5 marked as *minimum scattering* and *sub-optimal termination* model, respectively. As can be seen, the results as per [111] show optimistic performance (around 2 dB), while as per [113], antenna selection performs poorly (around 2 dB) compared to a full-complexity system. This clearly underscores the importance of inactive element modeling.

3.3.2 Uniform Circular Array

Fig. 3.6 shows the outage SNR performance of proposed parasitic antenna selection for a $N = 4,\ L = 2,\ d_{min} = 0.15\lambda$ circular array with optimal matching and optimal parasitic networks. Also shown are the curves for *traditional antenna selection* (open-circuited inactive elements) with self-matching and conjugate matching. Notice a $3-4$ dB improvement over traditional selection with optimal design, however, with optimal matching, optimal parasitic network only yields a fraction of a dB better performance. Unlike ULAs, optimal-matching by itself, provides a significant improvement over self-matching for UCA.

[1]Here, $\mathbf{D}, \mathbf{C}, \mathbf{M}$ are the corresponding $L \times L$ and $N \times N$ matrices, for $\mathbf{h}_1$ and $\mathbf{h}_2$, respectively. We point out that although, the model considered in these studies does not include amplifiers, and matching is handled by way of altering the load (i.e., $\mathbf{DCM} = \mathbf{I}$ and $\mathbf{Z}_L = \mathrm{diag}(\mathbf{Z}_A^H)$), these equations still retain the essence of inactive-element modeling.

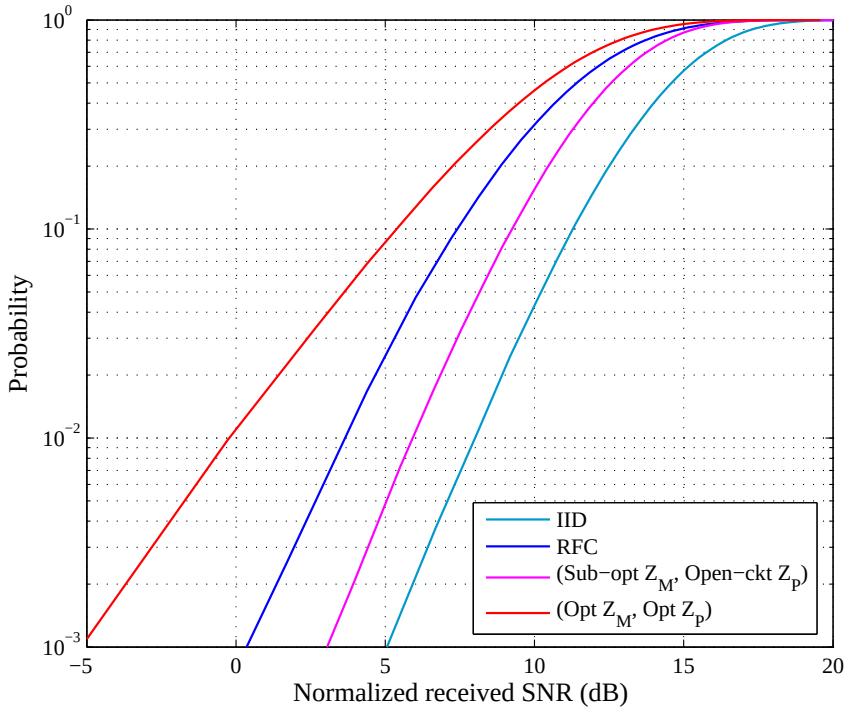

Figure 3.6: Parasitic antenna selection (UCA): $(4, 2)$

3.4 Alternative Designs

The optimal matching and parasitic networks presented in the previous section are subset-dependent and multiport in nature. These RF structures are hard to realize in practice, and essentially provide insights into the performance limits of compact arrays. In this section, we present a simpler parasitic scheme that adapts to the varying fading conditions while still avoiding the complexities of multiport networks.

We propose a novel but simple strategy, in which each of the inactive element is terminated into an impedance $z_p \in \mathcal{Z}_{\mathcal{P}}$, where, $\mathcal{Z}_{\mathcal{P}}$ represents the set of all available antenna terminations. The implementation complexity is considerably reduced by replacing multiport parasitic networks by two port terminations. The inactive element termination

not only changes with the active subset but potentially, may vary over time. Clearly, our ability to adaptively control the radiation pattern of the array lies in having a large set. However, as we shall see, even a small number of, but carefully chosen entries for $\mathcal{Z}_{\mathcal{P}}$ can provide significant improvements.

We evaluate the performance of parasitic antenna selection system for $\mathcal{Z}_{\mathcal{P}} = \{0, \infty, -jx_A\}$ where, 0 represents short-circuit, ∞ open-circuit and $-jx_A$ a purely-reactive termination experimentally found to be the best fit for such a parasitic selection system, in the same sense as z_A^* turns out to be an optimal match for active elements in the presence of mild coupling. This choice of $\mathcal{Z}_{\mathcal{P}}$ is simple and eliminates the need for a variable impedance under varying fading conditions. However, it turns out that due to directional sensitivity, the shorted parasitics do not offer much improvement and this set can as well be limited to $\mathcal{Z}_{\mathcal{P}} = \{\infty, -jx_A\}$.

It is worthwhile to talk about *electronically steerable passive array radiator* (ESPAR) antennas. ESPAR antennas work on the principle with one active element surrounded by a ring of parasitic elements terminated into variable reactive loads. This switching capability enables the array radiation pattern to be steered around the azimuth.

3.4.1 Antenna Selection with Parasitic Switching

Fig. 3.7 shows the performance of proposed antenna selection with parasitic switching for ULA $(5, 2)$. It is interesting to note that parasitic switching with appropriate matching (PS/AS (Optimal)) achieves a performance close to that of an i.i.d. antenna selection system, while with sub-optimal matching (PS/AS (Self)) it performs as good as traditional selection with optimal matching. At a 1% outage, optimal matching shows a 3 dB improvement over open-circuited antenna selection, once again highlighting how inactive

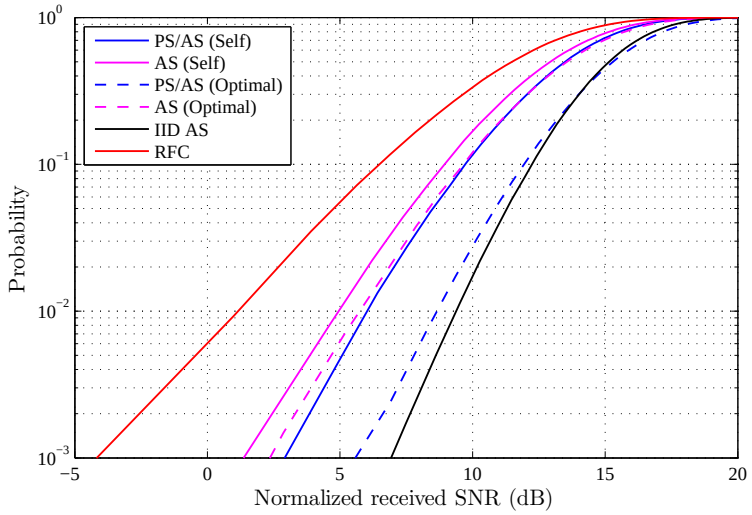

(a) $(5, 2)$

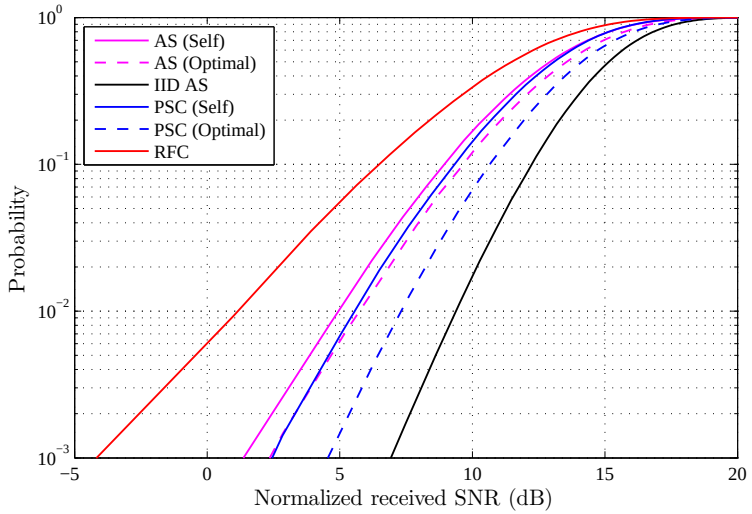

(b) $(5, 1)$

Figure 3.7: Parasitic switching (ULA)

element termination manifests itself in diversity gains.

A special case of this study surfaces when we consider selection combining (SC), i.e., single RF chain ($L = 1$). It turns out that PSC$(5, 1)$ system performs just as well as PS/AS$(5, 2)$, thereby simplifying the hardware design considerably and eliminating the

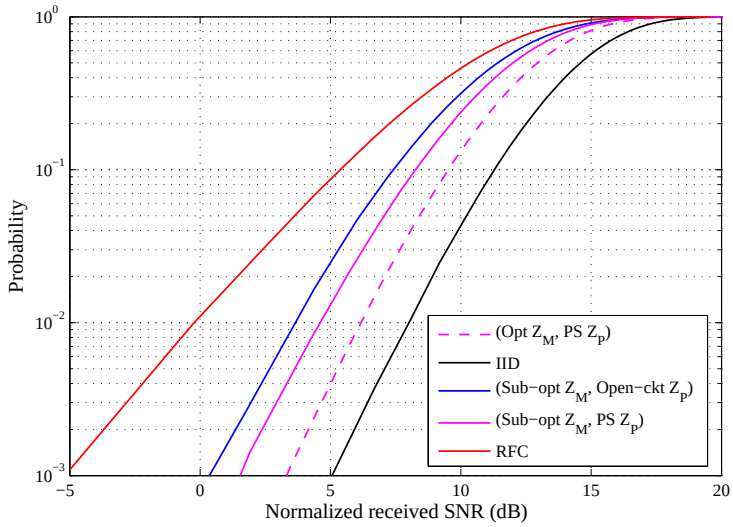

(a) $(4, 2)$

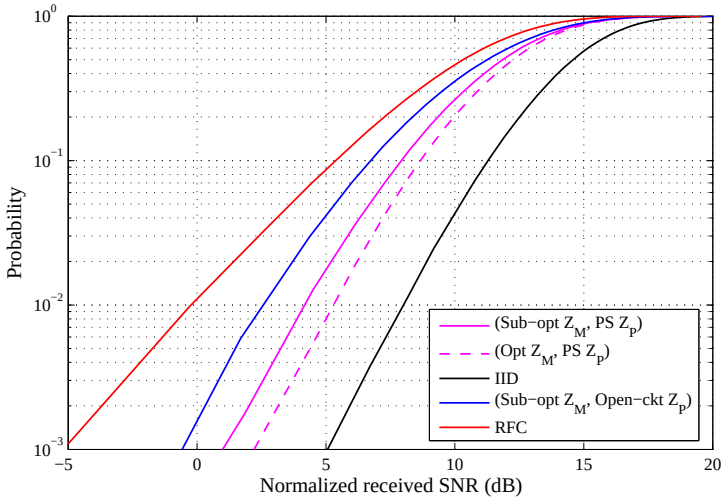

(b) $(4, 1)$

Figure 3.8: Parasitic switching (UCA)

need to build a multiport matching network. Apparently, the loss incurred by employing one less RF chain is recovered by the availability of an additional parasitic element at the cost of an increased overhead as far as the number of parasitic switching states is concerned. It is important to point out that the active element is selectable, unlike

ESPAR systems which employ a single active element with a set of parasitic elements arranged in a circular fashion around it. Similar results are observed for UCA$(4, 2)$ (see Fig. 3.8).

3.4.2 Parasitic Switching with Fixed Active Elements

One drawback of antenna selection is the insertion loss arising due to the presence of switches in the direct RF signal paths. This loss typically ranges from a fraction of a dB to several dB [72], which in our case, will ruin most of the benefits gained by employing any kind of selection in compact arrays. Although certain RF MEMS switches [9] are known to offer less than 1 dB insertion loss at low speeds (switching time in μs), we explore the possibility of ruling out any insertion losses by avoiding switches in the direct RF path.

We study parasitic switching *without selection*, that is, a predetermined set of elements (the ones that provide the optimal *expected* performance) is always active, however, the inactive elements are free to switch to any of the terminations available in $\mathcal{Z}_{\mathcal{P}}$. We consider two cases here: 2 RF chains for AS$(5, 2)$ with far-end elements always active, and 1 RF chain for SC$(5, 1)$ with center element always active.

The results are shown in Fig. 3.9 (F in legend entries denotes *fixed*). It is interesting to note that this technique incurs a loss of only about 1 dB for both optimal and self-matching, while still retaining most of the benefits offered by the parasitic antenna selection. We make a special mention here that having the inactive elements as open-circuited reduces to a conventional 2 element system. This strongly suggests that employing traditional antenna selection for compact arrays is definitely a sub-optimal strategy and that parasitic switching even without selection can offer significant diversity gains.

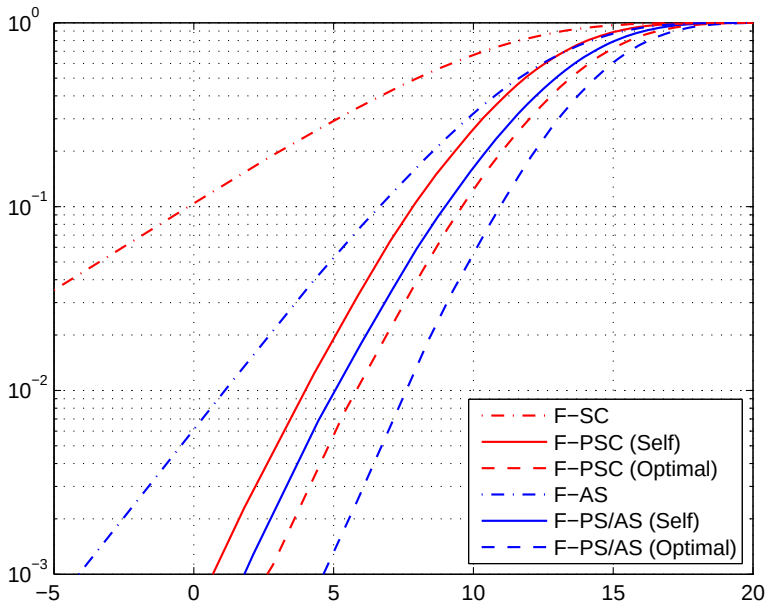

Figure 3.9: Parasitic switching w/o antenna selection (ULA)

3.5 Conclusion

3.5.1 Summary

We presented a realistic model for antenna selection applied to compact receive arrays which accounts for coupling among the elements and models the impact of inactive-element termination on the system performance. We also covered comprehensively various design approaches for antenna selection strategies primarily for two types of uniform arrays - linear and circular. Apart from considering optimal designs for matching networks and parasitic networks, we provided some simpler strategies that achieve near-optimal performance. We also considered designs where we only apply parasitic switching over a predefined set of elements in order to minimize losses arising due to RF switches.

Specifically, we showed that uniform linear arrays could indeed benefit from selection over using all of the available antennas, thereby reducing the number of RF chains and saving power and cost. The performance improvement though, depends on the spacing (i.e., amount of coupling in the system). Based on the space and cost constraints, different array geometries can be designed and employed differently as shown in this chapter. Simulations results reveal that it is critical to account for the behavior of inactive elements at close spacings and that wrong assumptions could result in misleading conclusions. We conclude that antenna selection offers a distinct advantage in portable/handheld or compact devices due to significant coupling among the antennas, and that packing more antennas in a constrained space with appropriate selection strategy can profoundly improve the system performance.

3.5.2 Bandwidth Sensitivity of Optimal Matching

There is one important point about optimal (multiport) matching networks, worth mentioning though. Apparently, these multiport networks can compensate for coupling, even at very close spacings and seem to offer almost i.i.d.-like system performance. Similar results have appeared in the literature elsewhere with regard to diversity and MIMO systems. This however, sounds counter-intuitive, because with reducing inter-element spacing, in limit, the performance of a diversity system should equal that of a single antenna system.

As evident, these gains come at the cost of a reduced RF bandwidth of the system [60], [31]. Fig. 3.10 shows the performance of a receive diversity system with optimal matching computed at the center frequency f_c but employed on a system with different relative bandwidths of 0.2%, 2% and 10%. As can be seen, optimal match is non-robust

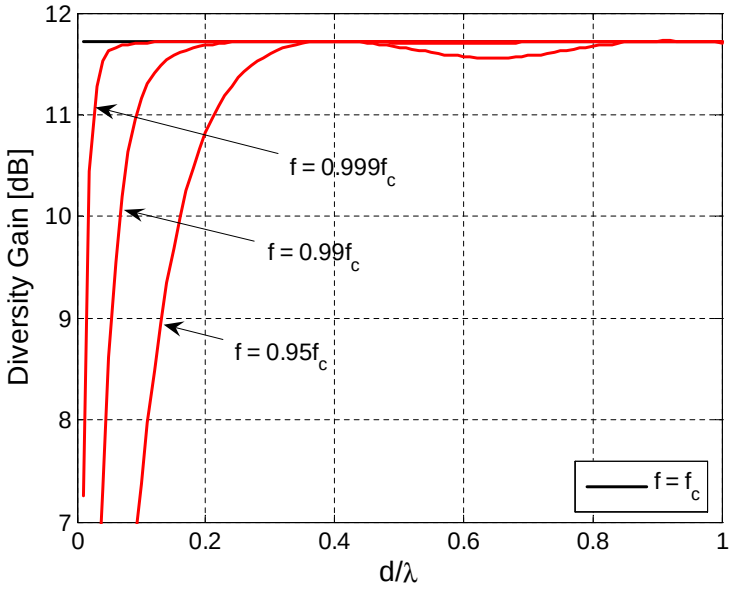

Figure 3.10: Bandwidth sensitivity of optimal matching ([31])

with regard to variations in the actual system bandwidth. However, very little is known about the relationship between the RF bandwidth of a system and antenna coupling, and this intriguing issue motivates us to pursue the design of matching networks suitable for broadband systems, in the remainder of this dissertation.

Chapter 4

Optimal Broadband Matching for SISO Systems

The problem of mutual coupling in MIMO systems, thus far, has been studied from an optimal matching network design standpoint for narrowband systems only. The study and design of matching networks for broadband systems is commonly referred to as *broadband matching theory* or *gain-bandwidth theory* - originally proposed by Bode [5] and later generalized by Fano [35]. In this chapter, we present the fundamentals of Fano's broadband matching theory and establish the theoretical limitations imposed on single antenna systems using a finite lumped element impedance model. We address the issue of SISO optimal broadband matching from an information theory perspective here, and defer the study of optimal matching for coupled broadband MIMO systems to Chapter 5 and Chapter 6.

4.1 Introduction

We introduce the concept of information-theoretic optimal broadband matching with a simple example. Consider a wireless communication system with two antennas placed a distance d apart communicating over the line-of-sight (LOS) at carrier frequency f_c. From Friis' transmission equation [40], the received power-spectral-density (PSD) is given by

$$P_r(f) \quad = \quad P_t(f)G_t(\theta_t, \phi_t)G_r(\theta_r, \phi_r)\left(\frac{c}{4\pi f d}\right)^2 \tag{4.1}$$

where, $P_t(f)$ is the transmitted PSD, G_t, G_r model the antenna gains in the cylindrical co-ordinates and c is the speed of light. For simplicity, we assume both the antennas to be omni-directional with unit gain, i.e., $G_t = G_r = 1$.

The Shannon capacity [86] of such a communication system is given by

$$C = \max_{P_t(f)} \int_{f \in W} \log_2\left(1 + \frac{|H(f)|^2 P_t(f)}{N(f)}\right) df \tag{4.2}$$

where $N(f)$ represents the noise PSD at the receiver, and $|H(f)|^2$ represents the overall transfer function of the system

$$|H(f)|^2 = \left(\frac{c}{4\pi f d}\right)^2$$

The notation, $f \in W$, represents the frequency range such that $P_t(f) \neq 0$. For ease of mathematical tractability, we shall use natural logarithm to use the following definition

of capacity in the rest of the paper

$$C = \max_{P_t(f)} \int_{f \in W} \ln \left(1 + \frac{|H(f)|^2 P_t(f)}{N(f)} \right) df \tag{4.3}$$

Typically, the maximum transmit power available at the output of the power amplifiers in the RF chain is limited. If the power is constrained to be P_0

$$\int_{f \in W} P_t(f) df \leq P_0 \tag{4.4}$$

the optimal power allocation is the well-known *water-pouring* solution [41]

$$P_t(f) = \left[\frac{1}{\xi_{wp}} - \frac{N(f)}{|H(f)|^2} \right]^+ \tag{4.5}$$

where, $[x]^+ = \max(0, x)$ and ξ_{wp} is chosen to satisfy (4.4). Ideally, this is the power radiated from the antenna terminals. However, we know that due to impedance mismatch, the transfer of power from the RF chain to the antennas is not ideal. This loss is typically characterized by *antenna efficiency* or *matching efficiency*

$$|T(f)|^2 = 1 - |\Gamma(f)|^2$$

where, $0 \leq \Gamma(f),\ T(f) \leq 1$ is called the *reflection* and *transmission coefficient*, respectively - a measure of how much signal power is reflected (or rejected) by the antenna. The reflection coefficient is usually defined with the network terminated on both sides in 1 Ω resistances[1] (see Fig. 4.1)

$$\Gamma(f) = \frac{Z_M(f) - 1}{Z_M(f) + 1}$$

[1] A more generalized definition shall be introduced in Chapter 5.

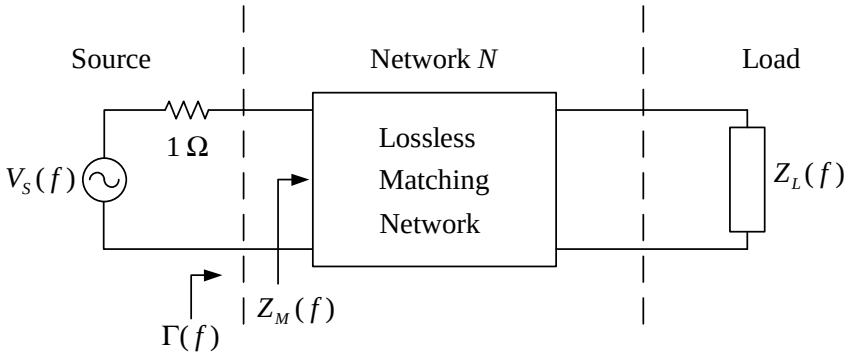

Figure 4.1: A simple matching network

where $Z_M(f)$ is the *driving-point* or input impedance seen looking into the matching network.

Friis' modified transmission equation [97], accounts for this matching efficiency at the transmitter and the receiver by

$$P_r(f) \;=\; P_t(f)|H(f)|^2\left(1-|\Gamma_t(f)|^2\right)\left(1-|\Gamma_r(f)|^2\right)$$

where, $\Gamma_t(f)$, $\Gamma_r(f)$ are the reflection coefficients at the transmit and receive antennas, respectively. The Shannon capacity for the example under consideration is easily altered due to this mismatch as

$$C=\max_{P_t(f)}\int_{f\epsilon W}\ln\left(1+|H(f)|^2(1-|\Gamma_t(f)|^2)(1-|\Gamma_r(f)|^2)\frac{P_t(f)}{N(f)}\right)df \tag{4.6}$$

Ideally, one would want $\Gamma_t(f)=\Gamma_r(f)=0$ throughout the bandwidth of interest, however, broadband matching theory reveals how based on the load and source impedance models, it may not be possible to achieve ideal matching efficiencies.

4.2 Broadband Matching Theory

Bode's [5, Sec. 16.3] investigation of the bandwidth limitations of a matching network terminated into a resistance R shunted by a capacitance C, i.e., $Z_L(s) = (1/R + Cs)^{-1}$, points out the following integral constraint on the reflection coefficient

$$\int_0^\infty 2\pi \ln \frac{1}{|\Gamma(f)|} df \leq \frac{\pi}{RC} \ . \tag{4.7}$$

Here, $s = \sigma + j\omega$ is the Laplace variable and $\omega = 2\pi f$ is the radian frequency. The above equation lays down the trade-off between the magnitude of the reflection coefficient and the bandwidth. In microwave literature, it is customary to assume $\Gamma(f) = \Gamma_{min}$ over a bandwidth W and unity outside, such that from (4.7)

$$|\Gamma|_{min} = e^{-1/2WRC} \ . \tag{4.8}$$

It is the resulting transducer-power gain characteristic $G_p(f^2) = 1 - |\Gamma(f)|^2$, which is realized in practice in the form of a well-known filter response such as Butterworth, Tchebyshev, etc. Fano in his seminal work [35], extended these results and laid the foundations of broadband matching theory. His theory outlines the fundamental limits on the design of broadband matching networks composed of *lumped passive* elements (positive resistors, inductors and capacitors, i.e., $R, L, C \geq 0$), for systems with a resistive source and an arbitrary load impedance. For advances in broadband matching theory and various implementation aspects, [16] is a classic reference.

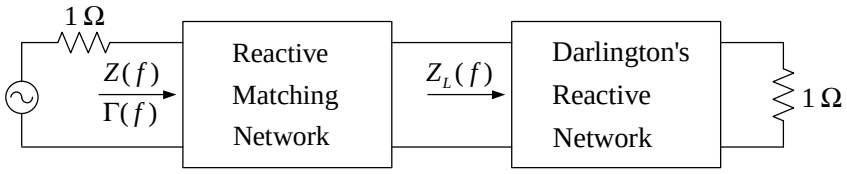

Figure 4.2: Matching network and Darlington's equivalent for Z_L

4.2.1 Matching Constraints

Consider the 2-port network shown in Fig. 4.1, where a resistive source is connected to a frequency-dependent load $Z_L(f)$ by a matching network N. According to Darlington [27], any impedance physically realizable using a finite number of linear passive elements, can be considered as the input impedance of a reactive two-terminal-pair network terminated in a pure resistance which can be transformed into 1 Ω by an appropriate ideal transformer in the reactive network (cf. Fig. 4.2).

As in [35], we turn the network of Fig. 4.2 end to end, as indicated in Fig. 4.3, and call the network resulting from the Darlington representation of the load impedance as N' and the matching network as N''. The reflection and transmission coefficients for the primed networks are denoted by the corresponding primed quantities with the networks terminated on both sides in 1 Ω resistances. The reflection coefficients $\Gamma_1(f)$ and $\Gamma_2(f)$ refer to the whole network N terminated on both sides in 1-ohm resistances. Since N is lossless, $|\Gamma_1(f)| = |\Gamma_2(f)|$.

Using

$$\Gamma_1(f) = \Gamma_1'(f) + \Gamma_1''(f)\frac{T'^2(f)}{1 - \Gamma_2'(f)\Gamma_1''(f)} \ ,$$

it can be shown that [35], the first $2K$ coefficients of the Taylor series for $\ln(1/\Gamma_1(f))$

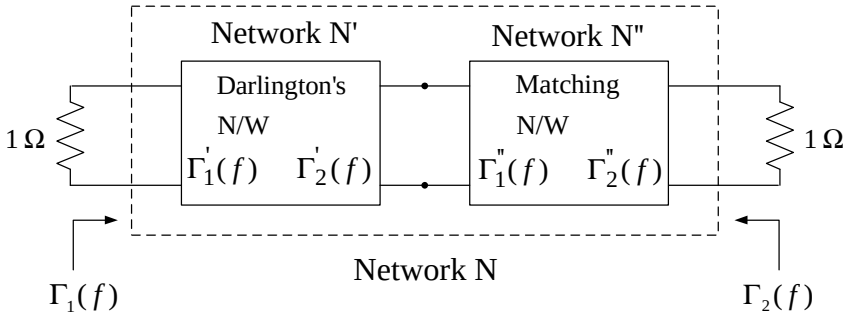

Figure 4.3: Equivalent representation of Fig. 4.2

about a zero of transmission f_z of the network N' (i.e., $T'(f_z) = 0$) of multiplicity K in the right hand s-plane (RHS) or the imaginary axis will be independent of N''. And based on the number of such zeros, there are one or more integral equation constraints that need to be satisfied for a physically realizable matching network.

For a load that has $(k+1)$ zeros of transmission at infinity (i.e., $\lim_{f_z \to \infty} T'^{k+1}(f_z) = 0$), the Taylor series expansion of $\ln(1/\Gamma_1(f))$ about infinity yields an integral equation constraint of the form [2]

$$\int_0^\infty \omega^{2k} \ln \frac{1}{|\Gamma_1(\omega)|} d\omega \leq (-1)^k \frac{\pi}{2} F_{2k+1}^\infty \tag{4.9}$$

where,

$$F_{2k+1}^\infty = \frac{1}{2k+1} \sum_i \left(\lambda_{oi}^{2k+1} - \lambda_{pi}^{2k+1}\right) - \frac{2}{2k+1} \sum_i \lambda_{ri}^{2k+1} \ . \tag{4.10}$$

[2] In general, we evaluate the function around a closed contour C: a semi-circle around the $j\omega$-axis and use

$$\oint_C \log \frac{1}{\Gamma(s)} \, ds = \int_{-j\omega}^{j\omega} \log \frac{1}{\Gamma(s)} \, ds \Big|_{s=j\omega}$$

Here, λ_{pi} and λ_{oi} are the poles and zeros of $\Gamma_1(s)$, respectively, and λ_{ri} are those zeros that lie in the RHS.

For a load that has $(k+1)$ zeros of transmission at zero (i.e., $T'^{k+1}(0) = 0$), the Taylor series expansion of $\ln(1/\Gamma_1)$ about zero yields the following constraint

$$\int_0^\infty \omega^{-(2k+1)} \ln \frac{1}{|\Gamma_1(\omega)|} d\omega \leq (-1)^k \frac{\pi}{2} F_{2k+1}^0 \tag{4.11}$$

where,

$$F_{2k+1}^0 = \frac{1}{2k+1} \sum_i \left(\lambda_{oi}^{-(2k+1)} - \lambda_{pi}^{-(2k+1)} \right) - \frac{2}{2k+1} \sum_i \lambda_{ri}^{-(2k+1)} \ . \tag{4.12}$$

In our study, we consider the case, where the load impedance imposes at least one zero of transmission at infinity:

$$2 \int_0^\infty \ln \frac{1}{|\Gamma_1(f)|^2} df \leq F_1^\infty \tag{4.13}$$

4.3 SISO Optimal Broadband Matching

Consider the LOS communication system shown in Fig. 4.4. It assumes a simplistic transceiver model, where the RF front-end is terminated into 1 Ω resistances (representing downstream components of the RF chain) by a broadband matching network. The Shannon capacity for this system is given by

$$C = \max_{P,\ \Gamma} \int_{f \epsilon W} \ln \left(1 + |H(f)|^2 (1 - |\Gamma(f)|^2) \frac{P(f)}{N(f)} \right) df \tag{4.14}$$

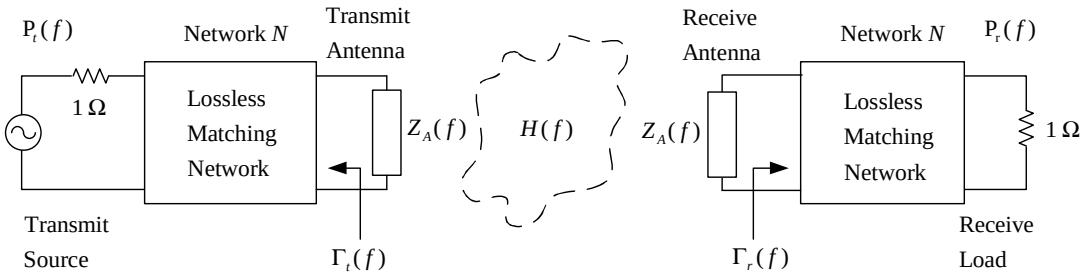

Figure 4.4: LOS communication illustration: System model

where, $\Gamma(f) = \Gamma_r(f)$, $P(f) = P_t(f)$ and

$$|H(f)|^2 = \left(\frac{c}{4\pi f d}\right)^2 \left(1 - |\Gamma_t(f)|^2\right) \ .$$

Observe that we have assumed a fixed or rather a sub-optimal $\Gamma_t(f)$, optimal only at the center frequency. It is straightforward to include $\Gamma_t(f)$ in the optimization, however, to illustrate our point, we limit the optimization over $P(f)$ and $\Gamma(f)$. Also, $H(f)$ can represent any of the frequency-selective transfer functions, e.g., a wireless fading-channel characteristic or a Digital Subscriber Line (DSL) with appropriate modeling of the impedances. We limit the scope of this paper to LOS communications.

Clearly, (4.8) is sub-optimal for (4.14) and does not provide any insight into the optimal bandwidth. To begin, let

$$G(f) = \ln \frac{1}{|\Gamma(f)|^2} \ . \tag{4.15}$$

In microwave literature, a variant of $G(f)$ $(-20 \log_{10} |\Gamma|)$ is commonly referred to as

return loss in dB. We can now rewrite (4.13) as

$$\int_{f\in W} G(f)df \leq G_0 \tag{4.16}$$

where,

$$G_0 = \frac{1}{2}\ F_1^{\infty}\ , \quad 0 \leq G(f) \leq G_0\ .$$

Problem Definition: Maximize the Shannon capacity (in nats/sec)

$$C = \max_{P,\ G} \int_{f\in W} \ln\left(1 + \frac{(1-e^{-G(f)})|H(f)|^2 P(f)}{N(f)}\right) df \tag{4.17}$$

for a given $H(f)$ and $N(f)$, subject to the constraints:

$$(i)\ \int_{f\in W} P(f)df \leq P_0 \tag{4.18}$$

$$(ii)\ \int_{f\in W} G(f)df \leq G_0\ . \tag{4.19}$$

Optimal Solution: The optimal solution is given by

$$P_{opt}(f) = \left[\frac{1}{\xi} - \frac{N(f)}{|H(f)|^2(1-e^{-G_{opt}(f)})}\right]^+\ , \tag{4.20}$$

$$G_{opt}(f) = \left[\ln(1+\mu^{-1}) - \ln\left(1 + \frac{N(f)}{|H(f)|^2 P_{opt}(f)}\right)\right]^+\ , \tag{4.21}$$

where, ξ and μ are chosen to satisfy the power and broadband matching constraints. For detailed optimization, see Appendix B.1. An iterative mutual-water-pouring algorithm based on the optimal solution is presented in Appendix B.2.

4.4 Numerical Results

We now present numerical results for optimal broadband matching.

4.4.1 Impedance Model

We assume a simple resonant model [49] for the transmit and receive antennas: a series RLC circuit. The impedance offered by the transmit (and receive) antenna is given by

$$Z_A(s) = R + Ls + \frac{1}{Cs}$$

The resonant radian-frequency $\omega_0 = 2\pi f_0$ of the circuit is defined such that $Z_L(\omega_0)$ is purely resistive: $\omega_0 = 1/\sqrt{LC}$. It is customary to build systems with the same resonant and carrier-frequencies (i.e., $f_c = f_0$), however, to distinguish modulation and circuit terminology, we shall retain this distinctive nomenclature for reasons that will become clear in the next chapter.

A resonant antenna with its quality-factor Q is well modeled by a series RLC circuit with $R = 1$, $L = Q/\omega_0$ and $C = 1/Q\omega_0$ [49]. The corresponding transmission and reflection coefficient is given, respectively, by

$$T(s) = \left(1 + \frac{Q}{2}\left(\frac{\omega_0}{s} + \frac{s}{\omega_0}\right)\right)^{-1} \tag{4.22}$$

and

$$\Gamma(s) = \frac{1 + (s/\omega_0)^2}{1 + (s/\omega_0)^2 + 2(s/Q\omega_0)} \ . \tag{4.23}$$

The antenna Q is closely related to the 3-dB bandwidth in Hz (B_{3dB}) of a resonant

circuit, defined as the range such that the antenna frequency response

$$1 - |\Gamma(f)|^2 \;\geq\; \frac{1}{2} \,.$$

For the transmit antenna

$$|T_t(f)|^2 = 1 - |\Gamma_t(f)|^2 = \frac{4f^2}{4f^2 + Q^2(f^2 - f_0^2)^2} \,.$$

Using $f_0 = 1$ in the above expression, we get

$$f - \frac{1}{f} = \frac{2}{Q} \implies f \approx 1 \pm \frac{1}{Q}$$

and

$$B_{3dB} \approx \frac{2}{Q} \,.$$

We assume the receiver noise PSD in (4.14) to be

$$N(f) = N_{sky}(f)(1 - |\Gamma(f)|^2) + N_{amp}(f)$$

where, $N_{sky}(f)$ represents the sky-noise and $N_{amp}(f)$ amplifier-noise. We however focus on amplifier-noise-dominant scenarios [43] such that $N(f) = N_{amp}(f)$ and it is assumed to be additive white Gaussian with variance N_0.

Without loss of generality, it is convenient to work with the normalized frequency $f_n = f/f_0$ such that

$$\int_{W_n} P(f_n) df_n \leq P_n = \frac{P_0}{f_0} \,,$$

$$\int_{W_n} G(f_n)df_n \leq G_n = \frac{G_0}{f_0}$$

with W_n being the normalized bandwidth and $C_n = C/f_0$:

$$C_n = \max \int_{f \epsilon W_n} \ln \left(1 + |H(f_n)|^2 (1 - e^{-G(f_n)}) \frac{P(f_n)}{N_0}\right) df_n$$

the normalized capacity, where

$$\begin{aligned} |H(f_n)|^2 &= \alpha f_n^{-2}(1 - |\Gamma_t(f_n)|^2), \quad \alpha = \left(\frac{c}{4\pi f_0 d}\right)^2 \\ &= \frac{1}{f_n^2 + (Q(f_n^2 - 1)/2)^2} \end{aligned} \tag{4.24}$$

and we set $\alpha = 1$.

The transmission coefficient (4.22) has a single zero at origin and a single zero at infinity. The corresponding reflection coefficient (4.23) has zeros $\lambda_o = \pm i\omega_0$ and poles

$$\lambda_p = \frac{\omega_0}{Q}\left(-1 \pm i\sqrt{Q^2 - 1}\right) \ .$$

Therefore, the set of matching constraints are given by

$$\int_{W_n} G(f_n)df_n \leq \frac{2\pi}{Q} = G_n \tag{4.25}$$

$$\int_{W_n} f_n^{-2} G(f_n)df_n \leq \frac{4\pi^2}{Q} = 2\pi G_n \ . \tag{4.26}$$

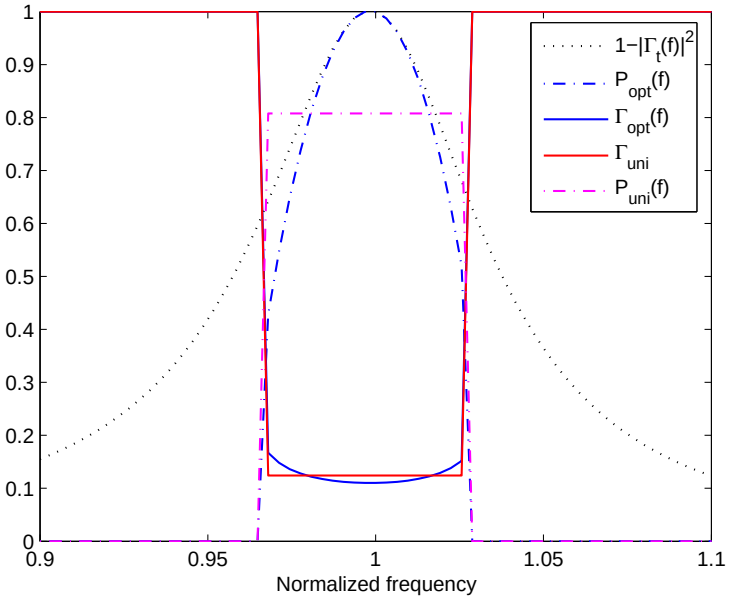

Figure 4.5: Optimal and sub-optimal power spectral density and reflection coefficient characteristic for the antenna example with Q=25

4.4.2 Simulation

Fig. 4.5 shows the result for an antenna with[3] $Q = 25$. The other parameters used for the simulation are $P_n = 1$ and $N_0 = 13$ dB resulting in a peak SNR of 0 dB. The $P(f)$ shown in the figure is normalized such that $\max[P(f)] = 1$. The optimal relative bandwidth W_o in this case is found to be 6.02%. A typical value for the bandwidth of an antenna is characterized by its 3 dB double-sided relative bandwidth [3], which in this case amounts to $W_{3dB} = Q^{-1} = 4\%$. However, it is important to point out that since this is a joint optimization, W_o is a function of SNR.

Fig. 4.5 also shows the performance for a frequency-flat reflection coefficient $\Gamma_{uni}(f) = e^{-G_0/2W_n}$ and the corresponding white $P_{uni}(f) = P_0/W_n$, when optimal bandwidth ($W_o = 6.02\%$) is employed. A nominal penalty of 0.70% in normalized capacity is observed

[3]An overview of typical Q values can be found in [3, Sec. 11.5] and [97, Sec. 8.2]

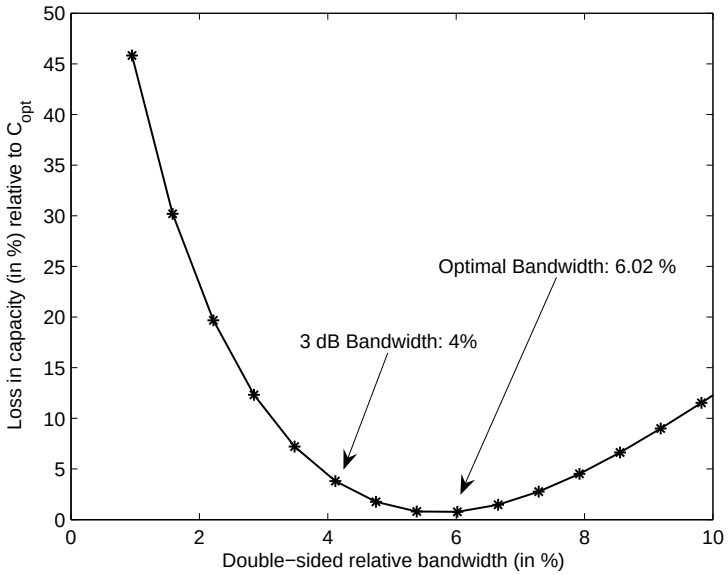

Figure 4.6: Percentage loss in capacity for arbitrary bandwidths relative to the optimal bandwidth

compared to the optimal solution. One of the reason for this lies in the term $1 - e^{-G(f)}$ which for $G_0 \gg 1$ has a negligible impact on the capacity compared to a box-car $G(f) = G_0/W_o$. To further quantify the sub-optimality of bandwidth for (P_{uni}, Γ_{uni}), see Fig. 4.6 which shows the loss in capacity relative to the optimal capacity for different values of W_n.

4.5 Conclusion

We presented an information theoretic approach to characterize the optimal matching of a broadband communication system. We also proposed an iterative algorithm for the optimal solution and demonstrated that a frequency-flat reflection coefficient over an arbitrary bandwidth is not optimal, although, such an approach with optimal bandwidth gives near-optimal results.

In real-world problems, the source or the load impedance may not always be modeled using a finite lumped element model. To circumvent this problem, there exist numerical methods such as real-frequency technique [14]. It is important to point out that there may exist impedances which do not have a constraint like (4.16) to start with, however, a similar approach can be employed. In the next chapter, we address the issue of optimal broadband matching in coupled MIMO systems.

Chapter 5

Matching Theory for Coupled MIMO Systems

In the previous chapter, we witnessed how the trade-off between matching efficiency and bandwidth manifests itself for single antenna systems. In this chapter, we shall build upon our understanding of optimal broadband matching for SISO systems and extend it to coupled MIMO systems. It is worthwhile to develop some intuition before we proceed. Clearly, SISO systems do not exhibit any kind of coupling, but we saw how there exists a constraint on the amount of power that can be absorbed by an antenna. In MIMO systems, we should expect a similar constraint on each antenna, except that, unlike SISO systems, where the incident power can either be absorbed (or rejected), coupled MIMO systems have an additional dimension the power can be channeled through - *coupling*. That is, a part of total power can also be coupled (or transferred) to the other antennas. Thus, as a precursor to what we shall observe later in this chapter, it makes sense to argue a *matrix constraint* on broadband matching for coupled MIMO systems. We begin with a

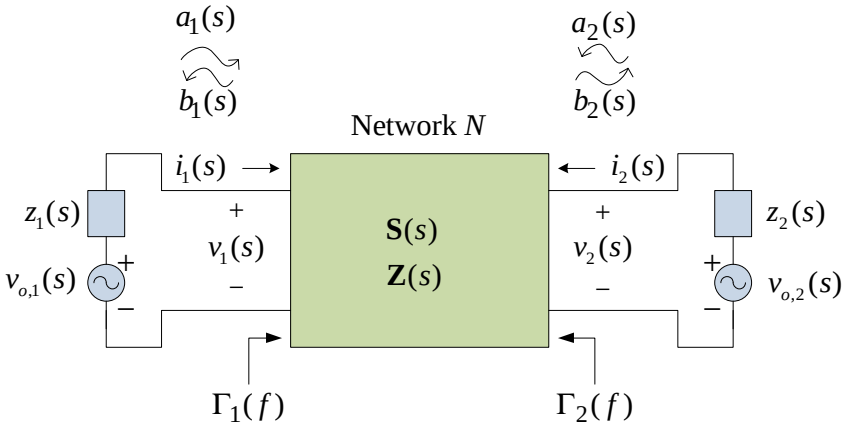

Figure 5.1: Input and output wave vectors for a two-port network

proposition of broadband matching theory for MIMO systems in the presence of mutual coupling, followed by a broadband antenna array impedance model characterization.

5.1 Broadband Matching for Coupled Arrays

In Chapter 3, we saw the impedance-matrix (or Z-matrix) characterization of a multiport network which relates the open-circuit voltages, terminal voltages and currents for each port. Fig. 5.1 shows a broadband 2-port network terminated into *reference impedances* $z_1(s)$ and $z_2(s)$ on either side, such that the corresponding voltage and current vectors, given by

$$\mathbf{v}(s) = \begin{bmatrix} v_1(s) \\ v_2(s) \end{bmatrix} \ , \ \mathbf{v}_o(s) = \begin{bmatrix} v_{o,1}(s) \\ v_{o,2}(s) \end{bmatrix} \ , \ \mathbf{i}(s) = \begin{bmatrix} i_1(s) \\ i_2(s) \end{bmatrix} \ ,$$

share a similar relationship

$$\begin{aligned} \mathbf{v}_o(s) &= \mathbf{v}(s) + \mathbf{z}(s)\mathbf{i}(s) \\ &= (\mathbf{Z}(s) + \mathbf{z}(s))\,\mathbf{i}(s)\ , \end{aligned}$$

where, $\mathbf{z}(s)$ is the *reference impedance* matrix

$$\mathbf{z}(s) = \begin{bmatrix} z_1(s) & 0 \\ 0 & z_2(s) \end{bmatrix}\ ,$$

$\mathbf{Z}(s)$ is the *broadband* impedance matrix of the network. However, when dealing with broadband systems, it is rather convenient to work with S-matrices[1] instead [12], [116]-[119].

5.1.1 Scattering-parameter Matrix

For the 2-port network N considered in Chapter 4, the elements of S-matrix are actually the reflection and transmission coefficients Γ_1, Γ_2 and T, respectively:

$$\mathbf{S}(s) = \begin{bmatrix} \Gamma_1(s) & T(s) \\ T(s) & \Gamma_2(s) \end{bmatrix}\ .$$

The S-matrix relates these voltages and currents through incident and reflected normalized *wave vectors* $\mathbf{a}$ and $\mathbf{b}$, respectively, such that

$$\mathbf{b}(s) = \mathbf{S}(s)\mathbf{a}(s) \tag{5.1}$$

[1] S-matrix is shorthand for *scattering-parameter* or *S-parameter* matrix.

where, as shown in Fig. 5.1,

$$\mathbf{a}(s) = \begin{bmatrix} a_1(s) \\ a_2(s) \end{bmatrix} = \frac{1}{2}\,\mathbf{r}_{mp}^{-1}(s)(\mathbf{v}(s) + \mathbf{z}(s)\mathbf{i}(s)) \ ,$$

$$\mathbf{b}(s) = \begin{bmatrix} b_1(s) \\ b_2(s) \end{bmatrix} = \frac{1}{2}\,\mathbf{r}_{mp}^{-1}(-s)(\mathbf{v}(s) - \mathbf{z}(-s)\mathbf{i}(s)) \ .$$

Here, $\mathbf{r}_{mp}(s)$ represents the *minimum phase* factorization of $\mathbf{r}_z(s)$ - the para-hermitian part $\mathbf{z}(s)$, given as

$$\mathbf{r}_z(s) = \frac{1}{2}(\mathbf{z}(s) + \mathbf{z}(-s)) = \mathbf{r}_{mp}(s)\mathbf{r}_{mp}(-s) \ .$$

Given $\mathbf{z}(s)$ and $\mathbf{Z}(s)$, the S-matrix is readily computed as [16]

$$\mathbf{S}(s) = \mathbf{r}_{mp}(s)(\mathbf{Z}(s) + \mathbf{z}(s))^{-1}(\mathbf{Z}(s) - \mathbf{z}(-s))\mathbf{r}_{mp}^{-1}(-s) \ .$$

When all the ports are terminated into 1 Ω, i.e., $\mathbf{z}(s) = \mathbf{I}\ \Omega$, we have $\mathbf{r}_{mp}(s) = \mathbf{I}\ \Omega$ and

$$\mathbf{S}(s) = (\mathbf{Z}(s) + \mathbf{I})^{-1}(\mathbf{Z}(s) - \mathbf{I}) \ . \tag{5.2}$$

If the network is lossless and reciprocal, its S-matrix has special properties:

$$\mathbf{S}(j\omega)\mathbf{S}^H(j\omega) = \mathbf{I} \ , \quad \mathbf{S}(j\omega) = \mathbf{S}^T(j\omega) \ .$$

For more details and in-depth discussion on scattering-parameter representation, the interested reader is referred to [16]. Having introduced the tools necessary for broadband

MIMO network analysis, we are now ready to present broadband matching theory for coupled MIMO systems, and derive bandwidth constraints imposed by coupled antenna arrays.

5.1.2 Matching Constraints

Fig. 5.2 shows a network model for an N-antenna receiver in S-matrix representation. It shows a cascade of two $2N$-port networks - N_a, representing a coupled lossless and reciprocal antenna array[2], and N_m representing the lossless and reciprocal matching network - terminated into a bank of uncoupled load impedances z_L. The load here is indicative of low noise amplifiers and other downstream components of an RF chain, primarily, demodulators and A/D converters. The EM field incident on the receive antenna array in a wireless propagation environment through multipaths, induces an open-circuit voltage across the antenna terminals, which acts as the *source excitation*, represented by the input wave vector $\mathbf{a}_1$ toward the left of the antenna array.

The individual $2N \times 2N$ S-matrices for the antenna array and matching network, in $N \times N$ block-matrix format normalized with respect to 1 Ω reference impedances, are given by

$$\mathbf{S}_A = \begin{bmatrix} \mathbf{S}_{11a} & \mathbf{S}_{12a} \\ \mathbf{S}_{21a} & \mathbf{S}_{22a} \end{bmatrix}, \quad \mathbf{S}_M = \begin{bmatrix} \mathbf{S}_{11m} & \mathbf{S}_{12m} \\ \mathbf{S}_{21m} & \mathbf{S}_{22m} \end{bmatrix},$$

where we have omitted the frequency-dependence by suppressing (s) for aesthetic reasons. We shall henceforth, assume it implied, unless stated otherwise. Note that we have

[2]It is important to point out that the antenna array is essentially an N-port network *appropriately extended* to a $2N$-port network for mathematical convenience [100].

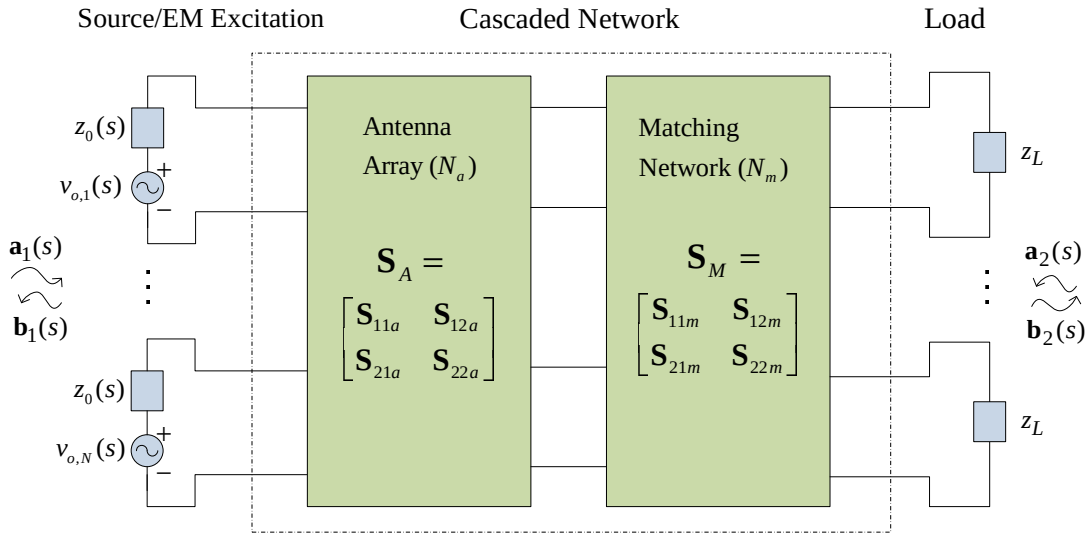

Figure 5.2: S-matrix representation of RF front-end

assumed the source and load impedances to be 1 Ω. Clearly, this is a very simplified model for a multi-antenna transceiver. However, in order to get our point across, it is necessary, so as not to get lost in the details. We shall revisit this issue later with emphasis on a much detailed model and its implications.

The overall $2N$-port network of cascades has an S-matrix

$$\mathbf{S}_C = \mathbf{S}_A \odot \mathbf{S}_M = \begin{bmatrix} \mathbf{S}_{11c} & \mathbf{S}_{12c} \\ \mathbf{S}_{21c} & \mathbf{S}_{22c} \end{bmatrix}$$

where, $\odot$ represents the cascading operation. The inward and outward traveling wave vectors are related by (5.1) except that, the input and output wave-vectors at the left are now vectors, denoted by $\mathbf{a}_1$ and $\mathbf{b}_1$, respectively. Those on the right side are denoted

by $\mathbf{a}_2$ and $\mathbf{b}_2$. These are related to the sub-blocks of $\mathbf{S}_C$

$$\mathbf{S}_{11c} = \mathbf{S}_{11a} + \mathbf{S}_{12a}(\mathbf{I} - \mathbf{S}_{11m}\mathbf{S}_{22a})^{-1}\mathbf{S}_{11m}\mathbf{S}_{21a} \tag{5.3a}$$

$$\mathbf{S}_{12c} = \mathbf{S}_{12a}(\mathbf{I} - \mathbf{S}_{11m}\mathbf{S}_{22a})^{-1}\mathbf{S}_{12m} \tag{5.3b}$$

$$\mathbf{S}_{21c} = \mathbf{S}_{21m}(\mathbf{I} - \mathbf{S}_{22a}\mathbf{S}_{11m})^{-1}\mathbf{S}_{21a} \tag{5.3c}$$

$$\mathbf{S}_{22c} = \mathbf{S}_{22m} + \mathbf{S}_{21m}(\mathbf{I} - \mathbf{S}_{22a}\mathbf{S}_{11m})^{-1}\mathbf{S}_{22a}\mathbf{S}_{12m} \ . \tag{5.3d}$$

in the fashion

$$\begin{bmatrix} \mathbf{b}_1 \\ \mathbf{b}_2 \end{bmatrix} = \begin{bmatrix} \mathbf{S}_{11c} & \mathbf{S}_{12c} \\ \mathbf{S}_{21c} & \mathbf{S}_{22c} \end{bmatrix} \begin{bmatrix} \mathbf{a}_1 \\ \mathbf{a}_2 \end{bmatrix} \ . \tag{5.4}$$

From the above relation, the output wave vector from the matching network - representing the input to the rest of the RF chain, is given by

$$\mathbf{b}_2(s) = \mathbf{S}_{21c}(s)\mathbf{a}_1(s) + \mathbf{S}_{22c}(s)\mathbf{a}_2(s) \tag{5.5}$$

Zero of Transmission: Similar to the approach by Fano (as discussed in Chapter 3), we shall describe a zero of transmission s_0 as a point where the output of the matching network is zero:

$$\mathbf{b}_2(s)|_{s=s_0} = \mathbf{0} \tag{5.6}$$

Since the excitation is assumed toward the left of antenna network N_a ($\mathbf{a}_2(s_0) = \mathbf{0}$), it

suffices to conclude from (5.5) that

$$\mathbf{S}_{21c}(s_0)\mathbf{a}_1(s_0) = \mathbf{0}$$

To find gain-bandwidth bounds *independent* of N_m and valid for *all* input wave-vectors, from (5.3c) we must have[3]

$$\mathbf{S}_{21a}(s)|_{s=s_0} = \mathbf{0} \ . \tag{5.7}$$

That is, matrix $\mathbf{S}_{21a}$ must identically go to zero.

Previous studies on broadband matching theory, have addressed the problem of multiport matching network design for uncoupled 2-port networks. This is equivalent to having a block-diagonal $\mathbf{S}_A$ in Fig. 5.2, and hence a block-diagonal $\mathbf{S}_C$. The matching constraints on the overall network are imposed by these 2-port networks on the reflection coefficient at each of the port, in other words, the diagonal[4] entries of $\mathbf{S}_C$. The physical interpretation of these constraints is that the amount of power that can be transfered from the input port to the output is bounded.

Along those lines, it can be argued that for coupled systems, matching constraints are a measure of how much power can be absorbed by an antenna itself and how much can be coupled to the neighboring elements. This leads us to conclude that the matching constraints must be imposed on $\mathbf{S}_C$ matrix. The challenge then, is to devise matching networks build from lumped passive elements that obey these constraints in order to ensure optimal matching efficiency. For a lossless and reciprocal matching network, the

[3]Recall, for 2 port problem addressed by Fano, this reduces to having $T'(s_0) = 0$.

[4]Since the off-diagonal entries are related to the diagonal entries by the lossless property.

cascaded network is lossless and reciprocal too, i.e.,

$$\mathbf{S}_C^H \mathbf{S}_C = \mathbf{I} \ , \ \mathbf{S}_C = \mathbf{S}_C^T$$

which yields the following conditions:

$$\begin{aligned} \mathbf{S}_{11c}^H \mathbf{S}_{11c} + \mathbf{S}_{21c}^H \mathbf{S}_{21c} &= \mathbf{I} \ , \\ \mathbf{S}_{12c}^H \mathbf{S}_{12c} + \mathbf{S}_{22c}^H \mathbf{S}_{22c} &= \mathbf{I} \ , \\ \mathbf{S}_{11c}^H \mathbf{S}_{12c} + \mathbf{S}_{21c}^H \mathbf{S}_{22c} &= \mathbf{0} \ . \end{aligned}$$

Based on the above relationships, it suffices to look at the Laurent series expansion of the entries of $\mathbf{S}_{11c}$ only, about the zeros of transmission of $\mathbf{S}_{21a}$. Thus, the constraints assume the most general form

$$\oint_C \log \mathbf{S}_{11c}(s) ds = \lim_{\omega \to \infty} \left[\begin{array}{cc} \int_{i\omega}^{-i\omega} \log \frac{1}{\Gamma_1(s)} ds & \int_{i\omega}^{-i\omega} \log \frac{1}{T_{12}(s)} ds \\ \int_{i\omega}^{-i\omega} \log \frac{1}{T_{12}(s)} ds & \int_{i\omega}^{-i\omega} \log \frac{1}{\Gamma_1(s)} ds \end{array} \right]_{s=j\omega} . \qquad (5.8)$$

However, before arriving at the appropriate constraints, we must characterize the antenna array S-matrix $\mathbf{S}_A$.

5.1.3 Characterizing Antenna Array S-Matrix

In order to establish $\mathbf{S}_A$, it is convenient to look at the impedance matrix $\mathbf{Z}_A$ of the antenna array. An antenna array with $N = 2$ identical elements placed a distance d

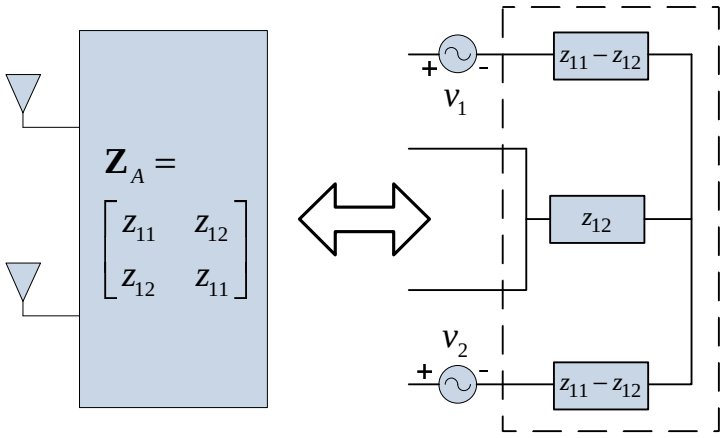

Figure 5.3: Impedance matrix representation of a 2-element array

(normalized to the center-wavelength[5] λ_c) apart, has a symmetric impedance matrix of the form (cf. Fig. 5.3)

$$\mathbf{Z}_A(j\omega) = \begin{bmatrix} z_{11}(j\omega) & z_{12}(j\omega) \\ z_{12}(j\omega) & z_{11}(j\omega) \ . \end{bmatrix}$$

The circulant nature of $\mathbf{Z}_A$ above, lets us rewrite it in terms of its eigen-value decomposition (EVD)

$$\mathbf{Z}_A(j\omega) = \mathbf{Q}\mathbf{\Lambda}_A(j\omega)\mathbf{Q}^H \ , \tag{5.9}$$

where the set of unitary eigen-vectors is given by

$$\mathbf{Q} \ = \ \frac{1}{\sqrt{2}} \begin{bmatrix} 1 & 1 \\ 1 & -1 \end{bmatrix} \ .$$

[5]To distinguish narrowband systems (where we used λ to denote the system wavelength) from broadband, we introduce the term center-wavelength $\lambda_c = c/f_c$, where c is the speed of light.

The eigen-values are given by

$$\mathbf{\Lambda}_A(j\omega) = \begin{bmatrix} \lambda_1(j\omega) & 0 \\ 0 & \lambda_2(j\omega) \end{bmatrix} = \begin{bmatrix} z_{11}(j\omega) + z_{12}(j\omega) & 0 \\ 0 & z_{11}(j\omega) - z_{12}(j\omega) \end{bmatrix} . \quad (5.10)$$

Henceforth, we shall refer to the eigen-values $\lambda_n(j\omega)$, $n = 1, \ldots, N$, of antenna impedance $\mathbf{Z}_A$, as *eigen-impedances*. Observe the explicit frequency-independence of $\mathbf{Q}$ highlighted in (5.9). This will turn out to be quite useful in analyzing the matching constraints on coupled MIMO systems and implementing the optimal matching network, as will be discussed later.

Next, we examine $\mathbf{S}_A$ and its components. The antenna array is essentially an N-port network which can be appropriately extended to a $2N$-port network for mathematical convenience [100]. The N-port representation of the antenna array is the $\mathbf{S}_{22a}$ block itself which can be computed using (5.2), as

$$\mathbf{S}_{22a}(j\omega) = (\mathbf{Z}_A(j\omega) + \mathbf{I})^{-1}(\mathbf{Z}_A(j\omega) - \mathbf{I}) .$$

The other blocks must be evaluated based on the lossless ($\mathbf{S}_A^H\mathbf{S}_A = \mathbf{I}$) and reciprocal ($\mathbf{S}_A = \mathbf{S}_A^T$) properties of the antenna array. The symmetry of the system under consideration and that of the individual blocks constituting $\mathbf{S}_A$, further allows us to write (using EVD)

$$\mathbf{S}_A = \begin{bmatrix} \mathbf{S}_{22a} & \mathbf{S}_{21a} \\ \mathbf{S}_{21a} & \mathbf{S}_{22a} \end{bmatrix} = \begin{bmatrix} \mathbf{Q} & \mathbf{0} \\ \mathbf{0} & \mathbf{Q} \end{bmatrix} \begin{bmatrix} \mathbf{\Lambda}_{11a} & \mathbf{\Lambda}_{12a} \\ \mathbf{\Lambda}_{21a} & \mathbf{\Lambda}_{22a} \end{bmatrix} \begin{bmatrix} \mathbf{Q}^H & \mathbf{0} \\ \mathbf{0} & \mathbf{Q}^H \end{bmatrix} .$$

Since, broadband matching theory requires an impedance to be analytic over the

entire s-plane, the resistive part must be an even function of ω and the reactive part an odd function of ω. For simplicity and without loss of generality, we assume that the resistive part of the antenna impedance matrix ($\mathbf{R}_A = \mathrm{Re}(\mathbf{Z}_A)$) is fairly constant over the frequency range of interest. Although more rigorous models can be developed, it will be shown later that the system behavior is essentially governed by the antenna reflection coefficient, magnitude-squared. Notably, the bound on the matching efficiency is also determined by the poles and zeros of the reflection coefficient, which will be shown to closely approximate that of a series RLC model against the numerical data. Therefore, for eigen-impedances of the form $\lambda(j\omega) = R + jX(\omega)$, where R and X represent the real and imaginary parts, respectively, we have

$$\begin{aligned} \mathbf{\Lambda}_{22a}(j\omega) &= (\mathbf{\Lambda}_A(j\omega) + \mathbf{I})^{-1}(\mathbf{\Lambda}_A(j\omega) - \mathbf{I}) \\ &= \mathbf{\Lambda}_{11a}(j\omega) \ , \qquad (5.11) \\ \mathbf{\Lambda}_{21a}(j\omega) &= \mathbf{I} - \mathbf{\Lambda}_{22a}(j\omega) \\ &= \mathbf{\Lambda}_{12a}(j\omega) \ . \qquad (5.12) \end{aligned}$$

Details can be found in Appendix C.

5.1.4 Virtual Antennas

Observe that the zeros of transmission defined in (5.7), remain unchanged under the unitary transformation

$$\mathbf{S}_{21a}(j\omega) = \mathbf{Q}\mathbf{\Lambda}_{21a}(j\omega)\mathbf{Q}^H$$

Assuming a symmetric and reciprocal matching network due to the inherent symmetry in the problem, we have

$$\mathbf{S}_M = \begin{bmatrix} \mathbf{Q} & \mathbf{0} \\ \mathbf{0} & \mathbf{Q} \end{bmatrix} \begin{bmatrix} \mathbf{\Lambda}_{11m} & \mathbf{\Lambda}_{21m} \\ \mathbf{\Lambda}_{21m} & \mathbf{\Lambda}_{11m} \end{bmatrix} \begin{bmatrix} \mathbf{Q}^H & \mathbf{0} \\ \mathbf{0} & \mathbf{Q}^H \end{bmatrix} \tag{5.13}$$

such that (5.3) allows us to write the overall cascaded network in block-matrix format as

$$\mathbf{S}_C = \begin{bmatrix} \mathbf{Q} & \mathbf{0} \\ \mathbf{0} & \mathbf{Q} \end{bmatrix} \begin{bmatrix} \mathbf{\Lambda}_{11c} & \mathbf{\Lambda}_{12c} \\ \mathbf{\Lambda}_{12c} & \mathbf{\Lambda}_{11c} \end{bmatrix} \begin{bmatrix} \mathbf{Q}^H & \mathbf{0} \\ \mathbf{0} & \mathbf{Q}^H \end{bmatrix} .$$

Since we are interested in finding the coefficient constraints on the Laurent series expansion of $\mathbf{S}_{11c}$ as outlined in (5.8), it suffices to analyze the constraints on its eigen-values (cf. (5.3a)) given by

$$\mathbf{\Lambda}_{11c} = \mathbf{\Lambda}_{11a} + \mathbf{\Lambda}_{12a}(\mathbf{I} - \mathbf{\Lambda}_{11m}\mathbf{\Lambda}_{22a})^{-1}\mathbf{\Lambda}_{11m}\mathbf{\Lambda}_{21a} .$$

This is equivalent to saying that the problem of matching the coupled antenna array $\mathbf{Z}_A$ has been replaced by that of a uncoupled *virtual antenna array* $\mathbf{\Lambda}_A$, where the proposed matching structure is illustrated in Fig. 5.4. The unitary transformation represented by $\mathbf{Q}$ is essentially an orthogonal *beam-forming matrix* implemented using RF networks called *beam-formers* consisting of power-dividers and phase shifters [82]. These beam-formers are capable of producing N (number of antennas) spatially orthogonal beams. One of the well known and widely used matrix is the *Butler matrix* [11], representing *spatial* FFT operations and applicable to arrays with 2^n number of antennas (e.g., $N = 2, 4, 8, 16$). In terms of the antenna radiation patterns, this operation can be thought of

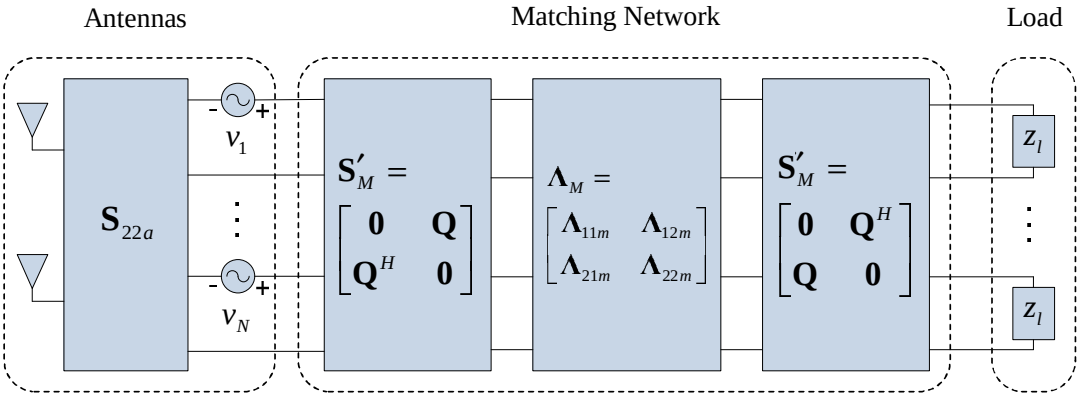

Figure 5.4: Optimal matching implementation using decoupling networks

as decomposing the composite *array pattern* into overlapping but mutually orthogonal patterns at the output of the beam-former.

It is worthwhile to realize that the entire analysis of broadband matching has been considerably simplified due to the frequency-independent nature of this spatial-unitary transformation. The complete set of diagonal matrices representing $\mathbf{S}_C$ is given by

$$\mathbf{\Lambda}_{11c} = \mathbf{\Lambda}_{11a} + \mathbf{\Lambda}_{12a}(\mathbf{I} - \mathbf{\Lambda}_{11m}\mathbf{\Lambda}_{22a})^{-1}\mathbf{\Lambda}_{11m}\mathbf{\Lambda}_{21a} \ , \tag{5.14a}$$

$$\mathbf{\Lambda}_{12c} = \mathbf{\Lambda}_{12a}(\mathbf{I} - \mathbf{\Lambda}_{11m}\mathbf{\Lambda}_{22a})^{-1}\mathbf{\Lambda}_{12m} \ , \tag{5.14b}$$

$$\mathbf{\Lambda}_{21c} = \mathbf{\Lambda}_{21m}(\mathbf{I} - \mathbf{\Lambda}_{22a}\mathbf{\Lambda}_{11m})^{-1}\mathbf{\Lambda}_{21a} \ , \tag{5.14c}$$

$$\mathbf{\Lambda}_{22c} = \mathbf{\Lambda}_{22m} + \mathbf{\Lambda}_{21m}(\mathbf{I} - \mathbf{\Lambda}_{22a}\mathbf{\Lambda}_{11m})^{-1}\mathbf{\Lambda}_{22a}\mathbf{\Lambda}_{12m} \ . \tag{5.14d}$$

It can easily be verified using (5.3) that the matching network $\mathbf{S}_M$ can be realized as a cascade of three $2N$-port networks [37]

$$\mathbf{S}_M = \mathbf{S}'_M \odot \mathbf{\Lambda}_M \odot \mathbf{S}''_M$$

with **S**-matrices given by

$$\mathbf{S}'_M = \begin{bmatrix} \mathbf{0} & \mathbf{Q} \\ \mathbf{Q}^H & \mathbf{0} \end{bmatrix}, \quad \mathbf{S}''_M = \begin{bmatrix} \mathbf{0} & \mathbf{Q}^H \\ \mathbf{Q} & \mathbf{0} \end{bmatrix}, \quad \mathbf{\Lambda}_M = \begin{bmatrix} \mathbf{\Lambda}_{11m} & \mathbf{\Lambda}_{21m} \\ \mathbf{\Lambda}_{21m} & \mathbf{\Lambda}_{11m} \end{bmatrix} .$$

This cascade realizes the block diagonalizing decomposition of $\mathbf{S}_M$ in (5.13). A quick observation of the cascade of $\mathbf{S}_{22a}$ and $\mathbf{S}'_M$ below

$$\begin{aligned} \mathbf{S} &= \mathbf{S}_{22a} \odot \mathbf{S}'_M \\ &= \mathbf{S}'_{22m} + \mathbf{S}'_{21m}(\mathbf{I} - \mathbf{S}_{22a}\mathbf{S}'_{22m})^{-1}\mathbf{S}_{22a}\mathbf{S}'_{12m} \\ &= \mathbf{Q}^H\mathbf{S}_{22a}\mathbf{Q} = \mathbf{\Lambda}_{22a} \ , \end{aligned}$$

reveals that $\mathbf{S}'_M$ is seen to *decouple* the antenna array into its eigen-values (cf. (5.11)). Therefore, optimal matching can be achieved by directly matching $\mathbf{\Lambda}_{22a}$ by $\mathbf{\Lambda}_M$, and the block $\mathbf{S}''_M$ is redundant. Hence, the new matching network has an S-matrix given by

$$\begin{aligned} \mathbf{S}_M &= \mathbf{S}'_M \odot \mathbf{\Lambda}_M \\ &= \begin{bmatrix} \mathbf{Q} & \mathbf{0} \\ \mathbf{0} & \mathbf{I} \end{bmatrix} \begin{bmatrix} \mathbf{\Lambda}_{11m} & \mathbf{\Lambda}_{12m} \\ \mathbf{\Lambda}_{21m} & \mathbf{\Lambda}_{22m} \end{bmatrix} \begin{bmatrix} \mathbf{Q}^H & \mathbf{0} \\ \mathbf{0} & \mathbf{I} \end{bmatrix} \end{aligned}$$

instead of (5.13), in which case, the overall S-matrix is given by (5.14d).

In either case, using EVD we can rewrite (5.8) as

$$\int_{-j\omega}^{j\omega} \log \mathbf{S}_{11c}(s)ds = \mathbf{Q}\left[\lim_{\omega\to\infty} \int_{j\omega}^{-j\omega} \log \mathbf{\Lambda}_{11c}(s)ds\right]\mathbf{Q}^H \ .$$

Having introduced the concept of virtual antennas above, we proceed to find the

integral constraints for the uncoupled eigen-impedances. To avoid unnecessary subscripts, we make a notational change

$$\begin{bmatrix} \mathbf{\Lambda}_{11c} & \mathbf{\Lambda}_{12c} \\ \mathbf{\Lambda}_{21c} & \mathbf{\Lambda}_{22c} \end{bmatrix} \triangleq \begin{bmatrix} \mathbf{\Gamma} & \mathbf{T} \\ \mathbf{T} & \mathbf{\Gamma} \end{bmatrix} , \tag{5.15}$$

such that the entries of

$$\mathbf{\Lambda}_{11c}(s) \;=\; \mathbf{\Gamma}(s) \;=\; \begin{bmatrix} \Gamma_1(s) & 0 \\ 0 & \Gamma_2(s) \end{bmatrix} ,$$

represent the reflection coefficients at the input of the virtual antennas. A coefficient constraint on $\Gamma_n(s)$, $n = 1, 2$, implies

$$\begin{aligned} \int_0^\infty G_n(f)\; df &= \int_0^\infty \log \frac{1}{|\Gamma_n(f)|^2}\; df \\ &= \pi \sum_{i=1}^{n_s} \mathrm{Res}\left(\log \frac{1}{\Gamma_n(s)}(s), s_i \right) \end{aligned}$$

where,

$$G_n(f) \triangleq \log \frac{1}{|\Gamma_n(f)|^2} , \tag{5.16}$$

and $\mathrm{Res}(g_n(s), s_i)$ represents the residue of a function $g_n(s)$ at singularity s_i, $i = 1, \ldots, n_s$.

The finding that exactly two quantities are being constrained for a 2-element coupled array, stems from the fact that the antenna array is essentially a 2-port network in this example. Physically, these constraints represent two things: (i) the amount of power being absorbed by each antenna and, (ii) the amount of power being coupled to the

other antenna.

Let us now consider an array of two ideal and identical antennas placed sufficiently far apart. Each resonant antenna can be well modeled by a series RLC circuit. For such an array, $\mathbf{Z}_A$ is diagonal. As we know, a resonant antenna with a series RLC equivalent, can alternatively be expressed in terms of its *resonant frequency* ω_0 and *quality factor* Q, where:

$$\omega_0 = \frac{1}{\sqrt{LC}}, \quad Q = \frac{1}{R}\sqrt{\frac{L}{C}}$$

As the spacing between the antennas decreases, electro-magnetic interactions start to alter the spectral responses of the individual antennas. Numerical simulations suggest that the eigen-impedances still conform to that of a resonant antenna, as will be discussed next.

5.1.5 Eigen-Impedance Characterization

Recall from (5.10) that the eigen-impedances are a linear function of self and mutual impedances, hence, they can be modeled using a series RLC equivalent as well:

$$\lambda_1(s) = R_1 + L_1 s + \frac{1}{C_1 s}$$

$$\lambda_2(s) = R_2 + L_2 s + \frac{1}{C_2 s}$$

where, $R_{1,2} > 0$, $L_{1,2} > 0$, $C_{1,2} > 0$ such that the self and mutual impedances are given by

$$\begin{aligned} z_{11}(s) &= \frac{1}{2}\left(\lambda_1(s) + \lambda_2(s)\right) \\ &= R_+ + L_+ s + \frac{1}{C_+ s} = z_{22}(s) \ , \\ z_{12}(s) &= \frac{1}{2}\left(\lambda_1(s) - \lambda_2(s)\right) \\ &= R_- + L_- s + \frac{1}{C_- s} = z_{21}(s) \ , \end{aligned}$$

where, $R_{+,-} > 0$, $L_{+,-} > 0$, $C_{+,-} > 0$. Observe that we can rewrite the eigen-impedances as

$$\lambda_n(j\omega) = R_n + j \underbrace{\left(L_n\omega - \frac{1}{C_n\omega}\right)}_{X_n(\omega)}, \quad n = 1, 2$$

which upon the substitution of

$$L_n = R_n Q_n/\omega_{0n} \ , \quad C_n = 1/Q_n R_n \omega_{0n} \ , \quad n = 1, 2$$

assumes the form

$$\lambda_n(j\omega) = R_n \left[1 + jQ_n \left(\frac{\omega}{\omega_{0n}} - \frac{\omega_{0n}}{\omega}\right)\right] \ .$$

The corresponding reflection and transmission coefficients

$$\mathbf{\Lambda}_{11a}(s) \;=\; \begin{bmatrix} \Gamma'_1(s) & 0 \\ 0 & \Gamma'_2(s) \end{bmatrix} \;,\; \mathbf{\Lambda}_{21a}(s) \;=\; \begin{bmatrix} T'_1(s) & 0 \\ 0 & T'_2(s) \end{bmatrix}$$

normalized to R_n Ω impedances are given by[6]

$$\Gamma'_n(s) \;=\; \frac{\lambda_n(s) - R_n}{\lambda_n(s) + R_n} \;=\; \frac{1 + (s/\omega_{0n})^2}{1 + (s/\omega_{0n})^2 + 2(s/Q_n\omega_{0n})} \tag{5.17}$$

$$T'_n(s) \;=\; \left(1 + \frac{Q_n}{2}\left(\frac{\omega_{0n}}{s} + \frac{s}{\omega_{0n}}\right)\right)^{-1} \tag{5.18}$$

for $n = 1, 2$. The frequency response of the *virtual antennas* can be written as

$$|T'_n(f)|^2 = 1 - |\Gamma'_n(f)|^2 = \frac{4f^2}{4f^2 + Q_n^2(f^2 - f_{0n}^2)^2} \tag{5.19}$$

which we shall refer to as the *eigen-modes* of the array.

Therefore, the matching constraints imposed on $\mathbf{\Gamma}(s)$ by $\mathbf{\Lambda}_{11a}(s)$ based on Laurent series expansion of $\mathbf{\Gamma}(s)$ about the zeros of transmission of $\mathbf{\Lambda}_{21a}(s)$ (which are at origin and infinity, with a single multiplicity), are given as

$$\int_0^\infty \log \frac{1}{|\Gamma_n(f)|^2}\; df \leq G_{0n} \;.$$

G_{0n}'s are evaluated using [35] (as discussed in Chapter 4 for single antenna)

$$G_{0n} = \frac{1}{2k+1}\left[\sum_i \left(z_{ni}^{2k+1} - p_{ni}^{2k+1}\right) - 2\sum_i r_{ni}^{2k+1}\right] \;. \tag{5.20}$$

[6]From (5.2), this can be shown in a trivial manner.

Here, z, p represent the zeros and poles of $\Gamma_n'(s)$ and r are the RHS zeros [49]:

$$z_n = \pm j\omega_{0n}, \quad p_n = \frac{\omega_{0n}}{Q_n}\left(-1 \pm j\sqrt{Q_n^2 - 1}\right) \ .$$

Finally, we have the set of broadband matching constraints for a coupled MIMO array:

$$(a) \qquad \int_W G_n(f)df \leq \frac{2\pi f_{0n}}{Q_n} = G_{0n} \qquad , \tag{5.21a}$$

$$(b) \qquad \int_W f^{-2} G_n(f)df \leq \frac{4\pi^2 f_{0n}^2}{Q_n} \qquad . \tag{5.21b}$$

The second constraint above was found to be inactive in almost all the cases that were considered in this study. For certain cases, it is straightforward to see this for bandwidths around 10%. We shall therefore, ignore the second constraint in the remainder of the dissertation.

5.2 Numerical Results

In this section, we present numerical results for optimal broadband matching for $N = 2$ element uniform circular array of dipole antennas with length[7] $0.475\lambda_c$ and radius $10^{-3}\lambda_c$, spaced $d = 0.25\lambda_c$ apart.

5.2.1 Impedance Parameters

Fig. 5.5(a) shows the self and mutual impedance for this array calculated using NEC. The corresponding eigen-impedance values are shown in Fig. 5.5(b). The resistive and reactive parts of the impedance are in general, a non-linear function of frequency. The

[7]The length is chosen such that each antenna in isolation, has a relative resonance frequency of 1.

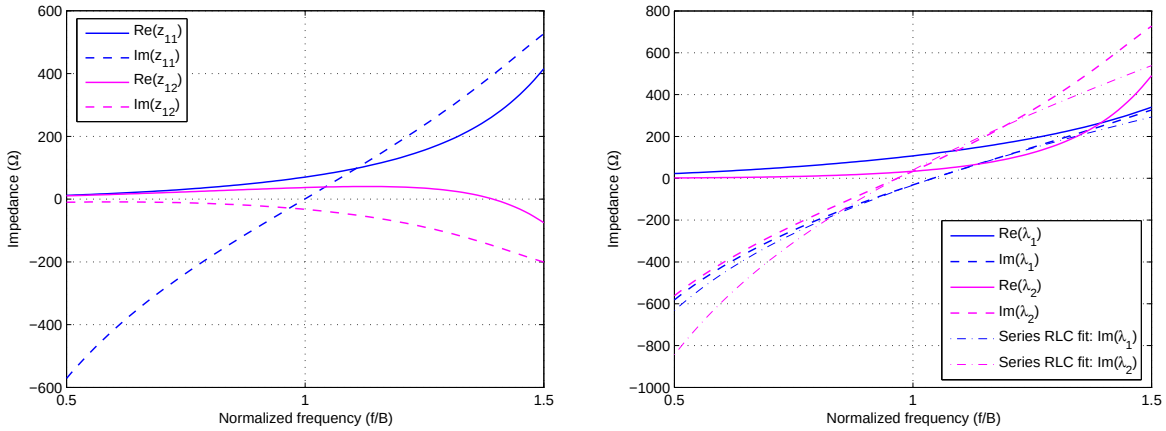

(a) Self- and mutual-impedance (b) Eigen-impedance

Figure 5.5: $N = 2$, $d = 0.25\lambda_c$

figure also shows the imaginary part of eigen-impedances obtained by series RLC-fit which evidently, is in close agreement for bandwidths on the order of 10%. Although it can be argued that the resistive part (using a series RLC model) may not be a good fit, we consider this simple model essentially because of its ease of analysis. The main results and ideas conveyed in this work can be applied to more rigorous models just as well. However, given the series RLC fit considerations of resonant antennas [88], we restrict our simulations to systems with relative bandwidths less than 10%.

Although 3-dB bandwidth (introduced in Chapter 4)

$$B_{3dB} \approx \frac{2}{Q} \ ,$$

relates the antenna Q with a way to characterize the system bandwidth, microwave/RF bandwidths are usually parameterized by *voltage standing-wave ratio* (VSWR) [4]. VSWR is a metric based on matching efficiency which is indicative of the range of voltage fluctuations in the standing wave formed due to reflections arising from the impedance-

mismatch:

$$\nu(\omega) = \frac{1 + |\Gamma(\omega)|}{1 - |\Gamma(\omega)|} \ .$$

The higher this ratio, the larger the mismatch and smaller the bandwidth. Note that $0 < |\Gamma(\omega)| < 1$, implies $\nu(\omega) \geq 1$. A convenient measure of the RF bandwidth is defined as the frequency range such that [4], [88], $1 \leq \nu(\omega) \leq 2$. In other words,

$$|\Gamma(\omega)| \leq 1/3 \ , \text{ or, } 1 - |\Gamma(\omega)|^2 \geq 8/9 \ .$$

For an antenna with series RLC model terminated in resistance R,

$$\Gamma(j\omega) = \frac{Z_A(j\omega) - R}{Z_A(j\omega) + R} \ , \tag{5.22}$$

while in terms of its resonance parameters (Q, ω_0)

$$\Gamma(j\omega) = \frac{1 - (\omega/\omega_0)^2}{1 - (\omega/\omega_0)^2 + 2j\omega/Q\omega_0} \ . \tag{5.23}$$

Fig. 5.6(a) and Fig. 5.6(c) shows VSWR for the eigen-impedances calculated using (5.22) with termination R_1 and R_2, respectively, for different spacings. Observe that for $d = 0.1\lambda_c$, the narrowband mode has a VSWR greater than 2. Under such scenarios, we consider this mode to be inactive. Fig. 5.6(d) shows the corresponding eigen-modes found numerically using NEC and by curve-fitting resonance parameters (Q, ω_0). Table 5.1 summarizes this data for the two-antenna system discussed above.

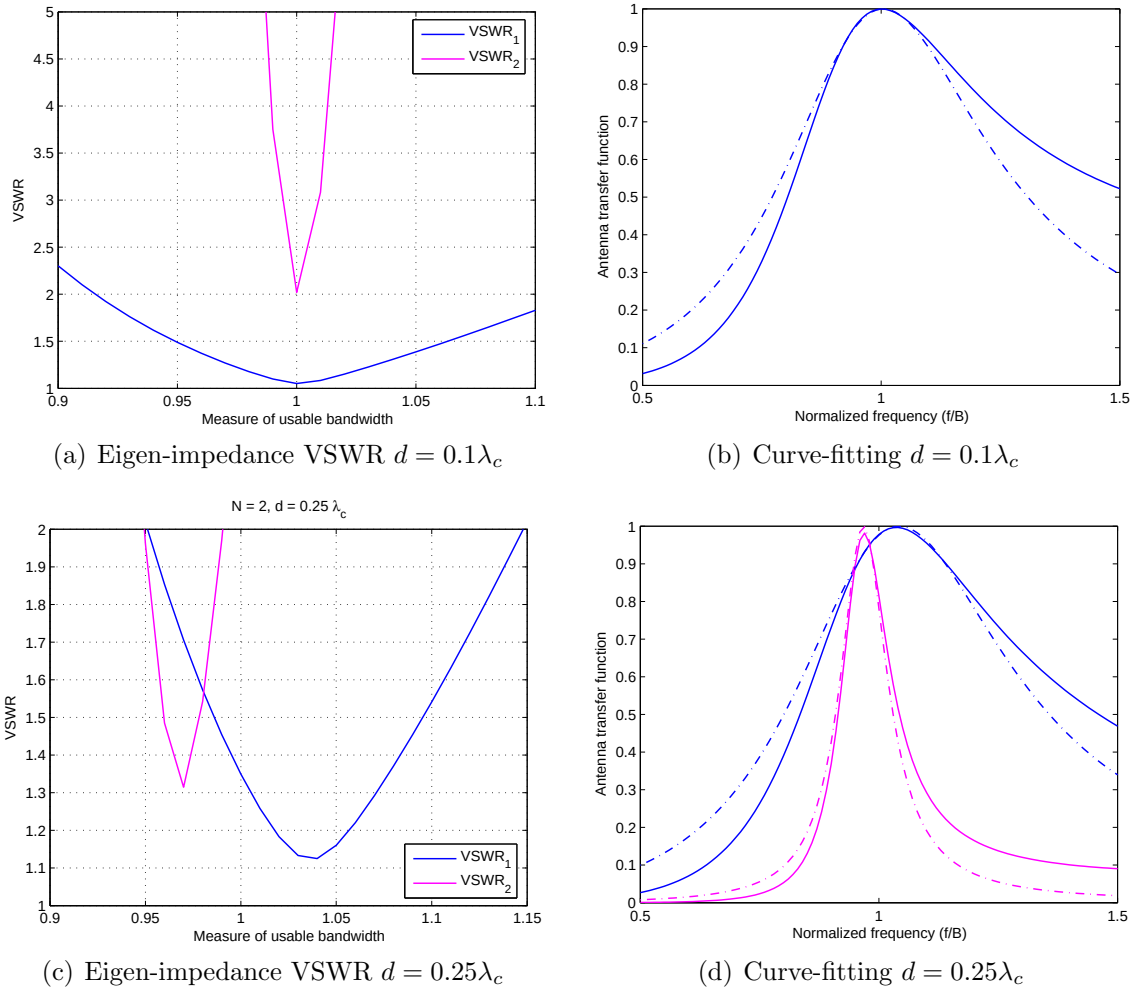

(a) Eigen-impedance VSWR $d = 0.1\lambda_c$

(b) Curve-fitting $d = 0.1\lambda_c$

(c) Eigen-impedance VSWR $d = 0.25\lambda_c$

(d) Curve-fitting $d = 0.25\lambda_c$

Figure 5.6: Eigen-impedance VSWR and eigen-modes $N = 2$

5.2.2 Eigen-Mode Behavior

The primary objective in using NEC was to gain insights into the impact of coupling on the antenna array behavior, particularly, RF bandwidth. Evidently, the impact of coupling can best be described in *lieu* of Fig. 5.6(d), as decomposing the two coupled seemingly-identical spatial modes into spectrally non-identical eigen-modes - one *broad-band* and the other *narrowband*. This finding sheds some insight into how the coupling

Table 5.1: Eigen-impedance parameters: $N = 2$, $d = 0.25\lambda_c$

Parameter	Value
Antenna type	Dipole
Antenna length	$0.475\lambda_c$
Antenna radius	$0.001\lambda_c$
Quality factor (Q_1)	3.75
Resonant frequency (f_{01})	$1.0425f_c$
R_1	118.76 Ω
$L_1 = Q_1R_1/\omega_{01}$	$67.99/f_c$ H
$C_1 = 1/Q_1R_1\omega_{01}$	$342.78/f_c$ μF
Quality factor (Q_2)	16
Resonant frequency (f_{02})	$0.9675f_c$
R_2	28.31 Ω
$L_2 = Q_2R_2/\omega_{02}$	$74.53/f_c$ H
$C_2 = 1/Q_2R_2\omega_{02}$	$1.4/f_c$ mF

impacts the bandwidth of a MIMO system. It also offers intuitively-coherent interpretations - as the spacing goes to zero, in limit, the narrowband mode must vanish, leaving behind a system that behaves like a single antenna system. Under very strong coupling, we might see a slight bandwidth enhancement of the broadband mode compared to a single antenna in isolation. This can be attributed to the fact that *thicker* dipoles (virtual broadband mode with almost double the diameter) have wider bandwidths than original dipole.

The other key observation is that, the two modes not only differ in bandwidths but are also centered at *different resonant frequencies*. This explains why a multiport matching network built for narrowband systems should collapse for wider bandwidths and that these optimal networks may be physically unrealizable. Since the gain of the narrowband mode is virtually zero near the center frequency of the system, it is no surprise that narrowband matching networks can not recover the diversity gains of an ideal MIMO

system at close spacings. Fig. 5.7 shows the usable bandwidths (VSWR < 2) of the eigen-modes with box-car matching. For example, at $d = 0.25\lambda_c$, we start to see a narrowband mode, however, for bandwidths less than 5% around the center frequency, it is essentially a single antenna system. Thus, for broadband systems we can argue that the system has a frequency-variant diversity gain that lies between 1 and 2. For very weak to no coupling, all the modes are identically broadband and centered at f_c.

Quarter-wave Transformer Analogy: The *differential bandwidth* behavior of eigen-modes can be explained with the help of a well known technique in RF/microwave literature [77], [78]. Consider an antenna modeled as an impedance z_A matched to a transmission line (z_0) by a quarter-wave transformer ($z_1 = \sqrt{z_0 z_A}$), near the resonant frequency. The antenna reflection coefficient magnitude, near resonant frequency, is given by

$$|\Gamma| \simeq \frac{|z_A - z_0|}{2\sqrt{z_A z_0}} |cos\ \theta| \ , \quad \pi/2 - \delta < \theta = \beta l < \pi/2 + \delta \ , \quad (\delta \ll \pi/2)$$

where l is the *electrical length* of the transformer ($l = \lambda_c/4$ at f_c). It can be seen that at $\theta = \pi/2$, the antenna is perfectly matched ($|\Gamma| = 0$). However, a transformer with a different length, is a perfect match for a frequency *other than* f_c, while the *usable bandwidth* depends on the impedance-ratio z_A/z_0 [77]. It can be argued that as an antenna is brought closer to another antenna, by virtue of mutual coupling it acts as an impedance matching similar to a quarter-wave transformer although with a *sub-optimal* length and impedance-ratio. The eigen-value decomposition offers the same matching problem on the sum and difference modes, instead. Consequently, each virtual antenna is imperfectly matched ($|\Gamma| > 0$) at the center frequency, i.e., perfectly matched at a different frequency with a different bandwidth.

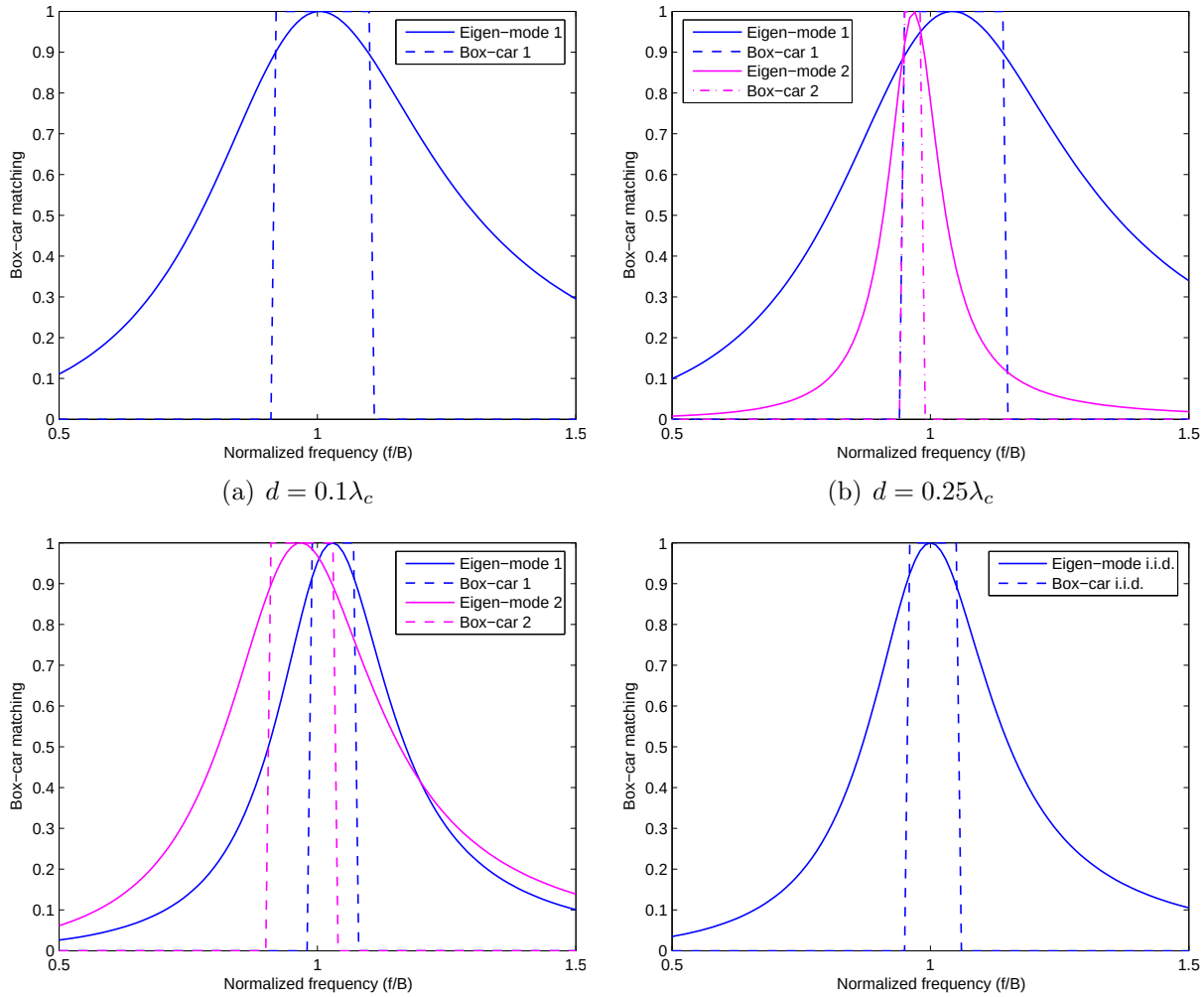

(a) $d = 0.1\lambda_c$ (b) $d = 0.25\lambda_c$

(c) $d = 0.5\lambda_c$ (d) i.i.d.

Figure 5.7: Box-car matching $N = 2$

5.2.3 Extension to Large MIMO Systems

A careful observation of the structure of $\mathbf{Z}_A$ and the unitary transformation $\mathbf{Q}$ reveals that it is straightforward to extend the entire theory developed so far, to a very special but practical class of antenna arrays - uniform circular arrays. A uniform circular array has a circulant impedance matrix. For a circulant $\mathbf{Z}_A$ with N elements, the eigen-vectors

for $\mathbf{Z}_A(j\omega) = \mathbf{Q}\mathbf{\Lambda}_A(j\omega)\mathbf{Q}^H$, are given by the columns of the unitary matrix

$$\mathbf{Q} = \frac{1}{\sqrt{N}} \begin{bmatrix} 1 & 1 & 1 & \dots & 1 \\ 1 & \alpha & \alpha^2 & \dots & \alpha^{N-1} \\ 1 & \alpha^2 & \alpha^4 & \dots & \alpha^{2(N-1)} \\ \vdots & \vdots & \vdots & & \vdots \\ 1 & \alpha^{N-1} & \alpha^{2(N-1)} & \dots & \alpha^{(N-1)(N-1)} \end{bmatrix}$$

where $\alpha = e^{-2\pi j/N}$. The eigen-values ($\mathbf{\Lambda}_A$) are given by the DFT of the first row of $\mathbf{Z}_A$. Once again, observe that we can realize the decoupling network for the entire range of frequencies of interest, owing to the frequency-independent nature of $\mathbf{Q}$. For uniform linear arrays, although a unitary transformation for complex-symmetric impedance matrix $\mathbf{Z}_A$ exists for each data-point over the frequency range, it is in general, frequency-dependent.

We now present NEC results to quantify the impact of coupling on circular arrays with 3 and 4 elements by observing their eigen-mode behavior. For $N = 3$ antennas, the spatial unitary transformation that decouples the antenna array is given by

$$\mathbf{Q} = \frac{1}{\sqrt{3}} \begin{bmatrix} 1 & 1 & 1 \\ 1 & -\frac{1}{2} - j\frac{\sqrt{3}}{2} & -\frac{1}{2} + j\frac{\sqrt{3}}{2} \\ 1 & -\frac{1}{2} + j\frac{\sqrt{3}}{2} & -\frac{1}{2} - j\frac{\sqrt{3}}{2} \end{bmatrix}$$

and the eigen-impedances by

$$\lambda_1(j\omega) = z_{11}(j\omega) + 2z_{12}(j\omega) \ , \tag{5.24a}$$

$$\lambda_2(j\omega) = z_{11}(j\omega) - z_{12}(j\omega) \ , \quad \lambda_3(j\omega) = \lambda_2(j\omega) \ . \tag{5.24b}$$

Similarly for $N = 4$ antennas, we have

$$\mathbf{Q} = \frac{1}{2}\begin{bmatrix} 1 & 1 & 1 & 1 \\ 1 & -j & -1 & j \\ 1 & -1 & 1 & -1 \\ 1 & j & -1 & -j \end{bmatrix}$$

and eigen-impedances as

$$\lambda_1(j\omega) = z_{11}(j\omega) + 2z_{12}(j\omega) + z_{13}(j\omega)\ , \quad \lambda_2(j\omega) = z_{11}(j\omega) - z_{13}(j\omega)\ , \quad (5.25a)$$

$$\lambda_3(j\omega) = z_{11}(j\omega) - 2z_{12}(j\omega) + z_{13}(j\omega)\ , \quad \lambda_4(j\omega) = \lambda_2(j\omega)\ . \quad (5.25b)$$

A series RLC fit with appropriate antenna Q values and resonant frequencies f_0 are presented in Fig. 5.8 for different array sizes. As can be seen, larger MIMO systems witness a clear loss of diversity benefits and spatial modes at close spacings, as is evident for $N = 3$ at $d = 0.1\lambda_c$ spacing and $N = 4$ at $d = 0.25\lambda_c$. Also observe that, one of the eigen-modes for $N = 4$ is completely nulled for spacings up to $d = 0.25\lambda_c$.

5.3 Conclusion

In this chapter, we primarily investigated the relationship between coupling and RF bandwidth of MIMO systems. In order to arrive at these results, we developed broadband matching theory for coupled impedance networks using S-matrix characterization. By way of optimal matching and power allocation, we analyzed the information theoretic limits of coupled MIMO-OFDM systems, and presented a sub-optimal practical design using box-car characteristics. Although we considered coupling only at the receiver, the

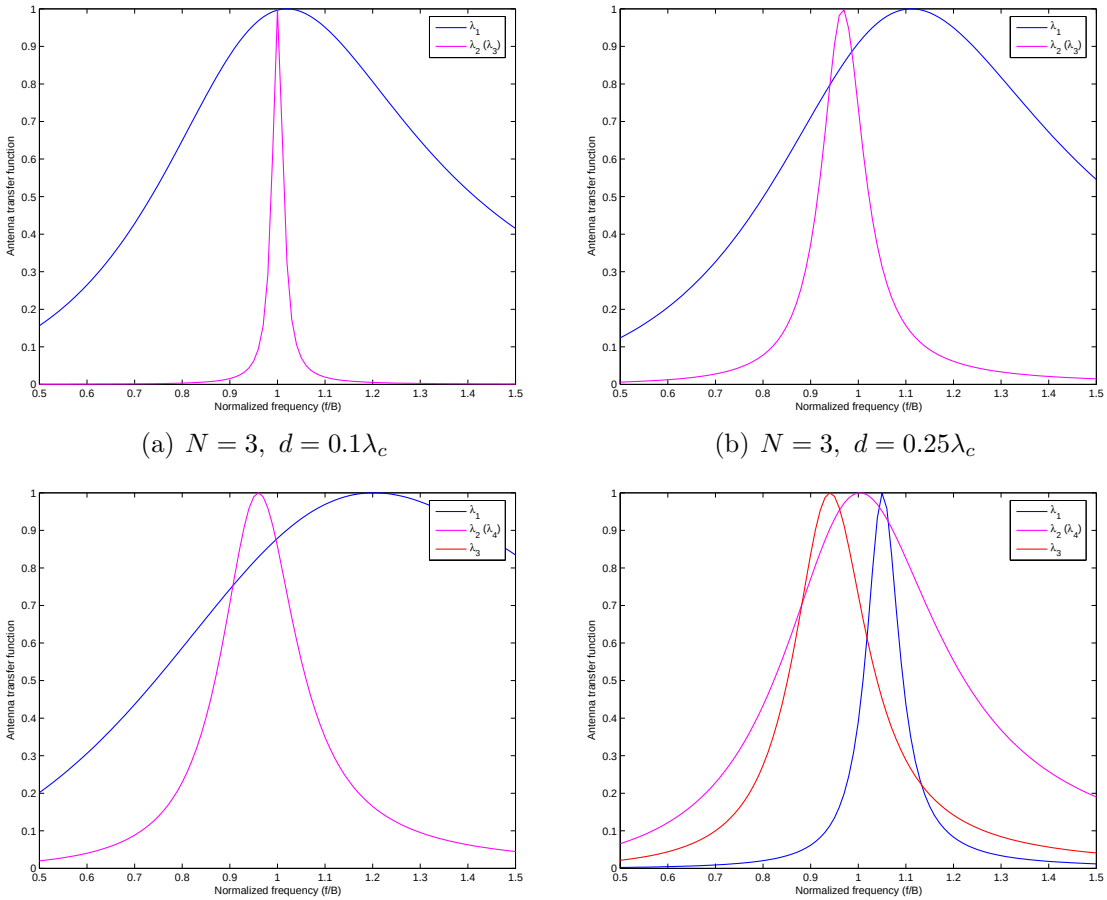

(a) $N = 3,\ d = 0.1\lambda_c$ (b) $N = 3,\ d = 0.25\lambda_c$

(c) $N = 4,\ d = 0.25\lambda_c$ (d) $N = 4,\ d = 0.5\lambda_c$

Figure 5.8: Eigen-modes, antenna-Q fit

entire analysis can easily be extended to incorporate coupling at both the ends.

We used series RLC approximation for modeling antenna array impedance, to analyze the behavior of eigen-modes of the array. Systems with much larger relative bandwidths can be analyzed by using more exact impedance models, either through analytic modeling for the entire frequency range, or by use of numerical techniques (such as real-frequency method), to compute the integral constraints. An extension to large circular arrays was also presented. Another form of arrays that is of considerable interest for MIMO systems

are uniform linear arrays. Although a straight-forward extension is not possible, this study does provide qualitative insights into how such a system might behave for varying amounts of coupling.

Chapter 6

Capacity Limits of Coupled MIMO-OFDM Systems

In the previous chapter, we established the constraints imposed by a coupled MIMO transceiver on the overall matching efficiency of the system. In this chapter, we develop a communication theory model that incorporates mutual coupling in the MIMO-OFDM system model presented in Chapter 2. We then formulate the information-theoretic approach to the problem of broadband matching and analyze the fundamentals capacity limits of coupled arrays. We present the optimal transceiver design and conclude with a few numerical examples to illustrate the impact of coupling on the overall bandwidth and capacity of the system.

6.1 Coupled MIMO-OFDM System Model

Consider an $N \times N$ MIMO-OFDM system with ideal transmit antennas, coupled receive antennas and K sub-carriers. The transmitted OFDM signal vector at k-th sub-carrier

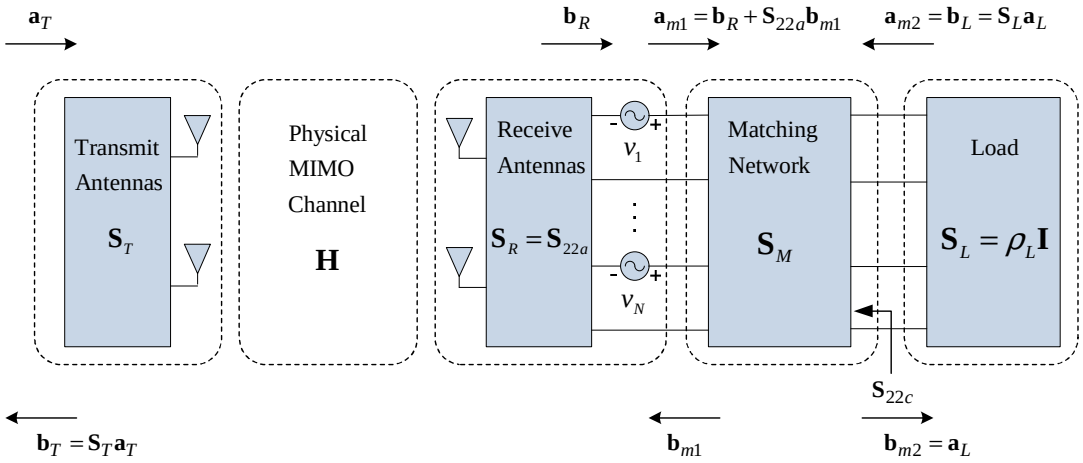

Figure 6.1: Network model for MIMO-OFDM with mutual coupling (sub-carrier index suppressed)

$\mathbf{s}_k$, is received at the coupled antenna array as $\mathbf{r}_k$ as [1]

$$\mathbf{r}_k = \mathbf{H}'_k\mathbf{s}_k + \mathbf{n}_k$$

where, $\mathbf{H}'_k$ represents the overall MIMO channel matrix at k-th sub-carrier, which incorporates the effects of fading, correlation and mutual coupling, and $\mathbf{n}_k$ is the additive noise at the receiver.

Fig. 6.1 shows a network model for MIMO-OFDM with mutual coupling (with suppressed sub-carrier index)[2]. The transmit and receive antennas are represented in terms of N-port networks with S-matrices at k-th sub-carrier, $\mathbf{S}_T(f_k)$ and $\mathbf{S}_R(f_k)$, respectively, where $\mathbf{S}_R(f_k) = \mathbf{S}_{22a}(f_k)$, as discussed earlier. The rest of the receive RF chain is modeled as a bank of uncoupled loads by an N-port $\mathbf{S}_L$. The transmit antennas are assumed to

[1]For convenience, we allow for some notational inconsistency vis-a-vis Chapter 2 and drop the accent from signal and channel variables for the remainder of this chapter, since we no longer need to explicitly distinguish them from their time-domain counter-parts. It shall be implied that symbols $\mathbf{x}$ mean $\widetilde{\mathbf{x}}$.

[2]This model is based on the narrowband model presented in [57, Chap. 1].

be ideal, however, we include $\mathbf{S}_T(f_k)$ for completeness. To model the impact of coupling, $\mathbf{H}_k$ (formerly denoted by $\widetilde{\mathbf{H}}_k$) must be modified to include the *transmission matrix* or *transmissivity* of the cascaded network (of antenna array and matching network) modeled by $\mathbf{S}_{21c}(f_k)$. We skip the tedious network analysis to Appendix D.1 and present the new MIMO channel matrix at k-th sub-carrier directly (cf. (D.8))

$$\begin{aligned} \mathbf{H}'_k &= \mathbf{S}_{21m,k}(\mathbf{I} - \mathbf{S}_{22a,k}\mathbf{S}_{11m,k})^{-1}\mathbf{S}_{21a,k}\mathbf{H}_k \\ &= \mathbf{S}_{21c,k}\mathbf{H}_k \ . \end{aligned} \tag{6.1}$$

Since we are interested in the bounds on capacity regulated solely by the coupled antenna array, we have made a simplifying assumption in arriving at this model that the loads for the receiver RF chain are perfectly matched to the RF front end. Some insights into the general load model are presented in Appendix D.2.

6.1.1 Receiver Noise Model

The additive noise $\mathbf{n}_k$ is usually modeled as a combination of noise from various sources in the RF chain [29]. Similar to narrowband noise characterization in Chapter 3, we can categorize the broadband noise into three types: (a) *sky noise* or antenna noise, consisting of thermal radiation, cosmic background, and interference from other devices, (b) *amplifier noise*, and (c) *downstream noise*, consisting of noise from the rest of the RF chain. However, based on our receiver model, we classify the noise as antenna noise, and load noise - a combination of amplifier and downstream noise. Furthermore, the load noise in general can be considered to be a combination of *forward traveling* noise $\mathbf{n}_f$, and *reverse traveling* noise $\mathbf{n}_r$ [57, Chap. 1]. Thus, the total noise at k-th sub-carrier

referenced to the load, is given by[3]

$$\mathbf{n}_k = \mathbf{S}_{21c,k}\mathbf{n}_{s,k} + \mathbf{n}_{f,k} + \mathbf{S}_{22c,k}\mathbf{n}_{r,k} \ , \tag{6.2}$$

The sky noise and load noise can be well modeled as statistically independent, ZMCSCG and spectrally white[4]:

$$\mathbf{n}_s \sim \mathcal{CN}(\mathbf{0}, 4kT_A B\mathbf{R}_A) \ , \ \mathbf{n}_f \sim \mathcal{CN}(\mathbf{0}, 4kT_\alpha B\mathbf{I}) \ , \ \mathbf{n}_r \sim \mathcal{CN}(\mathbf{0}, 4kT_\beta B\mathbf{I}) \ .$$

However, the reverse and forward traveling noise waves are in general, correlated to an extent determined by exact amplifier models (cf. [57, Chap. 1]). We redefine $\mathbf{S}_k \triangleq \mathbf{S}_{21c,k}$ such that the overall channel matrix in (6.1) is given by

$$\mathbf{H}'_k = \mathbf{S}_k\mathbf{H}_k \ ,$$

and the noise covariance by

$$\frac{1}{4kT_0B}\mathbf{R}_{\mathbf{n}_k} \ = \ \frac{T_A}{T_0}\ \mathbf{S}_k\mathbf{R}_A\mathbf{S}_k^H + \frac{T_\alpha}{T_0}\ \mathbf{I} + \frac{T_\beta}{T_0}\ (\mathbf{I} - \mathbf{S}_k\mathbf{S}_k^H) - 2\,\mathrm{Re}\left(\frac{T_\gamma^*}{T_0}\ \mathbf{S}_k\right)$$

where $\mathbf{R}_A = \mathrm{Re}(\mathbf{Z}_A)$ by assumption, is frequency independent. T_α, T_β and T_γ are *effective noise temperatures* which can be computed for example, using amplifier noise parameters as highlighted in [57, Chap. 1]. Due to the limited scope of this dissertation, we study the impact of various noise sources by varying the relative strengths governed by T_A, T_α,

[3]From [57, Chap. 1], the noise from components past matching network, becomes spatially correlated by the reflection coefficient seen looking into the matching network, i.e., $\mathbf{S}_{22c}$. Also, recall for a lossless network $\mathbf{S}_{22c}\mathbf{S}_{22c}^H = \mathbf{I} - \mathbf{S}_{21c}\mathbf{S}_{21c}^H$.

[4]This is a reasonable assumption for bandwidths less than 10%.

T_β, and assume T_γ to be negligible.

Observe that $\mathbf{S}_k$ and $\mathbf{R}_A$ admit the familiar EVD

$$\mathbf{S}_k = \mathbf{Q}\mathbf{T}_k\mathbf{Q}^H , \tag{6.3}$$

$$\mathbf{R}_A = \mathbf{Q}\,\mathrm{Re}(\mathbf{\Lambda}_A)\mathbf{Q}^H . \tag{6.4}$$

It is straightforward to observe that the noise covariance is also diagonalized by $\mathbf{Q}$, i.e.,

$$\begin{aligned} \mathbf{R}_{\mathbf{n}_k} &= \mathbf{Q}\mathbf{\Sigma}_{\mathbf{n}_k}\mathbf{Q}^H \\ \frac{1}{4kT_0B}\mathbf{\Sigma}_{\mathbf{n}_k} &= \frac{T_A}{T_0}\,\mathbf{T}_k\,\mathrm{Re}(\mathbf{\Lambda}_A)\mathbf{T}_k^H + \frac{T_\alpha}{T_0}\,\mathbf{I} + \frac{T_\beta}{T_0}\,(\mathbf{I}-\mathbf{T}_k\mathbf{T}_k^H) \\ &= \frac{T_A}{T_0}\,\mathrm{Re}(\mathbf{\Lambda}_A)(\mathbf{I}-\mathbf{\Gamma}_k\mathbf{\Gamma}_k^H) + \frac{T_\alpha}{T_0}\,\mathbf{I} + \frac{T_\beta}{T_0}\,\mathbf{\Gamma}_k\mathbf{\Gamma}_k^H \end{aligned} \tag{6.5}$$

where we have used the lossless property of the network, i.e., $\mathbf{T}_k\mathbf{T}_k^H = \mathbf{I} - \mathbf{\Gamma}_k\mathbf{\Gamma}_k^H$. We normalize the noise covariance such that for i.i.d. case $\mathbf{\Sigma}_{\mathbf{n}_k} = N_0\mathbf{I}$ where,

$$\frac{N_0}{4kT_0B} = \frac{T_A}{T_0}\,\mathrm{Re}(z_A)(1-|\Gamma_{iid}|^2) + \frac{T_\alpha}{T_0} + \frac{T_\beta}{T_0}|\Gamma_{iid}|^2 .$$

The power constraint P_0 is defined for a given SNR γ_0 as $P_0 = \gamma_0 N_0$.

6.1.2 MIMO-OFDM Signal Model

The cumulative MIMO-OFDM system in the presence of mutual coupling can be written in matrix format (similar to (2.16)), as

$$\boldsymbol{r} = \boldsymbol{\mathcal{H}}'\boldsymbol{s} + \boldsymbol{n} \tag{6.6}$$

where $\boldsymbol{r}$, $\boldsymbol{s}$ and $\boldsymbol{n}$ share the definitions specified in (2.18) and (6.2),

$$\boldsymbol{\mathcal{H}}' \;=\; \boldsymbol{\mathcal{S}}\boldsymbol{\mathcal{H}} \;, \tag{6.7}$$

and $\boldsymbol{\mathcal{S}}$ is the $KN \times KN$ block-diagonal matrix given by

$$\boldsymbol{\mathcal{S}} = \begin{bmatrix} \mathbf{S}_1 & & \\ & \ddots & \\ & & \mathbf{S}_K \end{bmatrix} .$$

Since the noise samples among the orthogonal sub-carriers are assumed to be spatially-correlated but spectrally-uncorrelated, we have

$$(a) \qquad \mathbb{E}[\mathbf{n}_i \mathbf{n}_j^H] = \mathbf{0} \;,\; i,j = 1,\ldots,K \;,\; i \neq j$$

$$(b) \qquad \mathbf{R}_{\mathbf{n}_k} = \mathbb{E}[\mathbf{n}_k \mathbf{n}_k^H] \;,\; k = 1,\ldots,K$$

such that the noise covariance $\boldsymbol{\mathcal{R}}_{\boldsymbol{n}}$ for (6.6) has a block-diagonal structure.

6.2 Problem Formulation

We now formulate the problem of information theoretic optimal broadband matching for coupled MIMO systems. With perfect channel state information at the transmitter (CSIT), our aim is to find the information theoretic limits of this system. From (2.10)

and (6.7), the spectral efficiency of the system can be written as

$$\begin{aligned} C &= \frac{1}{K} \max_{\mathrm{Tr}(\boldsymbol{\mathcal{R}_s}) \leq KP_0} \left\{ \log_2 \det \left(\boldsymbol{I} + \frac{1}{N} \boldsymbol{\mathcal{R}_n}^{-1} \boldsymbol{\mathcal{H}'} \boldsymbol{\mathcal{R}_s} \boldsymbol{\mathcal{H}'}^H \right) \right\} \\ &= \frac{1}{K} \max_{\boldsymbol{\mathcal{S}}, \mathrm{Tr}(\boldsymbol{\mathcal{R}_s}) \leq KP_0} \left\{ \log_2 \det \left(\boldsymbol{I} + \frac{1}{N} \boldsymbol{\mathcal{R}_n}^{-1} \boldsymbol{\mathcal{S}} \boldsymbol{\mathcal{H}} \boldsymbol{\mathcal{R}_s} \boldsymbol{\mathcal{H}}^H \boldsymbol{\mathcal{S}}^H \right) \right\} . \end{aligned} \tag{6.8}$$

We define $\boldsymbol{\mathcal{Y}} = \boldsymbol{\mathcal{H}} \boldsymbol{\mathcal{R}_s} \boldsymbol{\mathcal{H}}^H$, a positive-definite matrix whose EVD is given by

$$\begin{aligned} \boldsymbol{\mathcal{Y}} &= \boldsymbol{\mathcal{H}} \boldsymbol{\mathcal{R}_s} \boldsymbol{\mathcal{H}}^H \qquad (6.9) \\ &= \begin{bmatrix} \mathbf{H}_1 \mathbb{E}[\mathbf{s}_1 \mathbf{s}_1^H] \mathbf{H}_1^H & \dots & \mathbf{H}_1 \mathbb{E}[\mathbf{s}_1 \mathbf{s}_K^H] \mathbf{H}_K^H \\ \vdots & \ddots & \vdots \\ \mathbf{H}_K \mathbb{E}[\mathbf{s}_K \mathbf{s}_1^H] \mathbf{H}_1^H & \dots & \mathbf{H}_K \mathbb{E}[\mathbf{s}_K \mathbf{s}_K^H] \mathbf{H}_K^H \end{bmatrix} \\ &= \boldsymbol{\mathcal{V}} \boldsymbol{\Psi} \boldsymbol{\mathcal{V}}^H \qquad (6.10) \end{aligned}$$

where, $\boldsymbol{\mathcal{V}}$ is an $NK \times NK$ unitary matrix representing eigen-vectors corresponding to the eigen-values $\boldsymbol{\Psi}$. Also, observe that the block diagonal matrices $\boldsymbol{\mathcal{S}}$ and $\boldsymbol{\mathcal{R}_n}$ can be written as

$$\boldsymbol{\mathcal{S}} = \boldsymbol{\mathcal{Q}} \boldsymbol{T} \boldsymbol{\mathcal{Q}}^H \ , \ \boldsymbol{\mathcal{R}_n} = \boldsymbol{\mathcal{Q}} \boldsymbol{\Sigma_n} \boldsymbol{\mathcal{Q}}^H \ , \tag{6.11}$$

where,

$$\boldsymbol{T} = \begin{bmatrix} \mathbf{T}_1 & & \\ & \ddots & \\ & & \mathbf{T}_K \end{bmatrix} , \quad \boldsymbol{\Sigma_n} = \begin{bmatrix} \boldsymbol{\Sigma}_{\mathbf{n}_1} & & \\ & \ddots & \\ & & \boldsymbol{\Sigma}_{\mathbf{n}_K} \end{bmatrix} , \quad \boldsymbol{\mathcal{Q}} = \begin{bmatrix} \mathbf{Q} & & \\ & \ddots & \\ & & \mathbf{Q} \end{bmatrix} .$$

Substituting (6.10) and (6.11) in Shannon capacity (6.8) and using $\det(\mathbf{I}+\mathbf{XY}) = \det(\mathbf{I}+\mathbf{YX})$, we have[5]

$$C = \frac{1}{K}\max_{\boldsymbol{T},\boldsymbol{\Psi}}\left\{\log_2\det\left(\boldsymbol{I}+\frac{1}{N}\underbrace{\boldsymbol{\mathcal{Q}}\boldsymbol{T}^H\boldsymbol{\Sigma}_{\boldsymbol{n}}^{-1}\boldsymbol{T}\boldsymbol{\mathcal{Q}}^H}_{\boldsymbol{\mathcal{X}}}\underbrace{\boldsymbol{\mathcal{V}}\boldsymbol{\Psi}\boldsymbol{\mathcal{V}}^H}_{\boldsymbol{\mathcal{Y}}}\right)\right\} \tag{6.12}$$

For any two positive semi-definite matrices $\boldsymbol{\mathcal{X}}, \boldsymbol{\mathcal{Y}}$

$$\det\left(\boldsymbol{I}+\boldsymbol{\mathcal{X}}\boldsymbol{\mathcal{Y}}\right) = \prod_n\left(1+\lambda_n(\boldsymbol{\mathcal{X}}\boldsymbol{\mathcal{Y}})\right) \leq \prod_n\left(1+\lambda_n(\boldsymbol{\mathcal{X}})\lambda_n(\boldsymbol{\mathcal{Y}})\right)$$

with equality if and only if $\boldsymbol{\mathcal{X}}$ and $\boldsymbol{\mathcal{Y}}$ commute [64], where $\lambda_n(\cdot)$ denotes the n-th eigenvalue. For $\boldsymbol{\mathcal{X}} = \boldsymbol{\mathcal{Q}}\boldsymbol{T}^H\boldsymbol{\Sigma}_{\boldsymbol{n}}^{-1}\boldsymbol{T}\boldsymbol{\mathcal{Q}}^H$, we conclude that $\boldsymbol{\mathcal{V}}$ in (6.10) is block-diagonal

$$\boldsymbol{\mathcal{V}} = \boldsymbol{\mathcal{Q}}\ .$$

The Shannon capacity (6.12) in terms of block-diagonal matrices is thus given by

$$C \;=\; \frac{1}{K}\max_{\boldsymbol{\Psi},\boldsymbol{T}}\left\{\log_2\det\left(\boldsymbol{I}+\frac{1}{N}\boldsymbol{\Sigma}_{\boldsymbol{n}}^{-1}\boldsymbol{T}\boldsymbol{\Psi}\boldsymbol{T}^H\right)\right\}\ .$$

Observe that $\boldsymbol{\mathcal{V}} = \boldsymbol{\mathcal{Q}}$ ensures a block-diagonal structure for $\boldsymbol{\mathcal{Y}}$ as well,

$$\boldsymbol{\mathcal{Y}} = \boldsymbol{\mathcal{Q}}\boldsymbol{\Psi}\boldsymbol{\mathcal{Q}}^H = \begin{bmatrix}\mathbf{Y}_1 & & \\ & \ddots & \\ & & \mathbf{Y}_K\end{bmatrix}$$

[5]If we consider the cascade of $\mathbf{S}_{22a}$, the decoupling network to the left $\mathbf{S}'_M$, and a diagonal matching network $\boldsymbol{\Lambda}_M$, we have $\boldsymbol{\mathcal{S}} = \boldsymbol{T}\boldsymbol{\mathcal{Q}}^H$ and a diagonal noise covariance $\boldsymbol{\mathcal{R}}_{\boldsymbol{n}} = \boldsymbol{\Sigma}_{\boldsymbol{n}}$ due to a decoupled front-end, such that, the capacity is still given by (6.12).

where,

$$\mathbf{Y}_k = \mathbf{H}_k \mathbf{R}_{\mathbf{s}_k} \mathbf{H}_k^H = \mathbf{Q} \mathbf{\Psi}_k \mathbf{Q}^H \ . \tag{6.13}$$

Consequently, $\boldsymbol{\mathcal{R}_s}$ is block-diagonal (cf. (6.9)), i.e.,

$$\mathbb{E}[\mathbf{s}_i \mathbf{s}_j^H] = \mathbf{0} \ , \ i, j = 1, \ldots, K, \ i \neq j \ .$$

This means that the optimal power allocation strategy does not require modulating-symbols to be correlated, across sub-carriers. We define the transmit signal covariance for k-th sub-carrier as

$$\mathbf{R}_{\mathbf{s}_k} = \mathbb{E}[\mathbf{s}_k \mathbf{s}_k^H] \ , \ k = 1, \ldots, K$$

such that, the problem reduces to finding the optimal

$$\mathbf{R}_{\mathbf{s}_k} = (\mathbf{Q}^H \mathbf{H}_k)^{-1} \mathbf{\Psi}_k (\mathbf{Q}^H \mathbf{H}_k)^{-H} \ , \tag{6.14}$$

that renders $\mathbf{Y}_k$ in (6.13), circulant.

The spectral efficiency of this uncoupled system can be written as the sum of capacities of KN *space-frequency modes:*

$$\begin{aligned} C &= \frac{1}{K} \max_{\mathbf{\Psi}_k, \mathbf{T}_k} \sum_{k=1}^{K} \log_2 \det \left(\mathbf{I} + \frac{1}{N} \mathbf{\Sigma}_{\mathbf{n}_k}^{-1} \mathbf{\Psi}_k \mathbf{T}_k \mathbf{T}_k^H \right) \\ &= \frac{1}{K} \max_{\psi_{nk}, \Gamma_{nk}} \sum_{k=1}^{K} \sum_{n=1}^{N} \log_2 \left(1 + \frac{1}{N} \frac{\psi_{nk}}{\sigma_{nk}} \left(1 - |\Gamma_{nk}|^2 \right) \right) \end{aligned}$$

where $\psi_{nk} = [\mathbf{\Psi}_k]_{nn}$, $\sigma_{nk} = [\mathbf{\Sigma}_{\mathbf{n}_k}]_{nn}$ and $\Gamma_{nk} = [\mathbf{\Gamma}_k]_{nn}$. Notice from (6.5), the above

definition of $\mathbf{\Sigma}_{\mathbf{n}_k}$ ignores any dependence on matching (i.e., $\mathbf{T}_k$). For aesthetic reasons and to keep optimization straightforward, we assume a simple noise model. The details for the realistic noise model and optimal solutions are provided in Appendix D.6. We shall revisit the original noise model when we analyze numerical results for Diversity-OFDM systems in the presence of mutual coupling.

6.3 Optimal Solution

The problem, thus reduces to, finding the optimal $\psi_{nk},\ \Gamma_{nk}$ for $n = 1, \ldots, N$, $k = 1, \ldots, K$ that maximizes

$$C \;=\; \frac{1}{K} \max_{\psi_{nk}, \Gamma_{nk}} \sum_{k=1}^{K} \sum_{n=1}^{N} \log_2 \left(1 + \frac{1}{N} \frac{\psi_{nk}}{\sigma_{nk}} \left(1 - |\Gamma_{nk}|^2 \right) \right)$$

subject to the following constraints:

$$(i) \quad \frac{1}{K} \operatorname{Tr}(\boldsymbol{\mathcal{R}}_{\boldsymbol{s}}) \leq P_0 \tag{6.15}$$

$$(ii) \quad \frac{1}{K} \sum_{k=1}^{K} \log \frac{1}{|\Gamma_{nk}|^2} \leq \frac{1}{B}\, G_{0n}\ , \quad n = 1, \ldots, N \tag{6.16}$$

Before we proceed, we must formulate these constraints suitably. Observe that (i) can alternatively be expressed as

$$\frac{1}{K} \sum_{k=1}^{K} \operatorname{Tr}(\mathbf{R}_{\mathbf{s}_k}) \leq P_0\ ,$$

and using (5.16), (ii) as

$$\frac{1}{K} \sum_{k=1}^{K} G_{nk} \leq \frac{1}{B}\, G_{0n}\ ,$$

such that

$$C = \frac{1}{K} \max_{\psi_{nk}, G_{nk}} \sum_{k=1}^{K} \sum_{n=1}^{N} \log_2 \left(1 + \frac{1}{N} \frac{\psi_{nk}}{\sigma_{nk}} \left(1 - e^{-G_{nk}} \right) \right) \ . \tag{6.17}$$

Now, from (6.13)

$$\mathrm{Tr}\left(\mathbf{R}_{\mathbf{s}_k} \right) = \mathrm{Tr}\left(\mathbf{\Psi}_k \mathbf{\Omega}_k^{-1} \right) \ , \text{ where } \quad \mathbf{\Omega}_k = \mathbf{Q}^H \mathbf{H}_k \mathbf{H}_k^H \mathbf{Q} \ . \tag{6.18}$$

Therefore, in terms of $\psi_n(f_k)$, we have a linear power constraint

$$\mathrm{Tr}\left(\mathbf{R}_{\mathbf{s}_k} \right) \ = \ \sum_{n=1}^{N} w_n(f_k) \psi_n(f_k) \tag{6.19}$$

where the weights are given by

$$w_n(f_k) = \left[\ \mathbf{\Omega}_k^{-1} \right]_{nn} \ . \tag{6.20}$$

The power constraint thus assumes the form

$$\frac{1}{K} \sum_{k=1}^{K} \sum_{n=1}^{N} w_n(f_k) \psi_n(f_k) \leq P_0 \ . \tag{6.21}$$

Problem Definition: Maximize the Shannon capacity (in nats/sec/Hz)[6]

$$C = \frac{1}{K} \sum_{k=1}^{K} \sum_{n=1}^{N} \log \left(1 + \frac{1}{N} \frac{\psi_{nk}}{\sigma_{nk}} \left(1 - e^{-G_{nk}} \right) \right) \tag{6.22}$$

[6]For mathematical convenience, we use natural logarithm.

subject to the constraints:

$$(i) \quad \frac{1}{K}\sum_{n=1}^{N}\sum_{k=1}^{K} w_n(k)\psi_n(k) \leq P_0 \ , \tag{6.23}$$

$$(ii) \quad \frac{1}{K}\sum_{k=1}^{K} G_n(k) \leq \frac{1}{B}\, G_{n0} \ , \quad n = 1, \ldots, N \ . \tag{6.24}$$

Optimal Solution: The optimal solution to the problem described above, is given by

$$\begin{aligned} \psi_n(k) &= \left[\frac{1}{w_n(k)\xi} - \frac{N\sigma_n(k)}{1 - e^{-G_n(k)}}\right]^+ \ , \\ G_n(k) &= \left[\log\left(1 + \mu_n^{-1}\right) - \log\left(1 + \frac{N\sigma_n(k)}{\psi_n(k)}\right)\right]^+ \end{aligned}$$

where, ξ and μ_n are Lagrange multipliers chosen to satisfy the power and broadband matching constraints, respectively. For details on optimization, refer to Appendix D.3.

6.4 Space-Frequency Mutual-Water-Pouring

As can be seen from the solution above, optimal matching $G_n(k)$ has a water-pouring characteristic, while $\psi_n(k)$ does not. However, observe that the function

$$P_n(k) = \psi_n(k)w_n(k) \tag{6.25}$$

$$= \left[\frac{1}{\xi} - \frac{N\sigma_n(k)w_n(k)}{1 - e^{-G_n(k)}}\right]^+ \tag{6.26}$$

has a water-pouring distribution, where from (6.23)

$$\sum_{n=1}^{N}\sum_{k=1}^{K} P_n(k) \leq KP_0 \ , \tag{6.27}$$

is the equivalent power constraint. Substituting $P_n(k)$, we have,

$$G_n(k) \;=\; \left[\log\left(1+\mu_n^{-1}\right) - \log\left(1+\frac{N\sigma_n(k)w_n(k)}{P_n(k)}\right)\right]^+ \;.$$

Therefore, the optimal capacity (6.22) can be expressed as

$$C = \frac{1}{K}\max_{P_n,G_n}\sum_{k=1}^{K}\sum_{n=1}^{N}\log_2\left(1+\frac{P_n(k)}{\chi_n(k)}\left(1-e^{-G_n(k)}\right)\right) \tag{6.28}$$

where,

$$\chi_n(k) = N\sigma_n(k)w_n(k)\;. \tag{6.29}$$

The inverse of $w_n(k)$, can be considered as the *effective channel-gain* for n,k-th mode:

$$|h_n(k)|^2 = \frac{1}{w_n(k)}\;,$$

such that the multi-antenna counter-part to the single antenna capacity seen in Chapter 4, can be written as

$$C = \frac{1}{K}\max_{P_n,G_n}\sum_{k=1}^{K}\sum_{n=1}^{N}\log_2\left(1+\frac{1}{N}\,|h_n(k)|^2\left(1-e^{-G_n(k)}\right)\frac{P_n(k)}{\sigma_n(k)}\right)$$

It can also be shown that the eigen-values of $\mathbf{R}_{\mathbf{s}_k}$ have a water-pouring solution (cf. Appendix D.4).

Space-Frequency Mutual-Water-Pouring: The optimal solution can thus be rewritten as a space-frequency mutual-water-pouring characteristic:

$$P_n(k) = \left[\frac{1}{\xi} - \frac{\chi_n(k)}{(1-e^{-G_n(k)})}\right]^+ \tag{6.30}$$

$$G_n(k) = \left[\log\left(1+\mu_n^{-1}\right) - \log\left(1+\frac{\chi_n(k)}{P_n(k)}\right)\right]^+ \tag{6.31}$$

for $k = 1, \ldots, K$ and $n = 1, \ldots, N$ where, $\chi_n(k)$ is given by (6.29) and the term *mutual* denotes the inter-dependence of $P_n(k)$ and $G_n(k)$ on each other. An iterative mutual-water-pouring algorithm, outlined in Appendix D.5, is used to simulate the results presented in the next section.

6.5 Numerical Results

In this section, we present numerical results for optimal broadband matching for $N = 2$ element uniform circular array of dipole antennas with length[7] 0.475 λ_c and radius $10^{-3}\lambda_c$, spaced $d = 0.25\lambda_c$ apart.

6.5.1 MIMO-OFDM

We now present the MIMO-OFDM system parameters considered in our simulation. These are essentially the same as tabulated in Table 2.1. However, the spatial correlation at the receiver $\mathbf{R}_R$ is calculated using NEC, where the incident electric field is modeled as a superposition of $K' = 32$ vertically polarized plane waves as described in Sec. 3.3.

Fig. 6.2(a) shows the frequency response for $K = 64$ sub-carriers of a 2×2 MIMO-

[7]The length is chosen such that each antenna in isolation, has a relative resonance frequency of 1.

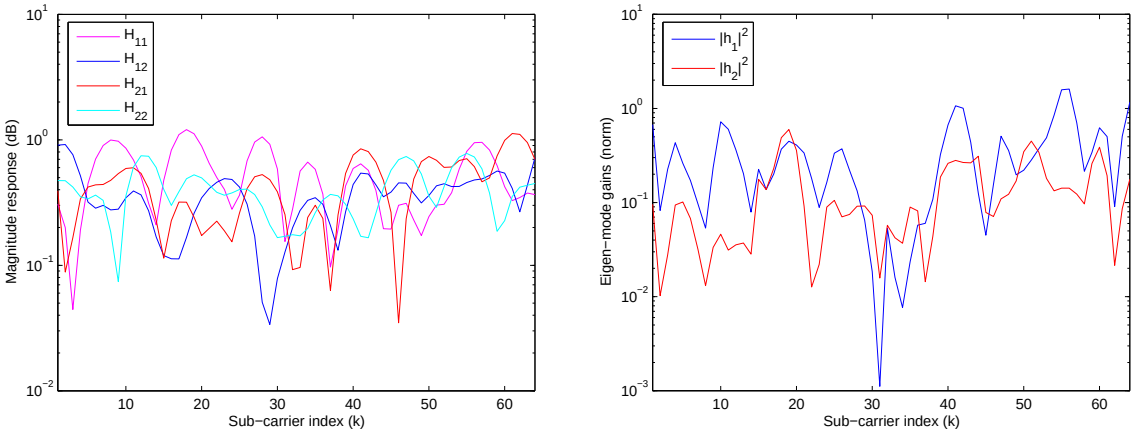

(a) MIMO channel (b) Effective channel gains

Figure 6.2: MIMO-OFDM channel, $N = 2$, $d = 0.25\lambda_c$, $N_t = 15$

OFDM system spread over a 20 MHz bandwidth, where each MIMO link represented by $N_t = 15$ taps. Fig. 6.2(b) shows the corresponding effective channel-gains for the example channel realization. Optimal space-frequency water-pouring solutions for $P_n(k)$ and $G_n(k)$ obtained by iterative mutual-water-pouring algorithm, are shown in Fig. 6.3(a) and Fig. 6.3(b), for an SNR of $\gamma_0 = 10$ dB.

6.5.2 Diversity-OFDM

The jointly-optimal solution provided above gives us information theoretic transceiver designs by enabling optimal matching, power and bandwidth allocation. Although water-pouring over transmit power can easily be done by bit/power loading in OFDM, channel state information feedback to the transmitter typically requires a high bandwidth feedback channel, and water-pouring matching characteristic may be hard to realize in practice. Nevertheless, the jointly-optimal water-pouring solution provides an upper bound on the performance limits of coupled MIMO-OFDM systems.

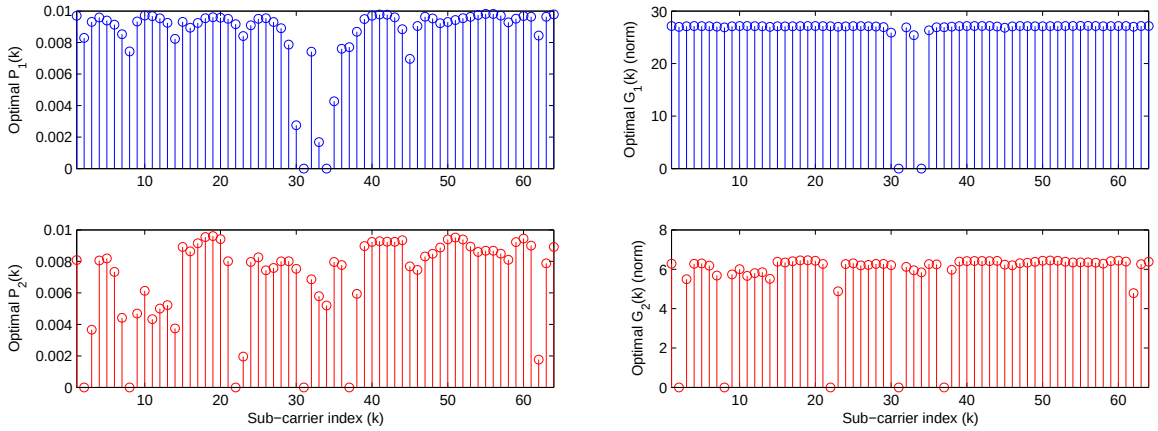

(a) Optimal $P_n(k)$ (b) Optimal $G_n(k)$

Figure 6.3: Optimal solution

It is often desirable to design receivers that operate fairly well over the entire signal bandwidth and are independent of the power allocation and channel fading conditions. Hence, we consider a sub-optimal but practical solution to the problem at hand - *box-car* matching characteristic at the receiver, along with the use of decoupling networks and uniform power allocation at the transmitter.

We consider an N Diversity-OFDM system with equal power allocation across K sub-carriers and box-car matching, i.e.,

$$P(k) = P_0 \ , \ G_n(k) = \frac{G_{0n}}{B} \ , \ n = 1, 2 \ .$$

The capacity of such a system is given by

$$C_{div} \ = \ \frac{1}{K} \sum_{k=1}^{K} \log_2 \left(1 + P_0 \mathbf{h}_k^H \mathbf{Q} \mathbf{\Sigma}_{\mathbf{n}_k}^{-1} (\mathbf{I} - \mathbf{\Gamma}_k \mathbf{\Gamma}_k^H) \mathbf{Q}^H \mathbf{h}_k\right)$$

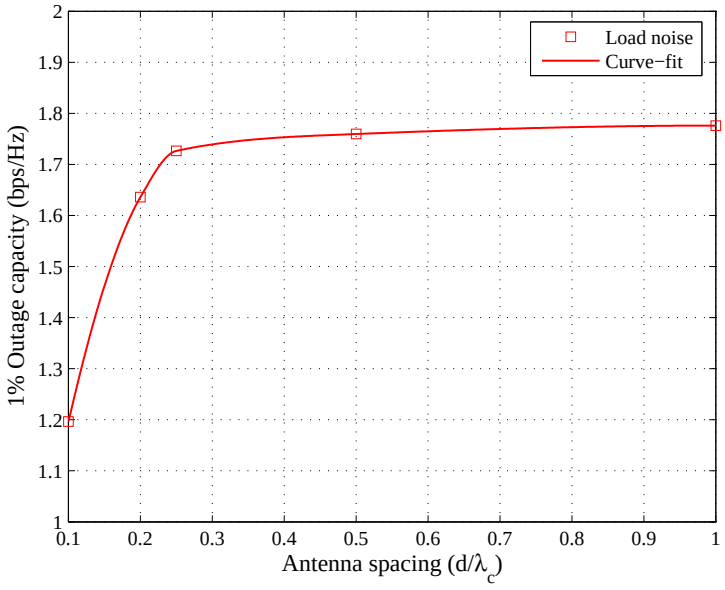

Figure 6.4: Diversity-OFDM: Outage capacity vs. spacing, $N = 2$

where from (6.5)

$$\mathbf{\Sigma}_{\mathbf{n}_k} = \frac{1}{T_0}\left((T_A - T_\beta)\,\mathrm{Re}(\mathbf{\Lambda}_A)(\mathbf{I} - \mathbf{\Gamma}_k\mathbf{\Gamma}_k^H) + (T_\alpha + T_\beta)\mathbf{I}\right) \ .$$

Fig. 6.4 shows 1% outage capacity for different antenna spacings for two element arrays at $\gamma_0 = 10$ dB SNR. The usable bandwidths for the eigen-modes are calculated based on the VSWR < 2 criteria. The results are presented for load-noise dominant $(1:2:0)$ scenarios for a 2% bandwidth. The performance predicted by these simulations shows that with increasing inter-element spacing, the capacity increases for small spacings and saturates around a quarter wave-length spacing. This behavior is in stark contrast to some of the results presented elsewhere assuming narrowband models. Although we have considered equal bandwidths for all of the eigen-modes, a differentiated approach with respect to the mode bandwidths can be applied to optimize the performance of

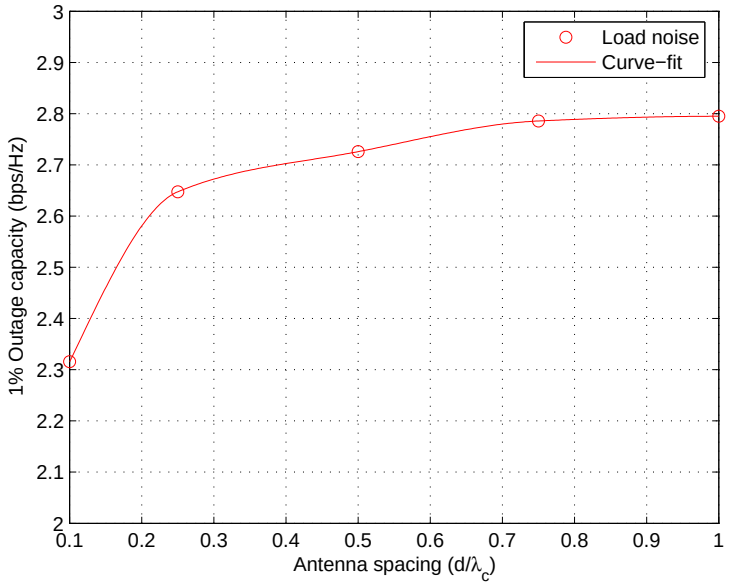

Figure 6.5: Diversity-OFDM: Outage capacity vs. spacing, $N = 4$

Diversity-OFDM systems.

Fig. 6.5 shows 1% outage capacity vs. antenna spacing for a four element UCA at $\gamma_0 = 10$ dB SNR. Once again, the results are presented for load-noise dominant $(1 : 2 : 0)$ scenarios for a 2% bandwidth.

6.6 Conclusion

In this chapter, we primarily investigated the relationship between coupling and RF bandwidth of MIMO systems. In order to arrive at these results, we developed broadband matching theory for coupled impedance networks using S-matrix characterization. By way of optimal matching and power allocation, we analyzed the information theoretic limits of coupled MIMO-OFDM systems, and presented a sub-optimal practical design using box-car characteristics. Although we considered coupling only at the receiver, the

entire analysis can easily be extended to incorporate coupling at both the ends.

We used series RLC approximation for modeling antenna array impedance, to analyze the behavior of eigen-modes of the array. Systems with much larger relative bandwidths can be analyzed by using more exact impedance models, either through analytic modeling for the entire frequency range, or by use of numerical techniques (such as real-frequency method), to compute the integral constraints. An extension to large circular arrays was also presented. Another form of arrays that is of considerable interest for MIMO systems are uniform linear arrays. Although a straight-forward extension is not possible, this study does provide qualitative insights into how such a system might behave for varying amounts of coupling.

Chapter 7

Conclusion

We conclude this dissertation with a summary of some of the main findings and suggest topics for future work.

7.1 Summary and Discussion

We began with an overview of some of the popular MIMO communication schemes in Chapter 2, and presented system models that incorporate fading correlation among the antennas. Later, we considered the impact of mutual coupling in compact transceivers for antenna selection systems in Chapter 3, by presenting a realistic model that considers the impact of inactive-element termination on the system performance. We primarily considered optimal matching and parasitic network design for uniform linear and circular arrays. We discussed some of the implementation aspects and provided simpler alternatives to transceiver design that achieve near-optimal performance. Specifically, we showed that parasitic selection designs benefit compact arrays significantly, due to coupling between the antennas. Thus, packing more antennas in a constrained space

and employing antenna selection offers, at least, $3-4$ dB performance improvement over conventional 2-element diversity systems for a $\lambda/2$-sized array.

We also highlighted how optimal multiport matching networks are known to be sensitive to the RF bandwidth of a coupled system. The lack of a sound understanding motivated us to investigate this phenomenon in greater detail. We addressed the issue of matching and bandwidth first, by looking at a single antenna example and formulated an information theoretic approach to characterize optimal broadband matching in Chapter 4. Based on broadband matching theory, we developed constraints imposed on a matching network using an impedance model for the antenna, and demonstrated that a frequency-flat reflection coefficient over an arbitrary bandwidth is not optimal, although, such an approach with optimal bandwidth gives near-optimal results.

In Chapter 5, we extended the problem to include coupling in MIMO systems and analyzed its impact on the bandwidth of MIMO systems. Using S-matrix characterization, we proposed a theory of broadband matching for coupled networks and formulated the matching constraints for uniform circular arrays. The main findings of the study revealed that the eigen-modes of the array start to behave asymmetrically when coupling is introduced in the system. The system starts to loose diversity advantages, and coupling diminishes the RF bandwidth of some of its eigen-modes. We illustrated this behavior by considering $2, 3$ and 4 element arrays.

7.2 Future Work

Several interesting research problems were encountered while pursuing the work addressed in this dissertation. Here, we discuss some of those issues as open problems for future work.

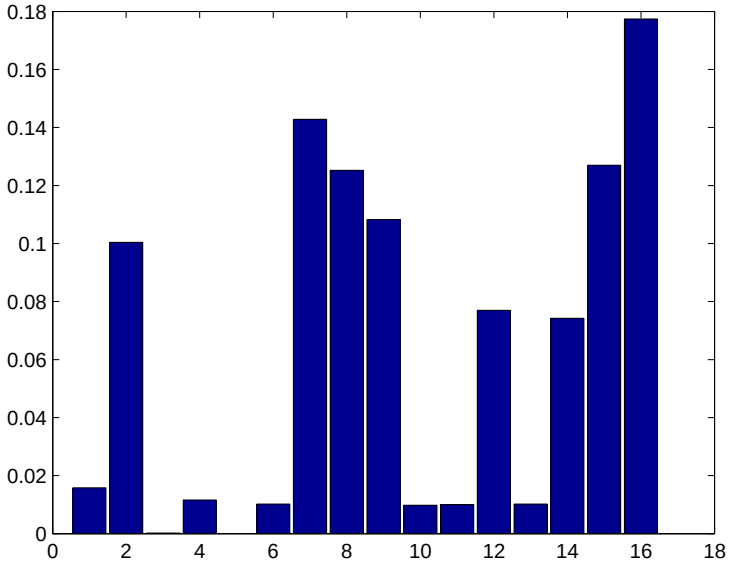

Figure 7.1: Histogram of parasitic switching combinations (ULA): $(5, 2)$

Antenna Selection: The performance benefits of an selection system come at the cost of an additional hardware-switching circuitry. Although, in selection systems with antennas spaced far apart, it suffices to pick the active antenna subset with L highest SNR branches, such is not the case in compact arrays. Ideally, the switching network should cycle through all combinations to estimate the optimal subset. When applied to parasitic switching scheme, the number of possible combinations grows exponentially with the number of inactive-element termination states (2^{N-L}) in $\mathcal{Z}_{\mathcal{P}}$. Fig. 7.1 shows the histogram of $\mathbf{Z}_P$ that maximizes the SNR at the receiver for parasitic selection combining systems with 1 active element out of 5. Evidently, only about half of the available combinations contribute to the overall performance, suggesting that a quick search procedure can be devised by ignoring the least likely candidates, to trade-off complexity with performance.

Besides, there are pertinent switching aspects in antenna selection systems that need to be considered, some of which we alluded to, in Chapter 3. The assumption of a noise-

less ideal switching network with low insertion loss is a rarely the case, although, certain RF MEMS switches [9] are known to offer less than 1 dB insertion loss at low speeds (switching time: few μs). Another important aspect of how often the active subset has to be computed, could be a significant overhead on the implementation costs, although, in slowly-varying or quasi-static channels, such as indoor WLAN channels, the switching frequency is considerably reduced. All these seemingly-tiny issues can play a crucial role in predicting the performance gains of antenna selection systems in compact arrays, and thus, mandate a closer look.

Adaptive Matching: The optimal matching network presented for broadband systems has certain limitations. While it provides optimal performance, limited area for electronics on a device, may create additional coupling from other hardware components and disturb the symmetry among the antennas. In such a case, it may be difficult to decouple a broadband antenna array using Butler matrices, rendering multiport matching almost unrealizable. The self-matching on the other hand, is robust but sub-optimal, in that it does not adapt to the varying channel conditions. Thus, an *adaptive* 2-port matching network should most likely, offer a good trade-off between optimal matching and non-adaptive self-matching. A similar idea for narrowband diversity systems has been studied in [36]. Another area where adaptive matching might manifest itself useful is the parasitic antenna selection and switching strategies proposed in this work. The optimal parasitic network and inactive element termination, could significantly benefit from the idea of adaptive reactive termination.

Broadband Matching for a given Transceiver: In analyzing the limits of a broadband coupled MIMO system, we assumed a simplistic transceiver model with ideal loads. However, practical transceivers may have a much more complex hardware circuitry, where all

the RF chains and their components are intrinsically coupled. For a given coupled RF front end, this would require analysis of additional matching constraints imposed on the matching network due to coupled amplifiers and downstream components. Such a study shall reveal optimal design methodologies for a complete broadband RF transceiver, one that consists of amplifiers, phasers, mixers and loads, such that minimal spectral efficiency loss occurs at each stage.

Miscellaneous: It should be interesting to look at more modern and practical kind of antennas (e.g., patch antennas and printed inverted-F antennas (PIFA)) and array structures (e.g. 2D planar arrays with concentric rings or squares useful for laptops, etc.). Besides, experimental work involving implementing these transceiver structures for antenna selection and MIMO systems, to analyze the performance improvements in practice as opposed to theory, should offer significant insights into challenges encountered in practical systems.

Bibliography

[1] http://datasheets.maxim-ic.com/en/ds/MAX2642-MAX2643.pdf

[2] S. M. Alamouti, "A simple transmit diversity technique for wireless communications," *IEEE Journal on Selected Areas in Communications*, 1998.

[3] C. A. Balanis, *Antennas Theory: Analysis and Design*, 3rd edition, John Wiley and Sons, 2005.

[4] C. A. Balanis, *Modern Antenna Handbook*, Wiley, New York, 2008.

[5] H. W. Bode, *Network Analysis and Feedback Amplifier Design*, Van Nostrand, New York, 1945.

[6] R. Blum and J. Winters, "On optimum MIMO with antenna selection," *IEEE Comm. Letters*, vol. 6(8), pp-322-324, Aug. 2002.

[7] H. Bolcskei, D. Gesbert and A. Paulraj, "On the Capacity of OFDM-Based Spatial Multiplexing Systems," *IEEE Transactions on Communications*, vol. 50, no. 2, pp. 225-234, Feb. 2002.

[8] D. G. Brennan, "Linear diversity combining techniques," *Proceedings of the IRE*, vol. 47, pp. 1075-1102, Jun. 1959.

[9] E. R. Brown, "RF-MEMS switches for reconfigurable integrated circuits," *IEEE Transactions on Microwave Theory and Techniques*, vol. 46, no. 11, pp. 1868-1880 Nov. 1998.

[10] G. J. Burke and A. J. Poggio, "Numerical Electromagnetics Code (NEC) – Method of moments," Tech. Doc. 11, Naval Ocean Systems Center, San Diego, CA, Jan. 1981.

[11] J. Butler and R. Lowe, "Beamforming matrix simplifies design of electronically scanned antennas," *Electron. Design*, Apr. 1961.

[12] H. J. Carlin, "The scattering matrix in network theory," *IRE Trans. Circuit Theory*, vol. CT-3, pp. 88-97, June 1956.

[13] H. J. Carlin and P. J. Crepeau, "Theoretical limitations on the broadband matching of arbitrary impedance," *IRE Trans. Circuit Theory (corresp.)*, vol. CT-S, p. 165, June 1961.

[14] H. J. Carlin, "A new approach to gain-bandwidth problems," *IEEE Transactions on Circuits and Systems*, vol. CAS-24, no. 4, Apr. 1977.

[15] R. W. Chang, "Synthesis of band-limited orthogonal signals for multi-channel data transmission," *Bell System Technical Journal*, vol. 46, pp. 1775-1796, 1966.

[16] W. K. Chen, *Broadband matching: Theory and Implementations*, 2nd edition, World Scientific, 1988.

[17] W. K. Chen, "Mathematical theory of broadband matching of multiport networks," *Journal of the Franklin Institute*, vol. 326, no. 5, pp. 737-747, 1989.

[18] W. K. Chen and Q. Z. Zha, "Factorizations and complex normalization of scattering matrices," *Proceedings of the 34th Midwest Symposium on Circuits and Systems*, vol. 2, pp. 716-718, May 1991.

[19] M. Chiani, M. Z. Win and A. Zanella, "On the capacity of spatially correlated MIMO Rayleigh-fading channels," *IEEE Trans. Info. Theory*, vol. 49, no. 10, pp. 2363-2371, Oct. 2003.

[20] T. M. Chien, "A Theory of Broadband Matching of Frequency Dependent Generator and Load," Ph.D. thesis, Polytechnic Institute of Brooklyn, New York, 1969.

[21] T. M. Chien, "A theory of broadband matching of a frequency-dependent generator and load - Part I: Theory," *Journal of the Franklin Institute* pp. 181-199, vol. 298, no. 3, Sep. 1974.

[22] T. M. Chien, "A theory of broadband matching of a frequency-dependent generator and load - Part II: Design procedures and applications," *Journal of the Franklin Institute* pp. 201-221, vol. 298, no. 3, Sep. 1974.

[23] C. Chuah, J. Kahn and D. Tse, "Capacity of multi-antenna array systems in indoor wireless environment," *Proc. IEEE Globecom*, pp. 1894-1899, Sydney, Australia, Nov. 1998.

[24] C. Chuah, D. Tse, J. Kahn and R. Valenzuela, "Capacity scaling in MIMO wireless systems under correlated fading," *Proc. IEEE Trans. on Information Theory*, vol. 48(3), pp. 637-650, Mar. 2002.

[25] R. H. Clarke, "A statistical theory of mobile-radio reception," *The Bell System Technical Journal*, vol. 47, pp. 957–1000, July 1968.

[26] T. Cover and J. Thomas, *Elements of Information Theory*, Wiley, New York, 1991.

[27] S. Darlington, "Synthesis of reactance 4-poles," *Journal of Mathematics and Physics*, vol. 18, pp. 275-353, Sep. 1939.

[28] C. A. Desoer, "The maximum power transfer theorem for n-ports," *IEEE Transactions on Circuit Theory*, pp. 328-330, May 1973.

[29] C. P. Domizioli et al., "Receive diversity revisited: correlation, coupling, and noise," in *Proc. 2007 IEEE Global Commun. Conf.*, Washington, D.C., pp. 3601-3606.

[30] C. P. Domizioli *et al.*, "Optimal front-end design for MIMO receivers," in *Proc. 2008 IEEE Global Commun. Conf.*, New Orleans, LA.

[31] C. P. Domizioli, "Noise analysis and low-noise design for compact multi-antenna receivers: A communication theory perspective," Ph.D. dissertation, North Carolina State University, Raleigh, NC, USA, 2009.

[32] Y. Dong *et al.*, "The Impact of Mutual Coupling on MIMO Maximum-Ratio Combining," in *Proc. 2007 IEEE Global Commun. Conf.*, Washington, D.C.

[33] Y. Dong *et al.*, "Mutual Coupling Effects in MIMO MRC Systems with Limited Feedback," in *Proc. 2008 IEEE Global Commun. Conf.*, New Orleans, LA.

[34] R. S. Elliot, *Antenna Theory and Design*, The IEEE Press Series on Electromagnetic Wave Theory, revised edition, John Wiley and Sons, 2003.

[35] R. M. Fano, "Theoretical limitations on the broadband matching of arbitrary impedances," *Journal of the Franklin Institute*, vol. 249, 1950.

[36] Y. Fei, Y. Fan, and J. S. Thompson, "Optimal single-port impedance matching for compact MIMO arrays," *IEEE Globecom*, pp. 4511-4515, Dec. 2007.

[37] F. D. Flaviis, L. Jofre and J. Romeu, *Multiantenna Systems for MIMO Communications*, Morgan and Claypool, 2008.

[38] G. Foschini, "Layered space-time architecture for wireless communication in a fading environment when using multi-element antennas," *Bell Labs. Technical Journal* pp. 41-59, 1996.

[39] G. J. Foschini and M. J. Gans, "On limits of wireless communications in a fading environment when using multiple antennas," *Wireless Personal Communications*, vol. 6, pp. 311-335, Feb. 1998.

[40] H. T. Friis, "A note on a simple transmission formula," *Proc. IRE*, vol. 34, pp. 254-256. 1946.

[41] R. G. Gallager, *Information Theory and Reliable Communication*, New York, Wiley, 1968.

[42] M. J. Gans, "Channel capacity between antenna arrays – Part I: Sky noise dominates," *IEEE Transactions on Communications*, vol. 54, no. 9, pp. 1587-1592, Sep. 2006.

[43] M. J. Gans, "Channel capacity between antenna arrays – Part II: Amplifier noise dominates," *IEEE Transactions on Communications*, vol. 54, no. 11, pp. 1983-1992, Nov. 2006.

[44] A. Goldsmith, S. A. Jafar, N. Jindal and S. Vishwanath, "Capacity limits of MIMO channels," *IEEE JSAC*, vol. 21, no. 5, pp. 684-702, Jun. 2003.

[45] A. Goldsmith, *Wireless Communications*.

[46] C. L. Goldsmith et al., "Performance of low-loss RF MEMS capacitive switches," *IEEE Microwave and Guidedwave Letters*, vol. 13, no. 10, pp. 437-439, Oct. 2003.

[47] D. Gore and A. Paulraj, "MIMO antenna sub-set selection for space-time coding," *IEEE Trans. Sig. Proc.*, vol. 50(10), pp-2580-2588, Oct. 2002.

[48] A. Gorokhov, D. Gore, and A. Paulraj, "Receive antenna selection for MIMO flat-fading channels: Theory and algorithms," *IEEE Trans. on Information Theory*, vol. 49, pp. 2687-2696, Oct. 2003.

[49] M. Gustafsson and S. Nordebo, "Bandwidth, Q factor, and resonance models of antennas," *PIER*, vol. 62, pp. 120, 2006.

[50] M. Gustafsson and S. Nordebo, "On the spectral efficiency of a sphere," *PIER*, vol. 67, pp. 275-296, 2007.

[51] M. Hamer and M. Butcher, "Experimental vehicular angle-diversity antenna using mutual coupling," in *Proc. Antennas Propagat. Soc. Int. Symp.*, Chicago, IL, vol. 2, pp. 1089-1091, Jul. 1992.

[52] R. F. Harrington, "Reactively controlled directive array," *IEEE Transactions on Antennas and Propagation*, vol. AP-26, no. 3, pp. 390-395, May 1978.

[53] H. A. Haus and R. B. Adler, *Circuit Theory of Linear Noisy Networks*, New York: Wiley, 1959.

[54] R. Heath and A. Paulraj, "Antenna selection for spatial multiplexing systems based on minimum error rate," *IEEE ICC*, vol. 7, pp-2276-2280, Helsinki, Finland, Jun. 2001.

[55] W. C. Jakes, *Microwave Mobile Communications*, IEEE Press, 1994.

[56] R. Janaswamy, "Effect of element mutual coupling on the capacity of fixed length linear arrays", *IEEE Antennas and Propagation Letters*, vol. 1, pp. 157-160, 2002.

[57] M. A. Jensen and J. W. Wallace, *Space-Time Processing for MIMO Communications: Chapter 1: MIMO Wireless Channel Modeling and Experimental Characterization*, Wiley, 2005.

[58] J. P. Kermoal et al, "A stochastic MIMO radio channel model with experimental validation," *IEEE Journal on Selected Areas in Communications*, vol. 20, pp. 1211-1226, August 2002.

[59] N. Kong and L. B. Milstein, "Combined average SNR of a generalized diversity selection combining scheme," *IEEE Communication Letters*, vol. 3, pp-57-59, Mar. 1999.

[60] B. K. Lau *et. al.*, "Impact of matching network on bandwidth of compact antenna arrays," *IEEE Trans. Antennas Propag.*, vol 54, no. 11, pp. 3225-3238, Nov. 2006.

[61] W. C. Y. Lee, "Mutual coupling effect on maximum-ratio diversity combiners and application to mobile radio," *IEEE Trans. on Comm. Technology*, vol. com-18, no. 6, pp. 779-791, Dec. 1970.

[62] A. Lozano and C. Papadias, "Layered space-time receivers for frequency-selective wireless channels," *IEEE Trans. Comm.*, vol. 50(1), pp. 65-73, Jan. 2002.

[63] D. Lu, D. K. C. So, and A. K. Brown, "Receive antenna selection scheme for V-BLAST with mutual coupling in correlated channels," *Proceedings of IEEE International Symposium on Personal, Indoor and Mobile Radio Communications*, pp. 15, Cannes, France, Sep. 2008.

[64] A. W. Marshall and I. Olkin, *Inequalities: Theory of Majorization and Its Applications*, Academic Press, 1979.

[65] T. Marzetta, "BLAST training: Estimating channel characteristics for high-capacity space-time wireless," *Proc. Allerton Conf. on Comm., Control and Computing*, Monticello, IL, Sep. 1999.

[66] P. Mattheijssen et al., "Antenna-pattern diversity versus space diversity for use at handhelds," *IEEE Trans. on Veh. Tech.*, vol. 53, no. 4, pp. 1035-1042, Jul. 2004.

[67] N. B. Mehta and A. F. Molisch, *MIMO System Technology for Wireless Communications*, Taylor and Francis, 2006.

[68] C. D. Meyer, *Matrix Analysis and Applied Linear Algebra*, SIAM, 2000.

[69] A. F. Molisch, N. B. Mehta, H. Zhang, P. Almers, and J. Zhang, "Implementation aspects of antenna selection for MIMO systems," *First International Conference on Communications and Networking in China* pp. 1-7, Oct. 2006.

[70] A. F. Molisch, M. Z. Win, and J. H. Winters, "Capacity of MIMO systems with antenna selection," *Proc. IEEE Int. Conf. on Communications*, Helsinki, pp. 570-574, 2001.

[71] A. F. Molisch, X. Zhang, S. Y. Kung, and J. Zhang, "FFT-based hybrid antenna selection schemes for spatially correlated MIMO channels," *Proc. PIMRC*, pp. 1119-1123, 2003.

[72] A. F. Molisch and M. Z. Win, "MIMO systems with antenna selection," *IEEE Microwave Magazine*, March 2004.

[73] A. F. Naguib, A. Paulraj and T. Kailath, "Capacity improvement with base-station antenna arrays in Cellular CDMA," *IEEE Transactions on Vehicular Technology*, pp. 691-698, Aug. 1994.

[74] A. Papoulis, *Probability, Random Variables, and Stochastic Processes*, McGraw-Hill, New York, NY, 1984.

[75] J. Papoulis, *Digital Communications*, 3rd edition, McGraw-Hill, New York, NY, 1995.

[76] A. Paulraj, R. Nabar and D. Gore, *Introduction to Space-Time Wireless Communications*, 2nd edition, Cambridge University Press, 2005.

[77] D. M. Pozar, *Microwave Engineering*, Wiley, New York, 1998.

[78] D. M. Pozar, *Microwave and RF Design of Wireless Systems*, Wiley, New York, 2001.

[79] R. Prasad, *OFDM for Wireless Communications Systems*, Artech House Publishers, 2004.

[80] G. Raleigh and J. Cioffi, "Spatio-temporal coding for wireless communication," *IEEE Transactions on Communications*, vol. 46(3), pp. 357-366, Mar. 1998.

[81] H. Rothe and W. Dahlke, "Theory of noisy fourpoles," *Proc. IRE*, vol. 44, pp. 811-818, Jun. 1956

[82] A. W. Rudge *et. al*, "The Handbook of Antenna Design," *Electromagnetic Waves*, vol. 2, no. 15-16, 1983.

[83] H. Sampath, "Generalized linear precoder and decoder design for MIMO channels using the weighted MMSE criterion," *IEEE Trans. on Comm.*, vol. 49(12), pp. 2198-2206, Dec. 2001.

[84] A. Sayeed, "Deconstructing multiantenna fading channels," *IEEE Transactions on Signal Processing*, vol. 50, no. 10, pp. 2563-2579, Oct. 2002.

[85] N. L. Scott et al., "Diversity gain from a single-port adaptive antenna using switched parasitic elements illustrated with a wire and monopole prototype," *IEEE Transactions on Antennas and Propagation*, vol. 47, no. 6, pp. 1066-1070, Jun. 1999.

[86] C. E. Shannon, "A mathematical theory of communication," *The Bell Systems Technical Journal*, vol. 27, pp. 379-423, 623-656, Jul., Oct. 1948.

[87] J. P. Shelton and K. S. Kelleher, "Multiple beams from linear arrays," *Trans. IRE*, vol. AP-9, pp. 154-161, Mar. 1961.

[88] S. Stearns, "New Results on Antenna Impedance Models and Matching," *ARRL Pacificon Antenna Seminar*, San Ramon, CA, Oct. 2007.

[89] P. S. Taluja and B. L. Hughes, "Information theoretic optimal broadband matching for communication systems," in *Proc. 2010 IEEE Global Commun. Conf.*, Miami, FL.

[90] I. E. Telatar, "Capacity of multi-antenna Gaussian channels," *European Transactions on Telecommunications*, vol. 10, pp. 585-595, 1999.

[91] A. M. Tulino, A. Lozano and S. Verdu, "Impact of antenna correlation on the capacity of multiantenna channels," *IEEE Trans. Info. Theory*, vol. 51, no. 7, pp. 2491-2509, Jul. 2005.

[92] D. V. Theil and S. Smith, *Switched Parasitic Antennas for Cellular Communications*, Artech House Publishers, 2002.

[93] D. Tse and P. Vishwanath, *Fundamentals of Wireless Communication*, Cambridge University Press, Cambridge, UK, 2005.

[94] A. M. Tulino, A. Lozano and S. Verdu, "MIMO capacity with channel state information at the transmitter," *IEEE ISSSTA*, Aug. 2004.

[95] R. Q. Twiss, "Nyquists and Thevenins theorems generalized for nonreciprocal linear networks," *J. Applied Physics*, vol. 26, pp. 599-602, May 1955.

[96] R. Vaughan, "Switched parasitic elements for antenna diversity," *IEEE Transactions on Antennas and Propagation*, vol. 47, no. 2, pp. 399-405, Feb. 1999.

[97] R. Vaughan and B. A. Andersen, *Channels, Propagation and Antennas for Mobile Communications*, 2nd edition, IEE Electromagnetic Waves Series 50, 2003.

[98] S. Verdu, *Multiuser Detection*, Cambridge University Press, Cambridge, UK, 1998.

[99] J. W. Wallace and M. A. Jensen, "Termination-Dependent Diversity Performance of Coupled Antennas: Network Theory Analysis," IEEE Transactions on Antennas and Propagation, vol. 52, no. 1, Jan. 2004.

[100] J. W. Wallace and M. A. Jensen, "Mutual coupling in MIMO wireless systems: A rigorous network theory analysis," *IEEE Transactions on Wireless Communications*, vol. 3, pp. 13171325, Jul. 2004.

[101] J. L. Wan and W. K. Chen, "Broadband matching of multi-port networks termination in frequency-dependent loads," *Circuits, Systems, Signal Process*, vol. 4, no. 3, pp. 385-411, 1983.

[102] S. Weinstein and P. Ebert, "Data transmission by frequency-division multiplexing using the discrete Fourier transform," *IEEE Transactions on Communication Technology*, vol. 19, no. 5, pp. 628634, Oct. 1971.

[103] M. Z. Win, G. Chrisikos, and J. H. Winters, "Error probability for M-ary modulation using hybrid selection-maximal-ratio combining in Raleigh fading," *Proc. Military Comm. Conf.*, vol. 2, pp. 944-948, Nov. 1999.

[104] M. Z. Win and J. H. Winters, "Exact error probability expressions for H-S/MRC in Rayleigh fading: A virtual branch technique," *Proc. IEEE Global Telecomm. Conf.*, vol. 1, pp. 537-542, Dec. 1999.

[105] M. Z. Win and J. H. Winters, "Analysis of hybrid selection/maximal ratio combining in Rayleigh fading," *IEEE Transactions on Communications*, vol. 47, pp. 1773-1776, Dec. 1999.

[106] M. Z. Win and J. H. Winters, "Virtual branch analysis of symbol error probability for hybrid selection/maximal-ratio combining in Rayleigh fading," *IEEE Transactions on Communications*, vol. 49, pp. 1926-1934, Nov. 2001.

[107] M. Z. Win, N. C. Beaulieu, L. A. Shepp, B.F. Logan, and J.H. Winters, "On the SNR penalty of MPSK with hybrid selection/maximal ratio combining over I.I.D. Rayleigh fading channels", *IEEE Transactions on Communications*, Jun. 2003.

[108] J. H. Winters, "Smart Antenna for Wireless Systems," *IEEE Personal Communications*, pp. 23-27, Feb. 1998.

[109] M. R. Wohlers, "Complex normalization of scattering matrices and the problem of compatible impedances," *IEEE Trans. Circuit Theory*, vol. CT-12, pp. 528-535, Dec. 1965.

[110] P. W. Woliansky, G. J. Foschini, G. D. Golden, and R. A. Valenzuela, "V-BLAST: An architecture for realizing very high data rates over the rich-scattering wireless channel", *Proc. URSI ISSSE*, pp. 295-300, Sep. 1998.

[111] Z. Xu, S. Sfar, and R. S. Blum, "On the importance of modeling the mutual coupling for antenna selection for closely-spaced arrays," *Conference on Information Sciences and Systems*, 2006.

[112] H. Yagi, "Beam transmission of ultra short waves," *Proceedings of the IEEE*, vol. 16, pp. 715-741, Jun. 1928.

[113] Y. Yang, S. Sfar, and R. S. Blum, "A Simulation Study of Antenna Selection for Compact MIMO Arrays," *Conference on Information Sciences and Systems*, 2008.

[114] Y. Yang, R. S. Blum, and S. Sfar, "Antenna selection for MIMO systems with closely spaced antennas," *EURASIP Journal on Wireless Communications and Networking*, 2009.

[115] Z. J. Yao et al., "Micromachined low-loss microwave switches," Journal of Microelectromechanical Systems, vol. 8, issue 2, pp. 129-134, Aug. 2002.

[116] D. C. Youla, "Solution to the problem of complex normalization," Polytechnic Institute of Brooklyn, New York, Memo 48, PIBMRI 891-61, Jan. 1961.

[117] D. C. Youla, "On scattering matrices normalized to complex port numbers," *Proc. IRE (corresp.)*, vol. 49, p. 1221, July 1961.

[118] D. C. Youla, "A new theory of broadband matching," *IEEE Tram. Circuit Theory*, vol. CT-II, pp. 30-50, March 1964.

[119] D. C. Youla, "An extension of the concept of scattering matrix," *IEEE Trans. Circuit Theory*, vol. CT-II, pp. 310-312, June 1964.

[120] Y. Zhang, K. Hirasawa, and K. Fujimoto, "Opened parasitic elements nearby a driven dipole", *IEEE Transactions on Antennas and Propagation*, vol. AP-34, no. 5, pp. 711-713, May 1986.

[121] X. Zhang, A. F. Molisch, and S. Y. Kung, "Phase-shift-based antenna selection for MIMO channels," *Proc. Globecom*, pp. 1089-1093, 2003.

[122] L. Zheng and D. Tse, "Diversity and Multiplexing: A fundamental tradeoff in multiple-antenna channels," *IEEE Trans. Info. Theory*, vol. 49, no. 5, pp. 1073-1096, May 2003.

Appendices

Appendix A

Antenna Selection

A.1 Equivalent Channel

Observe that we can rewrite (3.17) as

$$\begin{aligned}
\mathbf{C} &= \mathbf{Q}\underbrace{\left(z_{21}(\mathbf{\Lambda}'_{\mathcal{S}} + z_{11}\mathbf{I})^{-1}\right)}_{\mathbf{\Lambda}_C}\mathbf{Q}^H \\
\mathbf{D} &= \mathbf{Q}\left(z_l\left[(z_l + z_{22})\mathbf{I} - z_{12}\mathbf{\Lambda}_C\right]^{-1}\right)\mathbf{Q}^H \\
\mathbf{M} &= \mathbf{Q}\left(\mathbf{\Lambda}_{as}\left(\mathbf{\Lambda}_{\mathcal{S}} + \mathbf{\Lambda}_{ss}\right)^{-1}\right)\mathbf{Q}^H
\end{aligned}$$

The equivalent selection matrix (3.9) can similarly be broken into

$$\mathbf{T}_{\mathcal{S}} = \mathbf{I}_{\mathcal{S}} - \mathbf{Q}\mathbf{\Lambda}_{\mathcal{S}\bar{\mathcal{S}}}(\mathbf{\Lambda}_P + \mathbf{\Lambda}_{\bar{\mathcal{S}}\bar{\mathcal{S}}})^{-1}\mathbf{Q}^H\mathbf{I}_{\bar{\mathcal{S}}}$$

where, $\mathbf{D} = \mathbf{Q}\mathbf{\Lambda}_D\mathbf{Q}^H$ and $\mathbf{M} = \mathbf{Q}\mathbf{\Lambda}_M\mathbf{Q}^H$. From optimal matching, we note that

$$\mathbf{\Lambda}_{\mathcal{S}} + \mathbf{\Lambda}_{ss} = \mathrm{Re}[\mathbf{\Lambda}_{\mathcal{S}}]\ ,\ \mathbf{\Lambda}'_{\mathcal{S}} = z_{opt}\mathbf{I}$$

implying that $\mathbf{\Lambda}_C$ and $\mathbf{\Lambda}_D$ are independent of $\mathbf{Z}_P$, while

$$\begin{aligned}\mathbf{\Lambda}_M &= \sqrt{r_{opt}}\left(\mathrm{Re}[\mathbf{\Lambda}_{\mathcal{S}}]\right)^{-1/2} \\ &= \sqrt{r_{opt}}\left(\mathrm{Re}\left[\mathbf{\Lambda}_{\mathcal{S}\mathcal{S}} - \mathbf{\Lambda}_{\mathcal{S}\bar{\mathcal{S}}}\left(\mathbf{\Lambda}_P + \mathbf{\Lambda}_{\bar{\mathcal{S}}\bar{\mathcal{S}}}\right)^{-1}\mathbf{\Lambda}_{\bar{\mathcal{S}}\mathcal{S}}\right]\right)^{-1/2}\end{aligned}$$

The equivalent fading path-gains can thus be written as

$$\begin{aligned}\mathbf{h} &= \mathbf{Q}\mathbf{\Lambda}_D\mathbf{\Lambda}_C\mathbf{\Lambda}_M\mathbf{Q}^H(\mathbf{T}_{\mathcal{S}}\mathbf{h}_o) \\ &= \mathbf{Q}\mathbf{\Lambda}_D\mathbf{\Lambda}_C\mathbf{\Lambda}_M\mathbf{h}'\end{aligned}$$

and the noise covariance for amplifier-noise dominant scenarios, is given by

$$\begin{aligned}\mathbf{\Sigma}'_{\mathbf{n}} &= \mathbf{D}\mathbf{C}\left[r_a\mathbf{I} + g_a(\mathbf{Z}'_{\mathcal{S}} + z_{cor}\mathbf{I})(\mathbf{Z}'_{\mathcal{S}} + z_{cor}\mathbf{I})^H\right]\mathbf{C}^H\mathbf{D}^H \\ &= |\sigma_a|^2\mathbf{Q}\mathbf{\Lambda}_D\mathbf{\Lambda}_C\mathbf{\Lambda}_C^H\mathbf{\Lambda}_D^H\mathbf{Q}^H\end{aligned}$$

where

$$|\sigma_a|^2 = r_a + g_a|z_{opt} + z_{cor}|^2 \ .$$

A.2 Optimal Parasitic Network Evaluation

For $N = 4$, let us consider an example active subset

$$\mathbf{I}_{\mathcal{S}} = \begin{bmatrix} 1 & 0 & 0 & 0 \\ 0 & 0 & 1 & 0 \end{bmatrix}$$

such that

$$\begin{aligned}\mathbf{Q}^H\mathbf{T}_{\mathcal{S}} &= \mathbf{Q}^H\mathbf{I}_{\mathcal{S}} - \mathbf{\Lambda}_T\mathbf{Q}^H\mathbf{I}_{\bar{\mathcal{S}}} \\ &= \frac{1}{\sqrt{2}}\begin{bmatrix} 1 & -\lambda_{T1} & 1 & -\lambda_{T1} \\ 1 & -\lambda_{T2} & -1 & \lambda_{T2} \end{bmatrix}\end{aligned}$$

where we have used

$$\mathbf{T}_{\mathcal{S}} = \mathbf{I}_{\mathcal{S}} - \mathbf{Q}\mathbf{\Lambda}_T\mathbf{Q}^H\mathbf{I}_{\bar{\mathcal{S}}} \ , \ \mathbf{\Lambda}_T = \mathbf{\Lambda}_{\mathcal{S}\bar{\mathcal{S}}}\left(\mathbf{\Lambda}_P + \mathbf{\Lambda}_{\bar{\mathcal{S}}\bar{\mathcal{S}}}\right)^{-1}$$

From

$$\begin{aligned}\mathbf{h}' &= \mathbf{Q}^H\mathbf{T}_{\mathcal{S}}\mathbf{h}_o \\ &= \left(\mathbf{Q}^H\mathbf{I}_{\mathcal{S}} - \mathbf{\Lambda}_T\mathbf{Q}^H\mathbf{I}_{\bar{\mathcal{S}}}\right)\mathbf{h}_o \\ &= \frac{1}{\sqrt{2}}\begin{bmatrix} 1 & -\lambda_{T1} & 1 & -\lambda_{T1} \\ 1 & -\lambda_{T2} & -1 & \lambda_{T2} \end{bmatrix}\begin{bmatrix} h_1 \\ h_2 \\ h_3 \\ h_4 \end{bmatrix}\end{aligned}$$

To illustrate, let us consider the first entry of $\mathbf{h}'$

$$h_1' = \frac{1}{\sqrt{2}}\Big((h_1 + h_3) - \lambda_{T1}(h_2 + h_4)\Big)$$

such that

$$\begin{aligned}\mathbb{E}(|h_1'|^2) &= \frac{1}{2}\Big(\mathbb{E}(|h_1+h_3|^2)+|\lambda_{T1}|^2\mathbb{E}(|h_2+h_4|^2)-2\mathrm{Re}(\mathbb{E}((h_1^*+h_3^*)(h_2+h_4))\lambda_{T1})\Big)\\ &= \frac{1}{2}\Big(\mu_1+\mu_2|\lambda_{T1}|^2-2\mathrm{Re}(\mu_3\lambda_{T1})\Big)>0\end{aligned}$$

From

$$\mathbf{\Lambda}_P = \arg_{\mathbf{\Lambda}_P}\max\left\{\sum_{k=1}^{L}\left|[\lambda_M]_k\right|^2\mathbb{E}\left(\left|h_k'\right|^2\right)\right\}$$

the eigen-values of the optimal parasitic network can be obtained by maximizing each term in the summation above individually, that is

$$\lambda_P = \arg\max_x\left\{\left|\lambda_M\right|^2\left(\mu_1+\mu_2|\lambda_T|^2-2\mathrm{Re}(\mu_3\lambda_T)\right)\right\}$$

where

$$\begin{aligned}\lambda_T &= \lambda_{\mathcal{S}\bar{\mathcal{S}}}(jx+\lambda_{\bar{\mathcal{S}}\bar{\mathcal{S}}})^{-1}\\ \lambda_M &= r_o\mathrm{Re}\left[\lambda_{\mathcal{S}\mathcal{S}}-\lambda_{\mathcal{S}\bar{\mathcal{S}}}\left(jx+\lambda_{\bar{\mathcal{S}}\bar{\mathcal{S}}}\right)^{-1}\lambda_{\bar{\mathcal{S}}\mathcal{S}}\right]^{-1/2}\end{aligned}$$

and $\lambda_P = jx$ is the optimal reactive parasitic termination.

For a circular array with a full receive scattering, the fading path-gain covariance

matrix $\mathbf{\Sigma_h}$ has a circulant structure of the form

$$\mathbf{\Sigma_h} = \begin{bmatrix} 1 & \rho_1 & \rho_2 & \rho_1 \\ \rho_1 & 1 & \rho_1 & \rho_2 \\ \rho_2 & \rho_1 & 1 & \rho_1 \\ \rho_1 & \rho_2 & \rho_1 & 1 \end{bmatrix}$$

Using Kronecker spatial-correlation model $\mathbf{h}_o = \mathbf{\Sigma}_\mathbf{h}^{1/2}\mathbf{h}_w$, explicit relationships between μ's and ρ's can be calculated. Thus, the optimal values can be found by locating maxima of a polynomial of degree two.

Appendix B

SISO Broadband Design

B.1 Optimal Solution for SISO Systems

Proceeding as in [41, Chap. 8], it can shown that the above problem can be broken into an equivalent discrete optimization problem when $N(f)$ is represented on an orthonormal basis using Karhunen-Loeve expansion. Let $X_i = X(f_i)$ represent the i-th discrete sample of a continuous waveform $X(f)$, then for the continuous real-valued function C, we make use of the following property of Riemann integrals to write

$$C = \lim_{n\to\infty} \max_{\mathbf{P},\mathbf{G}} C_s(\mathbf{P},\mathbf{G})\triangle f_n$$

where, $\mathbf{P} = [P_1, \ldots, P_n]^T$, $\mathbf{G} = [G_1, \ldots, G_n]^T$,

$$C_s(\mathbf{P},\mathbf{G}) = \frac{1}{n}\sum_{i=1}^{n} \ln\left(1 + \frac{(1-e^{-G_i})|H_i|^2 P_i}{N_i}\right) \tag{B.1}$$

and $\triangle f_n = W/n$. Here, $(.)^T$ represents the transpose of a vector. Hence, it is equivalent to optimize (B.1) and extend the solution to the continuous case.

Now, consider the problem of maximizing

$$F(\mathbf{P}, \mathbf{G}) = \sum_{i=1}^{n} \ln \left(1 + \frac{(1 - e^{-G_i}) P_i}{Y_i} \right)$$

subject to

$$\sum_{i=1}^{n} G_i \leq G_0 \ , \ \sum_{i=1}^{N} P_i \leq P_0$$

where, $Y_i = N_i / |H_i|^2$.

Note that although F is increasing and concave in both $\mathbf{P}$ and $\mathbf{G}$, it is not jointly-concave in $(\mathbf{P}, \mathbf{G})$. The Karush-Kuhn-Tucker (KKT) conditions say that the necessary conditions for $\mathbf{x} = [x_1, \ldots, x_n]^T$ to minimize $f(\mathbf{x})$ subject to constraints $c_j(\mathbf{x}) \geq 0$, $j = 1, \ldots, k$ are that:

$$\begin{aligned} \frac{\partial}{\partial x_i} \left(f(\mathbf{x}) - \sum_j \lambda_j c_j(\mathbf{x}) \right) &= 0, \ i = 1, \ldots, n \\ c_j(\mathbf{x}) \geq 0 \quad &, \quad \lambda_j \geq 0 \\ \lambda_j c_j(\mathbf{x}) &= 0 \ , j = 1, \ldots, k \end{aligned}$$

For our problem, $\mathbf{x} = [\mathbf{P} \ \mathbf{G}]^T$ and we want to minimize $-F(\mathbf{P}, \mathbf{G})$ subject to the constraints:

$$c_1(\mathbf{x}) : [\mathbf{u}_n \ \mathbf{0}_n]^T \mathbf{x} \leq P_0 \ ,$$

$$c_2(\mathbf{x}) : [\mathbf{0}_n \ \mathbf{u}_n]^T \mathbf{x} \leq G_0 \ ,$$

where, $\mathbf{u}_n$ and $\mathbf{0}_n$ represent n-length vectors comprising all ones and zeros, respectively.

To proceed, we form the Lagrangian

$$L(\mathbf{P},\mathbf{G}) = -F(\mathbf{P},\mathbf{G}) + \lambda \sum_j P_j + \mu \sum_j G_j$$

which leads to the necessary conditions

$$\begin{aligned} \frac{\partial F}{\partial P_i} - \lambda &= 0 \ , \\ \frac{\partial F}{\partial G_i} - \mu &= 0 \ , \\ 0 \le P_i \le P_0 \ , \ 0 \le G_i \le G_0 \ , & \\ \lambda \ge 0 \ , \ \mu \ge 0 \ , & \\ \lambda P_i = \mu G_i &= 0 \ . \end{aligned}$$

These KKT conditions are met if there exist Lagrange multipliers λ and μ such that

$$\frac{\partial F}{\partial P_i} = \frac{(1-e^{-G_i})}{Y_i + (1-e^{-G_i})P_i} \begin{cases} = \lambda, & P_i > 0 \\ \le \lambda, & P_i = 0 \end{cases}$$

$$\frac{\partial F}{\partial G_i} = \frac{e^{-G_i}P_i}{Y_i + (1-e^{-G_i})P_i} \begin{cases} = \mu, & G_i > 0 \\ \le \mu, & G_i = 0 \end{cases}$$

Solving these, we get

$$P_i = \left[\frac{1}{\lambda} - \frac{Y_i}{1-e^{-G_i}}\right]^+ \ , \tag{B.2}$$

$$G_i = \left[\ln\left(1+\mu^{-1}\right) - \ln\left(1+\frac{Y_i}{P_i}\right)\right]^+ \tag{B.3}$$

where, λ and μ are chosen to satisfy the power and broadband matching constraints. It can seen that the optimal P_i and G_i satisfy a water-pouring solution, the continuous-frequency solution to which is given by

B.2 Iterative Mutual-Water-Pouring Algorithm

Observe that the optimal spectrum must satisfy a water-pouring solution of the form given in (B.2), (B.3). The optimal solution presented above can easily be obtained by an iterative algorithm presented below.

Algorithm *Iterative Mutual-Water-Pouring*

Input: P_0, G_0, Y_i, $i = \{1, 2, \ldots, n\}$ sorted in ascending order

Output: $\mathbf{P}, \mathbf{G}, C_{opt}, \lambda, \mu$

1. initialize $m = n, C_{opt} = 0$
2. **while** $m \neq 0$
3. **do**
4. $\mathbf{P} = [P_1, \ldots, P_m]$, $P_i = P_0/m$
5. $\mathbf{G} = [G_1, \ldots, G_m]$, $G_i = G_0/m$
6. $\mathbf{S} = [S_1, \ldots, S_m]$, $S_i = Y_i(1 - e^{-G_i})^{-1}$
7. $\mathbf{R} = [R_1, \ldots, R_m]$, $R_i = \ln(1 + Y_i/P_i)$
8. $(\mathbf{P}, \lambda) = \texttt{waterpour}(\mathbf{P}, \mathbf{S}, P_0)$
9. $(\mathbf{G}, \mu) = \texttt{waterpour}(\mathbf{G}, \mathbf{R}, G_0)$
10. **repeat** 8 & 9

11. **until** $(\mathbf{P}, \mathbf{G})$ converges to $(\mathbf{P}_{opt}, \mathbf{G}_{opt})$

12. evaluate C_s

13. **if** $C_s > C_{opt}$

14. update $C_{opt} = C_s, \mathbf{P}_{opt}, \mathbf{G}_{opt}, \lambda$ and μ

15. $m = m - 1$

16. **return**

The function `waterpour`$(\mathbf{P}, \mathbf{S}, P_0)$ distributes the total power P_0 such that $P_i = [\lambda^{-1} - S_i]^+$. This algorithm has been found to quickly converge to the optimal solution,[1] typically requiring less than 10 iterations for $n = 100$.

[1] Although KKT conditions are necessary and not sufficient, convergence to optimal solution has been ascertained analytically and via simulations for small n. Analysis of convergence for larger n is under study.

Appendix C

S-Parameter Matrix for Antenna Array

For an impedance of the form $\lambda(j\omega) = R + jX(\omega)$, the scattering parameters normalized to R (e.g., a characteristic impedance of 50 Ω or 75 Ω), the reflection coefficient is given by

$$\lambda_{22a}(j\omega) = \frac{\lambda(j\omega) - R}{\lambda(j\omega) + R} = \frac{jX(\omega)}{2R + jX(\omega)}$$
$$\implies |\lambda_{22a}(j\omega)|^2 = \frac{X^2}{4R^2 + X^2} = \mathrm{Re}(\lambda_{22a}(j\omega))$$

The above relation also implies that

$$\mathrm{Re}(\lambda_{21a}\lambda_{22a}^*) = \mathrm{Re}((1 - \lambda_{22a})\lambda_{22a}^*) = 0$$

Thus, the lossless and reciprocity requirements are met as follows:

$$\begin{aligned}
\mathbf{\Lambda}_{21a}\mathbf{\Lambda}_{21a}^{H} &= (\mathbf{I}-\mathbf{\Lambda}_{22a})(\mathbf{I}-\mathbf{\Lambda}_{22a})^{H} \\
&= \mathbf{I}-2\,\mathrm{Re}(\mathbf{\Lambda}_{22a})+\mathbf{\Lambda}_{22a}\mathbf{\Lambda}_{22a}^{H} \\
&= \mathbf{I}-\mathbf{\Lambda}_{22a}\mathbf{\Lambda}_{22a}^{H}
\end{aligned}$$

and

$$\mathrm{Re}(\mathbf{\Lambda}_{21a}\mathbf{\Lambda}_{22a}^{H})=\mathbf{0}$$

We must keep in mind that practical antenna designs may favor constant resistive parts.

Appendix D

Coupled MIMO-OFDM System

D.1 Equivalent System Model with Coupling

This section is based on [57]. Consider the system model shown in Fig. 6.1. Each of the S-matrix is calculated for 1 Ω reference impedance. We thus have

$$\mathbf{S}_{22a}(s) = (\mathbf{Z}_A(s) + \mathbf{I})^{-1}(\mathbf{Z}_A(s) - \mathbf{I})$$

Let $\mathbf{a}_T(s)$ represent the traveling wave-vector launched by the transmit array into the wireless channel and $\mathbf{b}_R(s)$ represent the traveling wave delivered by the receive antenna array to a set of independent loads of impedance $Z_0 = 1\ \Omega$. However, to avoid the needless clutter, we drop the notation (s). We suppress the frequency-dependence for the network analysis that follows.

Let $(\mathbf{a}_{m1}, \mathbf{b}_{m1})$ and $(\mathbf{a}_{m2}, \mathbf{b}_{m2})$ represent the input and output wave-vector pair at the

matching network N_m, respectively, as shown in Fig. 6.1. From $\mathbf{b}_m = \mathbf{S}_M \mathbf{a}_m$, we have

$$\begin{bmatrix} \mathbf{b}_{m1} \\ \mathbf{b}_{m2} \end{bmatrix} = \begin{bmatrix} \mathbf{S}_{11m} & \mathbf{S}_{12m} \\ \mathbf{S}_{21m} & \mathbf{S}_{22m} \end{bmatrix} \begin{bmatrix} \mathbf{a}_{m1} \\ \mathbf{a}_{m2} \end{bmatrix} \tag{D.1}$$

When the matching network is connected to the N antenna ports, by superposition

$$\mathbf{a}_{m1} = \mathbf{b}_R + \mathbf{S}_{22a}\mathbf{b}_{m1}$$

In order to find the equivalent MIMO channel matrix, we must find the relationship between $\mathbf{b}_R$ and $\mathbf{a}_T$.

First, observe that $\mathbf{b}_R$ is not affected by the choice of $\mathbf{S}_M$. Therefore, in order to establish the relationship between $\mathbf{a}_{m1}$ and $\mathbf{b}_R$, leaving the ports of the antenna array open-circuited (such that the net input is: $\mathbf{a}_{m1} - \mathbf{b}_{m1} = \mathbf{0}$), we have

$$\mathbf{a}_{m1} = (\mathbf{I} - \mathbf{S}_{22a})^{-1}\mathbf{b}_R \tag{D.2}$$

The open-circuit voltage induced across the antennas can be represented in terms of the incident and reflected wave-vectors as

$$\mathbf{v}_o = \sqrt{Z_0}(\mathbf{a}_{m1} + \mathbf{b}_{m1}) = 2\sqrt{Z_0}\mathbf{a}_{m1} \tag{D.3}$$

Using (D.2) and (D.3) alongwith

$$\mathbf{v}_o = 2Z_0\mathbf{H}\mathbf{i}_T, \quad \mathbf{i}_T = \frac{1}{\sqrt{Z_0}}(\mathbf{a}_T - \mathbf{b}_T)$$

we have

$$\begin{aligned}\mathbf{b}_R &= (\mathbf{I}-\mathbf{S}_{22a})\mathbf{H}(\mathbf{a}_T-\mathbf{b}_T)\\ &= (\mathbf{I}-\mathbf{S}_{22a})\mathbf{H}(\mathbf{I}-\mathbf{S}_T)\mathbf{a}_T;\quad \mathbf{b}_T=\mathbf{S}_T\mathbf{a}_T\\ &= \mathbf{S}_{21a}\mathbf{H}(\mathbf{I}-\mathbf{S}_T)\mathbf{a}_T \end{aligned} \tag{D.4}$$

Next, observe that in the absence of $\mathbf{b}_R$, $\mathbf{b}_{m2}=\mathbf{S}_{22}\mathbf{a}_{m2}$. Therefore, in the presence of $\mathbf{b}_R$ we see an additional wave-vector[1] $(\mathbf{I}-\mathbf{S}_{22a}\mathbf{S}_{11m})^{-1}\mathbf{b}_R$ scaled by the matching network's transmission matrix $\mathbf{S}_{21m}$, such that

$$\mathbf{b}_{m2}=\mathbf{S}_{21m}(\mathbf{I}-\mathbf{S}_{22a}\mathbf{S}_{11m})^{-1}\mathbf{b}_R+\mathbf{S}_{22c}\mathbf{a}_{m2} \tag{D.5}$$

where $\mathbf{S}_{22c}$ is given by (5.3d). Using (D.4), we can further write

$$\begin{aligned}\mathbf{b}_{m2} &= \mathbf{S}_{21m}(\mathbf{I}-\mathbf{S}_{22a}\mathbf{S}_{11m})^{-1}\mathbf{S}_{21a}\mathbf{H}(\mathbf{I}-\mathbf{S}_T)\mathbf{a}_T+\mathbf{S}_{22c}\mathbf{a}_{m2}\\ &= \mathbf{S}_{21c}\mathbf{H}(\mathbf{I}-\mathbf{S}_T)\mathbf{a}_T+\mathbf{S}_{22c}\mathbf{a}_{m2}\end{aligned}$$

where $\mathbf{S}_{21c}$ is given by (5.3c). However, we simplify our model by assuming that the rest of the RF chain is designed[2] such that $\mathbf{a}_{m2}=\mathbf{0}$, thereby yielding

$$\mathbf{b}_{m2} = \mathbf{S}_{21c}\mathbf{H}(\mathbf{I}-\mathbf{S}_T)\mathbf{a}_T \tag{D.6}$$

[1]The component $(\mathbf{I}-\mathbf{S}_{22a}\mathbf{S}_{11m})^{-1}\mathbf{b}_R$ reflects the matrix sum of an infinite geometric series for the wave traveling toward $\mathbf{S}_M$ due to excitation $\mathbf{b}_R$.

[2]The most general case is discussed in Appendix D.2.

In the absence of any coupling at the transmitter, $\mathbf{b}_{m2}$ is proportional to

$$\mathbf{b}_{m2} = \mathbf{S}_{21c}\mathbf{H}\mathbf{a}_T = \mathbf{S}_{21m}(\mathbf{I} - \mathbf{S}_{22a}\mathbf{S}_{11m})^{-1}\mathbf{S}_{21a}\mathbf{H}\mathbf{a}_T \tag{D.7}$$

We now make explicit, the frequency-dependence of the channel model, via sub-carrier index k. The overall channel matrix $\mathbf{H}_k$ that accounts for coupling is such that

$$\mathbf{r}_k = \mathbf{v}_L(f_k) = \mathbf{H}'_k\mathbf{v}_S(f_k) + \mathbf{n}_k = \mathbf{H}'_k\mathbf{s}_k + \mathbf{n}_k$$

where the covariance for noise component $\mathbf{n}_k$ may be altered due to mutual coupling. Further, we have

$$\begin{aligned}
\mathbf{v}_L(f_k) &= 2\sqrt{Z_0}\mathbf{a}_L(f_k) \\
&= 2\sqrt{Z_0}\mathbf{b}_{m2}(f_k) \\
&= 2\sqrt{Z_0}\mathbf{S}_{21c}(f_k)\mathbf{H}_k\mathbf{a}_T(f_k) \\
&= 2\sqrt{Z_0}\mathbf{S}_{21c}(f_k)\mathbf{H}_k\frac{1}{2\sqrt{Z_0}}\mathbf{v}_S(f_k)
\end{aligned}$$

yields

$$\mathbf{H}'_k = \mathbf{S}_{21c}(f_k)\mathbf{H}_k \ . \tag{D.8}$$

D.2 Accounting for a Given Load

It can be argued that we can not assume $\mathbf{a}_{m2} = \mathbf{0}$ in (D.5) since we may not have the freedom to choose the load in most cases. But at the same time, the aim of this study

is to provide bounds on the capacity based only on a given antenna geometry. However, we present the complete analysis for the case when $\mathbf{a}_{m2} \neq \mathbf{0}$. Note that the loads may impose their own matching constraints in addition to the ones by the antenna array.

In such a case, we can formulate the problem as one comprising of three networks with S-parameter matrices $\mathbf{S}_A, \mathbf{S}_M$ and $\mathbf{S}_L$ such that $\mathbf{b}_L = \mathbf{a}_{m2}$. Also, observe that $\mathbf{b}_L = \mathbf{S}_L\mathbf{a}_L$ implies

$$\begin{aligned}
\mathbf{a}_L &= \mathbf{b}_{m2} \\
&= \mathbf{S}_{21m}\mathbf{a}_{m1} + \mathbf{S}_{22m}\mathbf{a}_{m2} \\
&= \mathbf{S}_{21m}\mathbf{a}_{m1} + \mathbf{S}_{22m}\mathbf{b}_L \\
&= \mathbf{S}_{21m}\mathbf{a}_{m1} + \mathbf{S}_{22m}\mathbf{S}_L\mathbf{a}_L
\end{aligned}$$

Thus,

$$\begin{aligned}
\mathbf{a}_L &= (\mathbf{I} - \mathbf{S}_{22c}\mathbf{S}_L)^{-1}\mathbf{S}_{21m}\mathbf{a}_{m1} \\
&= (\mathbf{I} - \mathbf{S}_{22c}\mathbf{S}_L)^{-1}\mathbf{S}_{21m}(\mathbf{I} - \mathbf{S}_{22a})^{-1}\mathbf{b}_R \\
&= (\mathbf{I} - \mathbf{S}_{22c}\mathbf{S}_L)^{-1}\mathbf{S}_{21m}(\mathbf{I} - \mathbf{S}_{22a})^{-1}\mathbf{S}_{21a}\mathbf{H}\mathbf{a}_T \\
&= (\mathbf{I} - \mathbf{S}_{22c}\mathbf{S}_L)^{-1}\mathbf{S}_{21c}\mathbf{H}\mathbf{a}_T
\end{aligned}$$

and

$$\begin{aligned}
\frac{1}{\sqrt{Z_0}}\mathbf{v}_L &= \mathbf{a}_L + \mathbf{b}_L \\
&= (\mathbf{I} + \mathbf{S}_L)\mathbf{a}_L \\
&= (\mathbf{I} + \mathbf{S}_L)(\mathbf{I} - \mathbf{S}_{22c}\mathbf{S}_L)^{-1}\mathbf{S}_{21c}\mathbf{H}\mathbf{a}_T
\end{aligned}$$

Therefore,

$$\mathbf{v}_L = (\mathbf{I} + \mathbf{S}_L)(\mathbf{I} - \mathbf{S}_{22c}\mathbf{S}_L)^{-1}\mathbf{S}_{21c}\mathbf{H}\mathbf{v}_S$$

Substituting $\mathbf{S}_L = \rho_L\mathbf{I}$, the equivalent channel matrix is

$$\begin{aligned}
\mathbf{H}' &= (1+\rho_L)(\mathbf{I} - \rho_L\mathbf{S}_{22c})^{-1}\mathbf{S}_{21c}\mathbf{H} \\
&= \mathbf{Q}(1+\rho_L)(\mathbf{I} - \rho_L\mathbf{\Lambda}_{22c})^{-1}\mathbf{\Lambda}_{21c}\mathbf{Q}^H\mathbf{H} \\
&= \mathbf{Q}(1+\rho_L)(\mathbf{I} - \rho_L\mathbf{\Gamma})^{-1}\mathbf{T}\mathbf{Q}^H\mathbf{H}
\end{aligned}$$

Caution: This problem may be hard to optimize. And, we need to be careful about any constraints imposed by the load as well.

D.3 Optimization

Let x_{nk} denote $x_n(f_k)$ and define

$$\boldsymbol{w}_n = [w_{n1}, \ldots, w_{nK}]$$

$$\boldsymbol{\psi}_n = [\psi_{n1}, \ldots, \psi_{nK}]$$

$$\boldsymbol{G}_n = [G_{n1}, \ldots, G_{nK}]$$

for $n = 1, \ldots, N$ and

$$\mathbf{x} = [\boldsymbol{\psi}_1 \ \ldots \ \boldsymbol{\psi}_N \ \boldsymbol{G}_1 \ \ldots \ \boldsymbol{G}_N]^T$$

Now, consider the problem of maximizing

$$F(\mathbf{x}) = \frac{1}{K}\sum_{n=1}^{N}\sum_{k=1}^{K}\log\left(1+\frac{1}{N}\frac{\psi_n(f_k)}{\sigma_n(f_k)}\left(1-e^{-G_n(f_k)}\right)\right)$$

where (6.23) and (6.24) can be written as

$$\begin{aligned}
c_0(\mathbf{x}):&\ \frac{1}{K}\left[\boldsymbol{w}_1\ \ldots\ \boldsymbol{w}_N\ \mathbf{0}_K\ \ldots\ \mathbf{0}_K\right]^T\mathbf{x}\ \leq P_0\\
c_1(\mathbf{x}):&\ \frac{1}{K}\left[\mathbf{0}_K\ \ldots\ \mathbf{0}_K\ \mathbf{1}_K\ \ldots\ \mathbf{0}_K\right]^T\mathbf{x}\ \leq \frac{1}{B}\,G_{01}\\
&\vdots\\
c_N(\mathbf{x}):&\ \frac{1}{K}\left[\mathbf{0}_K\ \ldots\ \mathbf{0}_K\ \mathbf{0}_K\ \ldots\ \mathbf{1}_K\right]^T\mathbf{x}\ \leq \frac{1}{B}\,G_{0N}
\end{aligned}$$

where, $\mathbf{1}_K$ and $\mathbf{0}_K$ represent K-length vectors comprising all ones and zeros, respectively, and $(.)^T$ represents the transpose.

The Karush-Kuhn-Tucker (KKT) conditions say that the necessary conditions for $\mathbf{x} = [x_0, \ldots, x_{M-1}]^T$ to minimize $f(\mathbf{x})$ subject to constraints $c_j(\mathbf{x}) \geq 0$, $j = 0, \ldots, J-1$ are that:

$$\begin{aligned}
\frac{\partial}{\partial x_m}\left(f(\mathbf{x})-\sum_{j=0}^{J-1}\xi_j c_j(\mathbf{x})\right) &= 0,\ m=0,\ldots,M-1\\
c_j(\mathbf{x}) &\geq 0\ ,\ \xi_j \geq 0\\
\xi_j c_j(\mathbf{x}) &= 0\ ,\ j=0,\ldots,J-1
\end{aligned}$$

To proceed, we form the Lagrangian

$$L(\mathbf{x}) = -F(\mathbf{x}) + \xi\left(c_0(\mathbf{x}) - P_0\right) + \sum_{n=1}^{N}\mu_n\left(c_n(\mathbf{x}) - \frac{1}{B}\,G_{0n}\right)$$

which leads to the necessary conditions

$$\begin{aligned} \frac{\partial F}{\partial \psi_{nm}} - w_{nm}\xi &= 0 \ , \\ \frac{\partial F}{\partial G_{nm}} - \mu_n &= 0 \ , \end{aligned}$$

for $n = 1, \ldots, N,\ m = 0, \ldots, M-1$, where

$$\begin{aligned} & 0 \ \leq \ \psi_{nm} \ \leq \ P_0 \ , \ 0 \ \leq \ G_{nm} \ \leq \ G_{0n}/B \ , \\ & \xi \ \geq \ 0 \ , \ \mu_1 \ \geq \ 0 \ , \ \mu_2 \ \geq \ 0 \ , \\ & \xi \ \psi_m \ = \ \mu \ G_m \ = \ 0 \ , \ m \ = \ 0, \ldots, M-1 \end{aligned}$$

Solving these, we get

$$\begin{aligned} \psi_n(k) &= \left[\frac{1}{w_n(k)\xi} - \frac{N\sigma_n(k)}{1 - e^{-G_n(k)}} \right]^+ \ , \\ G_n(k) &= \left[\log\left(1 + \mu_n^{-1}\right) - \log\left(1 + \frac{N\sigma_n(k)}{\psi_n(k)}\right) \right]^+ \end{aligned}$$

where, $[z]^+ = \max\{0, z\}$, and ξ and μ_n are chosen to satisfy the power and broadband matching constraints, respectively.

D.4 Eigen-Values of Optimal Signal Covariance

For illustrative purposes, we consider a 2×2 MIMO system. It is easy to see that the eigen-values for the k-th sub-carrier are given by

$$\begin{aligned}\gamma_n &= \frac{1}{2}\Bigg[(w_1\psi_1 + w_2\psi_2) + (-1)^{n+1} \underbrace{\sqrt{(w_1\psi_1 - w_2\psi_2)^2 + 4\psi_1\psi_2 \det(\mathbf{\Omega}_k)}}_{\gamma_\Delta} \Bigg]^+ \\ &= \frac{1}{2}\Bigg[w_1\psi_1 + w_2\psi_2 + (-1)^{n+1}\gamma_\Delta \Bigg]^+, \qquad n = 1, 2\end{aligned}$$

In other words,

$$\gamma_n(k) = \left[\frac{1}{\xi} - \frac{N}{2}\frac{w_1(k)\sigma_1(k)}{(1 - e^{-G_1(k)})} - \frac{N}{2}\frac{w_2(k)\sigma_2(k)}{(1 - e^{-G_2(k)})} + (-1)^{n+1}\ \frac{1}{2}\ \gamma_\Delta(k) \right]^+ \quad \text{(D.9)}$$

represents a water-pouring solution[3] while the power constraint can be written as

$$\mathrm{Tr}\left(\boldsymbol{\mathcal{R}}_{\boldsymbol{ss}}\right) = \sum_{k=1}^{K} \mathrm{Tr}\left(\mathbf{\Upsilon}_k\right) \implies \sum_{n=1}^{N}\sum_{k=1}^{K} \gamma_n(k) \leq K P_0 \quad \text{(D.10)}$$

Although, $P_n(k)$ and $\gamma_n(k)$ have same constraints and similar distributions, it is important to point out that they essentially represent two different quantities.

[3]This property can be verified for $N > 2$ in a similar manner, realizing the fact that the sum of the roots of a degree-N polynomial are related by $\sum_{n=1}^{N} \gamma_n = \mathrm{Tr}(\mathbf{\Psi\Omega})$.

D.5 Iterative Mutual-Water-Pouring Algorithm

We now present an iterative algorithm to arrive at the optimal solution numerically. Recall from above that the optimal solution is of the form

$$P_{nk} = [F - \alpha_{nk}]^+ \ , \ G_{nk} \ = \ [J_n - \beta_{nk}]^+$$

where,

$$\begin{aligned} &\alpha_{nk} = \frac{\chi_{nk}}{1 - e^{-G_{nk}}} \ , \ \beta_{nk} = \log\left(1 + \frac{\chi_{nk}}{P_{nk}}\right) \\ &F = \frac{1}{\xi} \ , \ J_n = \log\left(1 + \mu_n^{-1}\right) \end{aligned} \tag{D.11}$$

such that

$$\begin{aligned} &(i) \ \sum_{n=1}^{N}\sum_{k=1}^{K} P_{nk} \leq KP_0 = P_0' \\ &(ii) \ \sum_{k=1}^{K} G_{nk} \leq \frac{K}{B}\, G_{0n} = \frac{2\pi K}{Q_n(B/f_{0n})} = G_{0n}' \ . \end{aligned}$$

We now propose the iterative algorithm. The case $N = 2$ is treated for illustration.

Algorithm *Iterative Mutual-Water-Pouring*

Input: $\boldsymbol{\chi} = [\boldsymbol{\chi}_1 \ \boldsymbol{\chi}_2],\ P_0',\ G_{01}',\ G_{02}'$

Output: $\boldsymbol{P}_{opt},\ \boldsymbol{G}_{opt},\ C_{opt},\ F,\ J_1,\ J_2$

1. $\boldsymbol{\chi}_n = \texttt{sort}(\boldsymbol{\chi}_n)$
2. initialize $m = K,\ C_{opt} = 0$
3. **while** $m \neq 0$
4. **do**

5. $\boldsymbol{P}_n = \texttt{initialize}(m, P'_0),\ n = 1, 2$

6. $\boldsymbol{G}_n = \texttt{initialize}(m, G'_{0n}),\ n = 1, 2$

7. $\boldsymbol{\alpha}_n = \texttt{evalalpha}(\boldsymbol{\chi}_n, \boldsymbol{G}_n),\ n = 1, 2$

8. $\boldsymbol{\beta}_n = \texttt{evalbeta}(\boldsymbol{\chi}_n, \boldsymbol{P}_n),\ n = 1, 2$

9. $(\boldsymbol{P}_1, \boldsymbol{P}_2, F) = \texttt{waterpour2D}(\boldsymbol{P}_1, \boldsymbol{P}_2, \boldsymbol{\alpha}_1, \boldsymbol{\alpha}_2, P'_0)$

10. $(\boldsymbol{G}_1, J_1) = \texttt{waterpour1D}(\boldsymbol{G}_1, \boldsymbol{\beta}_1, G'_{01})$

11. $(\boldsymbol{G}_2, J_2) = \texttt{waterpour1D}(\boldsymbol{G}_2, \boldsymbol{\beta}_2, G'_{02})$

12. **repeat** 6 to 10

13. **until** $(\boldsymbol{P}, \boldsymbol{G}) \longrightarrow (\boldsymbol{P}_{opt}, \boldsymbol{G}_{opt})$

14. evaluate C

15. **if** $C > C_{opt}$

16. update $C_{opt},\ \boldsymbol{P}_{opt},\ \boldsymbol{G}_{opt},\ F,\ J_1,\ J_2$

17. $m = m - 1$

18. $[\boldsymbol{P}_{opt}, \boldsymbol{G}_{opt}] = \texttt{unsort}(\boldsymbol{P}_{opt}, \boldsymbol{G}_{opt})$

19. **return**

The function `waterpour1D` and `waterpour2D` represent the standard water-pouring functions over one and two dimensions, respectively, whereas `evalalpha` and `evalbeta` evaluate α's and β's given by (D.11). The function `initialize` assigns equal P'_0 and G'_{0n} to corresponding m-length vectors.

D.6 Realisitic Noise Modeling

From (6.5)

$$\boldsymbol{\Sigma_n} \;=\; \frac{1}{T_0}\left((T_A - T_\beta)\boldsymbol{R}_A\boldsymbol{T}\boldsymbol{T}^H + (T_\alpha + T_\beta)\boldsymbol{I}\right) \;\triangleq\; \boldsymbol{D}\boldsymbol{T}\boldsymbol{T}^H + \sigma^2\boldsymbol{I}$$

where $\boldsymbol{R}_A$ is a $KN \times KN$ diagonal matrix representing the real part of eigen-impedance for K sub-carriers

$$\boldsymbol{R}_A = \begin{bmatrix} \mathrm{Re}(\boldsymbol{\Lambda}_{A,1}) & & \\ & \ddots & \\ & & \mathrm{Re}(\boldsymbol{\Lambda}_{A,K}) \end{bmatrix}$$

such that

$$\boldsymbol{\Sigma}_{\mathbf{n}_k} = \mathbf{D}_k\mathbf{T}_k\mathbf{T}_k^H + \sigma^2\mathbf{I}\ , \quad \mathbf{D}_k = \frac{T_A - T_\beta}{T_0}\boldsymbol{\Lambda}_{A,k}\ .$$

The spectral efficiency of this uncoupled system can be written as a sum of the capacities of KN space-frequency modes

$$\begin{aligned} C &= \frac{1}{K}\max_{\boldsymbol{\Psi}_k,\mathbf{T}_k}\sum_{k=1}^{K}\log_2\det\left(\mathbf{I} + \frac{1}{N}\boldsymbol{\Sigma}_{\mathbf{n}_k}^{-1}\boldsymbol{\Psi}_k\mathbf{T}_k\mathbf{T}_k^H\right) \\ &= \frac{1}{K}\max_{\boldsymbol{\Psi}_k,\mathbf{T}_k}\sum_{k=1}^{K}\log_2\det\left(\mathbf{I} + \frac{1}{N}\left(\mathbf{D}_k^{-1} + \frac{1}{\sigma^2}\mathbf{T}_k\mathbf{T}_k^H\right)\boldsymbol{\Psi}_k\right) \\ &= \frac{1}{K}\max_{\psi_{nk},\Gamma_{nk}}\sum_{k=1}^{K}\sum_{n=1}^{N}\log_2\left(1 + \frac{1}{N}\psi_{nk}\left(\frac{1}{d_{nk}} + \frac{1}{\sigma^2}\left(1 - |\Gamma_{nk}|^2\right)\right)\right)\ . \end{aligned}$$

The optimal solution in this case is given by

$$\begin{aligned} \psi_n(k) &= \left[\frac{1}{w_n(k)\xi} - \frac{Nd_{nk}\sigma^2}{\sigma^2 + d_{nk}\left(1 - e^{-G_{nk}}\right)}\right]^+, \\ G_n(k) &= \left[\log\left(1 + \mu_n^{-1}\right) - \log\left(1 + \frac{N\sigma^2}{\psi_n(k)}\right)\right]^+ . \end{aligned}$$